A TIME INTEGRATION SCHEME FOR STRESS -TEMPERATURE DEPENDENT VISCOELASTIC BEHAVIORS OF ISOTROPIC MATERIALS

A Thesis

by

KAMRAN-AHMED KHAN

Submitted to the Office of Graduate Studies of
Texas A&M University
partial fulfillment of the requirements for the degree of

MASTER OF SCIENCE

December 2006

Major Subject: Mechanical Engineering

A TIME INTEGRATION SCHEME FOR STRESS -TEMPERATURE DEPENDENT VISCOELASTIC BEHAVIORS OF ISOTROPIC MATERIALS

A Thesis

by

KAMRAN-AHMED KHAN

Submitted to the Office of Graduate Studies of
Texas A&M University
in partial fulfillment of the requirements for the degree of

MASTER OF SCIENCE

Approved by:

Chair of Committee,	Anastasia Muliana
Committee Members,	J. N Reddy
	Eyad Masad
Head of Department,	Dennis L. O'Neal

December 2006

Major Subject: Mechanical Engineering

ABSTRACT

A Time Integration Scheme for Stress-Temperature Dependent Viscoelastic Behaviors of Isotropic Materials. (December 2006)

Kamran-Ahmed Khan, B.Eng., NED University of Engineering and Technology, Pakistan

Chair of Advisory Committee: Dr. Anastasia Muliana

A recursive-iterative algorithm is developed for predicting nonlinear viscoelastic behaviors of isotropic materials that belong to the thermorheologically complex material (TCM). The algorithm is derived based on implicit stress integration solutions within a general displacement based FE structural analyses for small deformations and uncoupled thermo-mechanical problems. A previously developed recursive-iterative algorithm for a stress-dependent hereditary integral model which was developed by Haj-Ali and Muliana is modified to include time-temperature effects. The recursive formula allows bypassing the need to store entire strain histories at each Gaussian integration point. Two types of iterative procedures, which are fixed point and Newton-Raphson methods, are examined within the recursive algorithm. Furthermore, a consistent tangent stiffness matrix is formulated to accelerate convergence and avoid divergence. The efficiency and accuracy of the proposed algorithm are evaluated using available experimental data and several structural analyses. The performance of the proposed algorithm under multi-axial conditions is verified with analytical solutions of creep responses of a plate with a hole. Next, the recursive-iterative algorithm is used to predict the overall response of single

lap-joint. Numerical simulations of time-dependent crack propagations of adhesive bonded joints are also presented. For this purpose, the recursive algorithm is implemented in cohesive elements. The numerical assessment of the TCM and thermorheologically simple material (TSM) behaviors has also been performed. The result showed that TCM are able to describe thermo-viscoelastic behavior under general loading histories, while TSM behaviors are limited to isothermal conditions. The proposed numerical algorithm can be easily used in a micromechanical model for predicting the overall composite responses. Examples are shown for solid spherical particle reinforced composites. Detailed unit-cell FE models of the composite systems are generated to verify the capability of the above micromechanical model for predicting the overall nonlinear viscoelastic behaviors.

ACKNOWLEDGEMENTS

Above all I am very thankful to almighty Allah who gave me courage and strength to do my master's degree.

I am grateful to my advisor and committee chair, Dr. Anastasia Muliana, for her continuous guidance and encouragement through out this thesis. Her support at every stage of this project is really valuable for me. I would like to extend my gratitude to Dr. J. N. Reddy and Dr. Eyad Masad for their helpful comments on the work. I would also like to extend my gratitude to Dr. Harry Hogan for his fruitful comments on my thesis.

I am very thankful to my friends Sam, Kim, Sohaib, Ali, Salman and all other friends who guided me and supported me throughout my master's thesis. In the end, I am very thankful to my beloved mother, father, grandmother, brother and sisters for their support.

TABLE OF CONTENTS

Page

CHAPTER

LIST OF FIGURES

FIGURE Page

FIGURE Page

LIST OF TABLES

CHAPTER I

INTRODUCTION

Polymeric materials have received a tremendous attention in the past few years as an alternative material for engineering applications in automotive and electronic industries, sporting goods, adhesive bonded joints and many others. This is mainly due to the fact that polymers can be customized to meet a desired performance while maintaining low cost. As polymers become increasingly used, it is essential to understand their mechanical responses in terms of stresses and deformations under structural and environmental loadings. One of the most pronounced characteristic of polymers is their viscoelastic behavior. The viscoelastic behaviors of polymers are intensified under high stress levels and extreme environmental conditions. However, the effects of combined time-stress-temperature-moisture on the polymer performance have not been fully understood, which limits the ability in predicting the polymer's durability and long term responses. The temperature effects on the time-dependent behaviors of polymers are often incorporated through a time-scale shift factor only. This typed of polymers is categorized as thermo-rheologically simple materials (TSM). Other materials that do not belong to the TSM are referred to thermo-rheologically complex materials (TCM). In addition to understanding the mechanical performance of polymers it is necessary to build a tool that integrates the constitutive material models into the structural analyses. This allows the engineers to analyze short term and long term structural performances under various loading conditions.

This thesis follows the style of Composite Science and Technology.

The present study develops a time integration algorithm of nonlinear viscoelastic materials that belongs to a class of TCM. The Schapery nonlinear viscoelastic model is modified to include the time-stress-temperature variations. This numerical algorithm is generated for small deformation and uncoupled thermo-mechanical problems. The proposed algorithm can be easily implemented in general displacement based finite element (FE) structural analyses. Moreover, polymeric materials are often reinforced with nano or micro particles to improve their toughness. This leads to the use of micromechanical modeling frameworks. The proposed time-integration algorithm is also designated to be easily integrated within the micromechanical modeling framework.

This chapter presents a literature review of analytical, numerical, and experimental works on thermo-viscoelastic behaviors of polymeric materials.

1.1 CURRENT WORKS IN THERMO-VISCOELASTIC BEHAVIORS OF POLYMERS

1.1.1 ANALYTICAL AND EXPERIMENTAL STUDIES ON THERMO-VISCOELASTIC BEHAVIORS OF POLYMERS

Viscoelastic material responses can be described either with constitutive material models or phenomenological approaches. The constitutive material models are derived within the context of thermodynamics framework, which make them capable of describing material's physical behaviors. Detail constitutive material models often lead to complex analytical forms with significant number of material parameters and it is quite challenging to characterize these parameters. On the other hand, using phenomenological approaches reduce complexity and number of material parameters. However, these models are not fully capable in including the physical characteristic of the materials.

Staverman and Schwarzl [1] discussed the relation of a linear viscoelastic material response that consists of spring and dashpot chain models and the thermodynamics framework. The free energy was calculated by adding amounts of energy accumulated in the springs, while the rate of dissipated energy was obtained by summing of viscous work rate in all the dashpots. It was concluded that all modeling networks consisting of spring and dashpots satisfied local balanced of energy, provided that the equilibrium condition was fulfilled and the inertial effect was negligible.

Several constitutive equations were proposed to describe nonlinear viscoelastic behaviors of materials. Leaderman [2] developed a generalization of single integral equations of the Boltzman constitutive model to describe the nonlinear viscoelastic behavior of filamentous material, but this model was not general enough to describe nonlinear viscoelastic materials behavior. Generalization was done by introducing the empirical functions of time and stress, which were used to illustrate the nonlinear behavior. Green, Rivlin and Spencer [3]-[5] proposed a more general constitutive model for nonlinear materials by formulating stress relaxation in terms of a tensor functional of the strain history based on invariants. In this model, the stress at a point was not only a function of current deformation gradients but also a function of the deformation gradients at all time histories. Schapery [6] developed a single integral equation for predicting nonlinear viscoelastic material under isothermal condition. This integral form was derived based on thermodynamics of irreversible processes (TIP) with internal state variables (ISVs). Each ISV was used to describe the material physical behavior. The temperature-dependent properties were carried through a time-scale (reduced time). This simplification allowed applying the time-temperature superposition principle (TTSP). Four nonlinear material coefficients were introduced. The use of stresses, rather than strains, as independent variables was made for polymeric materials in a glassy phase. Caruthers et al. [7] and Adolf et al. [8] derived a thermodynamics based constitutive model for nonlinear viscoelastic behavior of isotropic and thermorheologically simple polymers. To fulfill the thermodynamics consistency for nonlinear viscoelastic materials, the rational mechanics framework of Noll and Coleman

[9] was imposed. The proposed constitutive model was capable in physically describing full range of relaxation behavior of glassy polymers under arbitrary combined time-temperature-deformation histories. Thus, no fitting for nonlinear parameters were required to capture the nonlinear behaviors. The proposed constitutive model was applied to four different polymers over a broad range of relaxation behaviors.

Several experimental works on thermo-mechanical and time-dependent behaviors of polymeric materials have been performed. Schapery [6] constitutive model has been widely used and modified to represent time-dependent behaviors of amorphous polymers under combined thermo-mechanical loadings. Both thermorheologically simple materials (TSM) and thermorheologically complex materials (TCM) have been considered. Ward and Onat [10] performed creep and recovery tests with various loading histories under isothermal conditions for an oriented polypropylene monofilament. By comparing the compliances generated from the tests and the ones from the linear creep and recovery equations it was concluded that the studied material exhibits nonlinear viscoelastic behavior. It was shown that the functional of first order and third order hereditary integral are sufficient to describe the nonlinear behavior of the polypropylene.

Peretz and Weitsman [11]-[12] characterized nonlinear viscoelastic behavior of FM-73 polymer from isothermal uniaxial creep-recovery tests at different stress levels and temperature range of 30-60 °C. The Schapery's single integral constitutive equation was used to describe the nonlinear behavior. It was mentioned that the transient temperature testing was required to separate the nonlinear temperature dependent parameters g_1 and g_2 in the Schapery integral model. Harper and Weitsman [13] presented the method to

characterize the response of a class of TCM, such as Hercules 3502 epoxy resin. Three characterization techniques were used, which are involving transient temperature data, isothermal data and a combination of transient and isothermal data. It was shown that, in order to obtain complete information, it is necessary to conduct sharp temperature-drop tests in addition to isothermal creep and recovery tests.

Knauss and Emri [14] studied the sensitiveness of the temperature effect on the viscoelastic behavior of the polyvinyl acetate. Nonlinear viscoelastic constitutive model based on free volume was modified to accommodate the transient deformation histories under hydrostatic loadings. The volume change under transient thermal histories in the glass transition range was analyzed. It was mentioned that temperature histories should be prescribed in such a way that the material functions can be accurately evaluated because it is impossible to achieve the step temperature histories. It was suggested that conducting experiments under constant temperature and/or maintaining constant temperature rates is best for evaluation of the material functions.

Zhang et al. [15] used the combined Schapery and Struik's model for predicting nonlinear viscoelastic behavior for an unsaturated polyester resin. A series of tests were carried out in order to characterize the material parameters and verify the prediction capabilities. The combined Schapery-Struik model was verified for several cyclic mechanical loading conditions. Zhu [16] studied nonlinear thermo-mechanical creep behaviors of polycarbonate at different temperatures (0 to 140^{o}C) under pure shear loading. The creep strain in the linear viscoelastic range was measured with a torsiometer. A master curve was then constructed using a horizontal time-shifting.

Next, the shear creep tests in the nonlinear viscoelastic range were conducted using the Arcan shear test fixture at different temperatures and under different stress levels. It was shown that nonlinearity started at 1% strain for all temperatures considered in that study. It was also found that time-temperature shifting at small strains did not apply in the nonlinear domain.

Park et al. [17] conducted multi-axial compression tests on epoxy material to determine the shear and bulk linear viscoelastic properties. The calibrated material properties were then validated with the data from separately conducted torsion and uniaxial tests. A hybrid nonlinear viscoelastic model, which combined Schapery's [6] integral equation and Popelar's shear [18] modified free volume model, was proposed. The torsion and uniaxial tension experiments were conducted at three different strain rates, temperature and humidity levels for calibrating time-dependent material parameters in the hybrid model. It was found that the vertical shifting of the compliance was required to capture the moisture effects.

1.1.2 TIME SCALING TECHNIQUE FOR PREDICTING LONG-TERM BEHAVIORS OF POLYMERS

Short term creep tests at several elevated temperatures have been conducted and used to create a master curve for predicting long-term behaviors of polymers. The time-temperature superposition principle (TTSP), proposed by Leaderman [2], has been extensively and successfully applied to characterize long-term behaviors of various viscoelastic materials. The method involves creating a master curve by shifting

relaxation moduli or creep compliances from a short-term test duration at different temperatures to the ones at a reference temperature. The master curve is associated with a long-term material behavior at the chosen reference temperature. For a class of thermorheologically simple material (TSM), a master curve can be formed by horizontal shifting alone in a logarithmic time scale. The horizontal distance required to shift the short-term creep/relaxation responses to the master curve is equal to the log of the inverse of the time-temperature shift factor a^T. It should be emphasized here that the parameter a^T is a time shift factor used to produce a creep/relaxation response at a non-reference temperature by performing time shifting of the response at the reference condition. For a class of thermorheologically complex material (TCM), vertical shifting of the short-term data prior to the horizontal shifting is required (Griffith et al., [19] Tuttle, [20] and Yen and Williamson [21]). Vertical shifting is associated with instantaneous nonlinear stress and temperature dependent behaviors.

Schwarzl and Staverman [22] classified materials as thermorheologically simple and non thermorheologically simple based on their micro and macro structural performances at different temperatures. It was shown that for the TSM the entire viscoelastic response can be described by one function of temperature only. This was due to the fact that the temperature change was equivalent to a shift factor on the logarithmic time scales. All deformation rates and times were affected in the same proportion with respect to the reference temperature. It was concluded that in TSM at different temperatures, the same molecular processes took place only with different speed. Feng et al. [23] carried out accelerated tests to determine long-term performances of neat epoxy resin under

different environmental conditions. The TTSP was used to create a master curve for the long-term material prediction. Temperature and moisture effects on the creep compliance of the epoxy adhesives were also studied. It was found that the long-term creep behavior of the epoxy structural adhesives can be reliably predicted using a set of short term accelerated creep tests at different temperatures and moisture conditions. Qvale and Chandar [24] introduced the confined compression configuration to conduct experiments under multiaxial loading on polymethyl methrylate (PMMA) and polycarbonate (PC). The bulk and shear relaxation moduli were obtained simultaneously from that experiment. TTSP was utilized to obtain master curves for bulk and shear moduli using the series of tests at different temperatures. A uniaxial relaxation modulus under confined tests corresponding to the measured bulk and shear behaviors was obtained and compared with the ones from the unconfined uniaxial relaxation experiments. It was found that the confined configuration decelerated the rate of relaxation of the polymers.

1.1.3 NUMERICAL ALGORITHM FOR THERMO-VISCOELASTIC BEHAVIORS OF POLYMERS

Numerical solutions that are compatible with finite element (FE) analyses have been developed for analyzing viscoelastic constitutive models of both isotropic and anisotropic materials. Zienkiewicz et al. [25] presented incremental algorithm for simulating creep behaviors on quasi-static problems. The incremental formulation was derived directly from a differential governing equation of a spring-dashpot mechanical

model. The constitutive material model was represented by a series of Kelvin elements coupled with an elastic spring. The strain rate was modeled as functions of current stress and accumulated creep strains; and the strain histories were stored only for the current time. The model was extended for multi-axial and isotropic materials with time-independent Poisson's effect. An alternative approach using hereditary integral model has been presented (Zienkiewicz and Cheung [26]). Bazant [27] developed higher order numerical algorithm of nonlinear first-order differential equations in terms of the components of stresses and strains, which can be solved by Runge-Kutta or predictor-corrector methods.

Constitutive viscoelastic model based on hereditary integral forms have gained advantages in terms of their capability in predicting time-dependent material responses under more general loading histories than those of differential equation models. Numerical algorithms have been formulated for several available hereditary integral models. A recurrence numerical algorithm for linear viscoelastic integral under thermo-mechanical loading for TSM was proposed by Taylor et al. [28]. The recursive algorithm allows formulating the current stress tensor as a function of the history variables stored at the previous time step, the current time increment, and the current strain increments. The recursive approach bypasses the need to store entire history variables, which minimizes the storage required to perform the constitutive integration. Similar recursive approach was used by Feng [29] for modeling linear viscoelastic materials described by the Voltera integral equation.

The Schapery's [6] nonlinear viscoelastic model has been extensively applied for isotropic and anisotropic materials. Henriksen [30] developed a recursive integration algorithm of the Schapery's nonlinear constitutive model for a uniaxial response. A Prony exponential series was used for the transient compliance to allow generating a recursive form of the hereditary integral. The computer storage requirement for using this method was proportional to the number of terms in the Prony series, at each integration point. Lai and Bakker [31] modified Henriksen recursive algorithm in order to include nonlinear effects due to temperature and physical aging in the reduced time functions. Isotropic material was considered by decoupling the deviatoric and volumetric parts. Haj-Ali and Muliana [32] formulated a recursive-iterative algorithm of the Schapery stress-dependent viscoelastic constitutive models. The formulation was derived with a constant incremental strain rate during each increment, which is compatible with a displacement based FE analyses. The linearized stress update part of this study followed the numerical formulation previously derived by Taylor et al. [28], Henriksen [30], and Lai and Bakker [31]. An iterative scheme based on Newton-Raphson method was performed for correcting trial linearized stress in order to minimize a strain residual. Simo and Hughes [33] presented several numerical algorithms of inelastic materials including viscoelasticity. Constitutive material models with internal state variables were used to derive a strain-based nonlinear viscoelastic models.

The hereditary integral models have been extended for anisotropic viscoelastic materials of TSM typed. Poisson's effect is often assumed to be time-independent. Kennedy and Wang [34] presented three-dimensional FE analysis of nonlinear

viscoelastic response of orthotropic media. The transient creep compliance in the viscoelastic model was represented as an exponential series plus a steady-flow term, which simplified the numerical procedure for handling hereditary effects. Time-dependent stress and strain distributions were calculated for un-notched and notched plates subjected to tensile loading or bending. Yi et al. [35] developed a FE integration procedure for orthotropic materials subjected to mechanical and hygrothermal loading. A recursive viscoelastic exponential series is generated from the time-domain integration of the virtual work with the nonlinear constitutive model. The terms of the integration can be expressed as residual nodal vectors that were stored only for the previous increment. Hilton and Yi [36] presented anisotropic viscoelastic numerical algorithm under a plane stress condition. A set of integral equation is solved by first transformed the equations into Laplace domain. Thus, no direct time integration was performed.

Zocher et al. [37] developed of a numerical algorithm for the solution of the boundary value problem involving orthotropic linear viscoelastic media undergoing thermal and/or mechanical deformation. The proposed FE scheme used an integration point update algorithm. Integral form of constitutive equation involving the relaxation moduli were first transformed into an incremental algebraic form. The relaxation modulus was represented by Prony series in order to derive the recursive relationship and thereby eliminated the storage problem that arises from numerically solving the integral equations. The stress increment was decomposed into a current linearized part and a history part stored from the previous increment. This method was suitable only for linear viscoelastic responses, in which the updated consistent tangent stiffness or

iterative procedure can be avoided. Poon and Ahmad [38]-[39] proposed an integration scheme for stress relaxation that followed Schapery's integral model with strain-based nonlinear functions. This model was applied independently for each of the anisotropic moduli. This explicit constitutive form can be directly integrated to the displacement-based FE environment because it did not require a correction scheme. A consistent tangent operator was calculated at each time increment. However, it is often more difficult to determine the strain based material parameters from experimental tests. Extensive literature reviews on the development of numerical algorithms of viscoelastic materials can be found in Zocher et al. [37]. All available numerical algorithms are developed for the class of TSM, while the ones for a class of TCM are still lacking.

1.2 RESEARCH OBJECTIVES

The present study deals with a time-integration algorithm for predicting nonlinear viscoelastic behaviors of isotropic materials that belong to a class of TCM. For this purpose, the Schapery [6] single integral equation is used and modified. The effects of stress and temperature on the elastic and time-dependent material properties and the loading rate are incorporated, which allow predicting time-dependent responses under general stress-temperature loading histories. The proposed integration algorithm is implemented in general FE code for performing structural analyses. In this study, the integrated material-structural analyses are performed on lap joint structural components having polymeric adhesives under combined thermo-mechanical loadings. Furthermore, the capability of the proposed numerical algorithm in integrating with a

micromechanical model of particle reinforced composites is presented. Experimental data and analytical models available in the literature are used to verify the proposed time- integration algorithm.

Chapter II describes the detailed numerical algorithm for the thermomechanical viscoelastic behavior. The algorithm is derived based on implicit stress integration solutions within a general displacement based FE structural analyses for small deformations and uncoupled thermo-mechanical problems. Previously developed recursive-iterative algorithm for a stress-dependent hereditary integral model (Haj-Ali and Muliana, [32]) is modified to include time-temperature effects. The recurrence formula allows bypassing the need to store entire strain histories at each Gaussian integration point. The linearized strain formulation is used within the recursive approach to give the trial stress solutions. The stress corrector scheme is added to minimize error arising from the linearization. Two types of iterative procedures, which are fixed point (FP) and Newton-Raphson (NR) methods, are examined within the recursive iterative algorithm. Furthermore, a consistent tangent stiffness matrix is formulated to accelerate convergence and avoid divergence at the structural level. Verification of the numerical algorithm is performed using thermo-mechanical viscoelastic experimental data available in the literature. The performance of the recursive-iterative algorithm under multi-axial conditions is also verified with analytical solutions of creep responses of a plate with a hole.

Chapter III deals with implementations of the proposed numerical algorithm in the FE structural analyses. The analysis is presented for lap joints having adhesive polymers

under thermo-mechanical viscoelastic loadings. For this purpose, the nonlinear viscoelastic responses for the adhesive are calibrated using the long term experimental data of Jurf and Vinson [40]. The adherends are made of aluminum with linear elastic material behaviors. The time-dependent behaviors of the lap-joint structural components are then compared with the experimental tests of Jurf and Vinson [40]. Next, FE analyses of time-dependent crack propagation of adhesive bonded joints under several thermo-mechanical loadings are also performed. For this purpose, the recursive-iterative algorithm is coupled with cohesive element models available in ABAQUS FE code [41]. Numerical predictions of crack initiation and complete debonding time for mode I (opening) and II (shearing) failures are presented.

Chapter IV presents the integration of the recursive-iterative algorithm with a micromechanical model of particle reinforced polymers. The composite microstructures are simplified with periodically distributed cubic particles over an infinite polymeric medium in the three dimensional Cartesian coordinate system. The representative volume element (RVE) consists of a single particle embedded in the cubic matrix. Due to the three plane symmetry, one eighth unit-cell model with four particle and polymer subcells is generated. The solid spherical particle is modeled as linear elastic, while the polymer follows nonlinear viscoelastic material responses. The responses of the micromechanical model are compared with the detailed FE unit cell model for different thermo-mechanical loading histories.

Conclusion and future research are given in Chapter V.

CHAPTER II

A TIME INTEGRATION SCHEME FOR TIME-STRESS-TEMPERATURE DEPENDENT BEHAVIORS OF ISOTROPIC MATERIALS

This chapter presents a recursive-iterative algorithm for modeling nonlinear viscoelastic responses of isotropic polymers. The studied polymers belong to a class of thermo-rheologically complex materials (TCM). The algorithm is derived based on implicit stress integration solutions within a general displacement based FE structural analyses for small deformations and uncoupled thermo-mechanical problems. Previously developed recursive-iterative algorithm for a stress-dependent hereditary integral model (Haj-Ali and Muliana [32]) is modified to include time-temperature effects. A consistent tangent stiffness matrix is also formulated to enhance convergence at the structural level. The proposed numerical algorithm is verified using experimental data available in the literature. The capability of the recursive-iterative algorithm in predicting thermo-viscoelastic responses under multi-axial loading conditions is also examined for creep response on a plate with a hole. Finally, the behaviors of the proposed numerical algorithm for TCM are assessed for several thermo-mechanical loading histories.

2.1. A RECURSIVE-ITERATIVE ALGORITHM

A numerical algorithm for stress-temperature dependent viscoelastic behavior of the isotropic polymers is presented in this section. The Schapery [6] nonlinear single integral constitutive model is modified to include the effects of stress and temperature on

time-dependent material responses. Schapery [42] and Sadkin and Aboudi [43] have derived constitutive material model for the TCM that involves two time-scales for representing temperature and stress variations. The use of two time-scales in the constitutive material models makes development of numerical algorithm very challenging and is often impossible to integrate this constitutive material models in general FE structural analyses. In this study, the time-stress-temperature effect on material behaviors is linked to one time scale without any restriction for modeling temperature or stress variations with time. The goal is to develop a numerical algorithm for predicting time-dependent material behaviors under general mechanical and temperature loading histories. The algorithm is derived based on implicit stress integration solutions within a general displacement based FE structural analyses for small deformations and uncoupled thermo-mechanical problems. Linearized solutions of the nonlinear constitutive equations and iterative schemes are performed at the structural (global) and material (local) levels. The purpose of adding iterative schemes is to minimize errors arising from the linearization; otherwise very small time increments are required. It is noted that solving nonlinear responses with small time increments is computationally expensive and often leads to significant mismatch after several incremental steps have been performed due to the accumulated errors.

At each global iteration within the incremental time-step $\Delta t^{(m)}$, trial incremental strain tensor $\Delta\varepsilon_{ij}^{t,(m)}$ and temperature $\Delta T^{t,(m)}$ are obtained, as illustrated in Eq. (2.1). The superscript (m) denotes global iteration counter within the current incremental time step. The goal is to calculate current total stresses $\sigma_{ij}^{t,(m)}$ and material's consistent

tangent stiffness $C_{ijkl}^{t,(m)}$ from given current variables and history variables stored from the previous converged solution at time $(t-\Delta t)$. The converged $C_{ijkl}^{t,(M)}$ after M global iteration at the current time t will be used to provide incremental trial strains for the next time step $(t+\Delta t)$. Due to the uncoupled thermo-mechanical problems, the trial incremental temperature is directly linked to the incremental time step. The procedure in Eq. (2.1) is performed at every material (Gaussian) integration point within elements at each structural iteration to achieve structural and material convergence simultaneously. Thus, an efficient and accurate numerical algorithm for solving the constitutive material model becomes necessary. For simplicity, the superscript (m) that indicates the global iteration counter will be ignored in the rest of this manuscript and the local iteration counter will be denoted by the superscript (k).

$$
\begin{aligned}
&\textit{Given}: \quad \Delta\varepsilon_{ij}^{t,(m)}, \quad \Delta T^{t,(m)}, \quad \Delta t^{(m)} \quad m = \textit{global iteration counter} \\
&\varepsilon_{ij}^{t,(m)} = \varepsilon_{ij}^{t-\Delta t} + \Delta\varepsilon_{ij}^{t,(m)} \\
&T^{t,(m)} = T^{t-\Delta t} + \Delta T^{t,(m)} \\
&t^{(m)} = (t-\Delta t) + \Delta t^{(m)}
\end{aligned}
\tag{2.1}
$$

$$
\begin{aligned}
&\textit{Calculate}: \quad \text{Increamental form} \\
&\sigma_{ij}^{t,(m)} = \sigma_{ij}^{t-\Delta t} + \Delta\sigma_{ij}^{t,(m)} \\
&\Delta\sigma_{ij}^{t,(m)} = f(\sigma_{ij}^{t,(m)}, T^{t,(m)}, \Delta\varepsilon_{ij}^{t,(m)}) \\
&C_{ijkl}^{t,(m)} = \frac{\partial\Delta\sigma_{ij}^{t,(m)}}{\partial\Delta\varepsilon_{ij}^{t,(m)}} \\
&\text{or} \quad \text{Total form} \\
&\sigma_{ij}^{t,(m)} = f(\sigma_{ij}^{t,(m)}, T^{t,(m)}, \varepsilon_{ij}^{t,(m)}) \\
&C_{ijkl}^{t,(m)} = \frac{\partial\sigma_{ij}^{t,(m)}}{\partial\varepsilon_{ij}^{t,(m)}}
\end{aligned}
$$

The Schapery [6] uniaxial stress-strain history relationship is modified for a time-stress-temperature dependent behavior of non-aging materials, which in the time interval [0,t] is written as

$$\varepsilon^t \equiv \varepsilon(t) = g_0(\sigma^t, T^t) D_0 \sigma^t + g_1(\sigma^t, T^t) \int_0^t \Delta D\left(\psi^t - \psi^\tau\right) \frac{d\left[g_2(\sigma^t, T^t)\sigma^t\right]}{d\tau} d\tau + \int_{T_0}^{T^t} \alpha(T^t) \frac{d(T^\tau)}{d\tau} d\tau \tag{2.2}$$

Here D_0 and ΔD are the uniaxial instantaneous elastic and transient compliances, ψ is the reduced-time (effective time) given by:

$$\psi^t \equiv \psi\left(t\right) = \int_0^t \frac{d\xi}{a(\sigma^\xi, T^\xi)} \qquad \psi^\tau \equiv \psi\left(\tau\right) = \int_0^\tau \frac{d\xi}{a(\sigma^\xi, T^\xi)} \tag{2.3}$$

The parameter g_0 measures the reduction or increase in elastic compliance due to stress and temperature. The parameter g_1 measures the nonlinearity effect in the transient compliance. The parameter g_2 accounts for the loading rate effect on the time-dependent response. The parameter $a(\sigma^t, T^t)$ is time shift (interchange) factors measured with respect to the reference stress and temperature. If the thermal effects are carried through the shift factor $a(T^t)$ only, the thermo-rheologically simple material (TSM) is exhibited. The parameters T and T_o are the current and reference temperatures, respectively. The superscript denotes a dependent time variable. In general, the coefficient of thermal expansion α is a material and temperature dependent; however

α for solid material at temperature ranges: ambient temperature to the material's service limit temperature is often assumed to be constant.

The uniaxial viscoelastic behavior in Eq. (2.2) is generalized for multiaxial (3D) constitutive relations of isotropic materials by separating the deviatoric and volumetric strain-stress relations and thermal strains as:

$$\begin{aligned}
\varepsilon_{ij}^{t} &= e_{ij}^{t} + \frac{1}{3}\varepsilon_{kk}^{t}\delta_{ij} + \alpha\left(T^{t} - T_{0}\right)\delta_{ij} \\
e_{ij}^{t} &= \frac{1}{2}g_{0}(\bar{\sigma}^{t}, T^{t})J_{0}S_{ij}^{t} + \frac{1}{2}g_{1}(\bar{\sigma}^{t}, T^{t})\int_{0}^{t}\Delta J\left(\psi^{t} - \psi^{\tau}\right)\frac{d\left[g_{2}(\bar{\sigma}^{\tau}, T^{\tau})S_{ij}^{\tau}\right]}{d\tau}d\tau \\
\varepsilon_{kk}^{t} &= \frac{1}{3}g_{0}(\bar{\sigma}^{t}, T^{t})B_{0}\sigma_{kk}^{t} + \frac{1}{3}g_{1}(\bar{\sigma}^{t}, T^{t})\int_{0}^{t}\Delta B\left(\psi^{t} - \psi^{\tau}\right)\frac{d\left[g_{2}(\bar{\sigma}^{\tau}, T^{\tau})\sigma_{kk}^{\tau}\right]}{d\tau}d\tau
\end{aligned} \tag{2.4}$$

The parameters J_0 and B_0 are instantaneous elastic shear and bulk compliances, respectively. The terms ΔJ and ΔB are the time-dependent shear and bulk compliances, respectively. A series of exponential functions (Prony series) is used for the transient part due to the advantage of this representation in solving the integral form in Eq (2.4) recursively. The nonlinear parameters of the multi-axial behaviors are modeled as a function of current effective stress $\bar{\sigma}^{t}$ and temperature T^{t}. The matrix Poisson's ratio, υ, is assumed to be time independent, which allows expressing the shear and bulk compliances as:

$$\begin{aligned}
J_{0} &= 2(1+\upsilon)D_{0} & B_{0} &= 3(1-2\upsilon)D_{0} \\
\Delta J^{\psi^{t}} &= 2(1+\upsilon)\Delta D^{\psi^{t}} & \Delta B^{\psi^{t}} &= 3(1-2\upsilon)\Delta D^{\psi^{t}}
\end{aligned} \tag{2.5}$$

Where the uniaxial transient compliance is expressed as:

$$\Delta D^{\psi^t} = \sum_{n=1}^{N} D_n \left(1 - \exp[-\lambda_n \psi^t]\right) \tag{2.6}$$

For simplicity, the nonlinear stress and temperature dependent material parameters will be written as:

$$\begin{aligned} & g_\beta(\bar{\sigma}^t, T^t) = g_\beta^t, \qquad \beta = 0,1,2 \\ & a\ (\bar{\sigma}^t, T^t) = a^t \\ & \bar{\sigma}^t = \sqrt{\frac{3}{2} S_{ij}^t S_{ij}^t} \end{aligned} \tag{2.7}$$

Using the Eqs. (2.5) and (2.6), the deviatoric and volumetric strains in Eq. (2.4) can be written as:

$$\begin{aligned} & e_{ij}^t = \frac{1}{2} g_0^t J_0 S_{ij}^t + \frac{1}{2} g_1^t g_2^t S_{ij}^t \sum_{n=1}^{N} J_n - \frac{1}{2} g_1^t \sum_{n=1}^{N} J_n q_{ij,n}^t \\ & where\ \ q_{ij,n}^t = \int_0^t \exp\left[-\lambda_n \left(\psi^t - \psi^\tau\right)\right] \frac{d\left(g_2^\tau S_{ij}^\tau\right)}{d\tau} d\tau \end{aligned} \tag{2.8}$$

$$\begin{aligned} & \varepsilon_{kk}^t = \frac{1}{3} g_0^t B_0 \sigma_{kk}^t + \frac{1}{3} g_1^t g_2^t \sigma_{kk}^t \sum_{n=1}^{N} B_n - \frac{1}{3} g_1^t \sum_{n=1}^{N} B_n q_{kk,n}^t \\ & where\ \ q_{kk,n}^t = \int_0^t \exp\left[-\lambda_n \left(\psi^t - \psi^\tau\right)\right] \frac{d\left(g_2^\tau \sigma_{kk}^\tau\right)}{d\tau} d\tau \end{aligned} \tag{2.9}$$

A recursive integration method, which was derived by Taylor et. al. [28] for linear viscoelastic integral model and extended by Haj-Ali and Muliana [32] for nonlinear stress-dependent viscoelastic constitutive model, is performed to solve the integral parts in Eqs. (2.8) and (2.9). A recursive method allows for developing incremental formulation and integration of the current stress state based on the given time, strain, and temperature increments and the history variables stored at the previous time step. Thus the hereditary integrals in Eqs. (2.8) and (2.9) are expressed as:

$$\begin{aligned} q_{ij,n}^{t} &= \int_{0}^{t-\Delta t} \exp\left[-\lambda_n\left(\psi^t-\psi^\tau\right)\right]\frac{d\left(g_2^\tau S_{ij}^\tau\right)}{d\tau}d\tau + \int_{t-\Delta t}^{t} \exp\left[-\lambda_n\left(\psi^t-\psi^\tau\right)\right]\frac{d\left(g_2^\tau S_{ij}^\tau\right)}{d\tau}d\tau \\ &= \exp[-\lambda_n\Delta\psi^t]q_{ij,n}^{t-\Delta t} + \left(g_2^t S_{ij}^t - g_2^{t-\Delta t}S_{ij}^{t-\Delta t}\right)\frac{1-\exp[-\lambda_n\Delta\psi^t]}{\lambda_n\Delta\psi^t} \end{aligned} \tag{2.10}$$

$$\begin{aligned} q_{kk,n}^{t} &= \int_{0}^{t-\Delta t} \exp\left[-\lambda_n\left(\psi^t-\psi^\tau\right)\right]\frac{d\left(g_2^\tau \sigma_{kk}^\tau\right)}{d\tau}d\tau + \int_{t-\Delta t}^{t} \exp\left[-\lambda_n\left(\psi^t-\psi^\tau\right)\right]\frac{d\left(g_2^\tau \sigma_{kk}^\tau\right)}{d\tau}d\tau \\ &= \exp[-\lambda_n\Delta\psi^t]q_{kk,n}^{t-\Delta t} + \left(g_2^t \sigma_{kk}^t - g_2^{t-\Delta t}\sigma_{kk}^{t-\Delta t}\right)\frac{1-\exp[-\lambda_n\Delta\psi^t]}{\lambda_n\Delta\psi^t} \end{aligned} \tag{2.11}$$

The first integral part includes the limits (0, t-Δt), i.e. up to the previous converged time step, which is stored as history variables of the hereditary strain integral. The limits of the second part are taken as (t-Δt , t), which is the current incremental step. The parameters $q_{ij,n}^{t-\Delta t}$ and $q_{kk,n}^{t-\Delta t}$, n=1..N are the hereditary integral for every term in the Prony series in the form of deviatoric and volumetric strains. These parameters are history

state variables stored from the last converged step at time (t-Δt). Total number of history variables is 7xNxN_{Gauss}; where 7 is the total number of deviatoric and volumetric components, N is the number of terms in the Prony series, and N_{Gauss} is the number of Gaussian integration points. The incremental reduced time is expressed as $\Delta\psi^t \equiv \psi^t - \psi^{t-\Delta t}$. Substituting the integral equations (2.10) and (2.11) into Eqs. (2.8) and (2.9) gives the deviatoric and volumetric total strains:

$$
\begin{aligned}
e_{ij}^t &= \frac{1}{2}\left[g_0^t J_0 + g_1^t g_2^t \sum_{n=1}^{N} J_n - g_1^t g_2^t \sum_{n=1}^{N} J_n \frac{1-\exp[-\lambda_n \Delta\psi^t]}{\lambda_n \Delta\psi^t} \right] S_{ij}^t \\
&- \frac{1}{2} g_1^t \sum_{n=1}^{N} J_n \left[\exp[-\lambda_n \Delta\psi^t] q_{ij,n}^{t-\Delta t} - g_2^{t-\Delta t} \frac{1-\exp[-\lambda_n \Delta\psi^t]}{\lambda_n \Delta\psi^t} S_{ij}^{t-\Delta t} \right] \\
e_{ij}^t &= \overline{J}^t S_{ij}^t - d_{ij}^t
\end{aligned}
\tag{2.12}
$$

$$
\begin{aligned}
\varepsilon_{kk}^t &= \frac{1}{3}\left[g_0^t B_0 + g_1^t g_2^t \sum_{n=1}^{N} B_n - g_1^t g_2^t \sum_{n=1}^{N} B_n \frac{1-\exp[-\lambda_n \Delta\psi^t]}{\lambda_n \Delta\psi^t} \right] \sigma_{kk}^t \\
&- \frac{1}{3} g_1^t \sum_{n=1}^{N} B_n \left[\exp[-\lambda_n \Delta\psi^t] q_{kk,n}^{t-\Delta t} - g_2^{t-\Delta t} \frac{1-\exp[-\lambda_n \Delta\psi^t]}{\lambda_n \Delta\psi^t} \sigma_{kk}^{t-\Delta t} \right] \\
\varepsilon_{kk}^t &= \overline{B}^t \sigma_{kk}^t - V_{kk}^t
\end{aligned}
\tag{2.13}
$$

The incremental forms of the deviatoric and volumetric strains are:

$$
\begin{aligned}
\Delta e_{ij}^t &= e_{ij}^t - e_{ij}^{t-\Delta t} \\
&= \overline{J}^t S_{ij}^t - \overline{J}^{t-\Delta t} S_{ij}^{t-\Delta t} - \frac{1}{2} \sum_{n=1}^{N} J_n (g_1^t \exp[-\lambda_n \Delta\psi^t] - g_1^{t-\Delta t}) q_{ij,n}^{t-\Delta t} - \\
&\frac{1}{2} g_2^{t-\Delta t} \sum_{n=1}^{N} J_n \left[g_1^{t-\Delta t} \left(\frac{1-\exp[-\lambda_n \Delta\psi^{t-\Delta t}]}{\lambda_n \Delta\psi^{t-\Delta t}} \right) - g_1^t \left(\frac{1-\exp[-\lambda_n \Delta\psi^t]}{\lambda_n \Delta\psi^t} \right) \right] S_{ij}^{t-\Delta t}
\end{aligned}
\tag{2.14}
$$

$$\Delta\varepsilon_{kk}^{t} = \varepsilon_{kk}^{t} - \varepsilon_{kk}^{t-\Delta t}$$
$$= \overline{B}^{t}\sigma_{kk}^{t} - \overline{B}^{t-\Delta t}\sigma_{kk}^{t-\Delta t} - \frac{1}{3}\sum_{n=1}^{N} B_n (g_1^t \exp[-\lambda_n \Delta\psi^t] - g_1^{t-\Delta t}) q_{kk,n}^{t-\Delta t} - \tag{2.15}$$
$$\frac{1}{2} g_2^{t-\Delta t} \sum_{n=1}^{N} B_n \left[g_1^{t-\Delta t} \left(\frac{1-\exp[-\lambda_n \Delta\psi^{t-\Delta t}]}{\lambda_n \Delta\psi^{t-\Delta t}} \right) - g_1^{t} \left(\frac{1-\exp[-\lambda_n \Delta\psi^{t}]}{\lambda_n \Delta\psi^{t}} \right) \right] \sigma_{kk}^{t-\Delta t}$$

Equations (2.12)-(2.13) and (2.14)-(2.15) define complete solutions for the current total and incremental strain tensors, respectively. The nonlinear parameters in Eqs. (2.12) - (2.13) and (2.14)-(2.15) are expressed as functions of current temperature and total stresses, which at the current time (t) are not known. Linearized trial stress tensors are used as starting points for solving the stress tensor using Eqs. (2.12)- (2.13) or (2.14)-(2.15). Therefore, an iterative scheme is needed in order to find the correct stress tensor. The chosen trial values (initial approximation solutions) and iterative method can significantly determine the convergence solutions. Poor initial approximation values often lead to divergence.

Two iterative methods within the recursive algorithm, which is used to solve the integral in Eq. (2.4), are presented within the procedure in Eq. (2.1). The first iterative method is using a Fixed Point (FP) method to directly satisfy the equilibrium conditions in Eq. (2.1). The FP method gives slower convergence rate but require less computational effort during each iteration step. The second iterative method is the Newton-Raphson's (NR) method, which approximates a complicated function with a linear tangent function to satisfy equilibrium conditions locally. The NR's method can increase convergent process rapidly, however, linearized tangent functions often lead to

divergence solutions if during the iteration process the convergence is not monotonic or if the magnitude of the tangent functions is very small (approaching zero).

2.1.1 FIXED POINT (FP) METHOD

The iteration procedure to find a solution for x that satisfies x=f(x) using the FP method is summarized as:

$$\begin{aligned} &x^{k+1} = f(x^{(k)}) \\ &R = \| x^{k+1} - x^{(k)} \| \\ &\textit{Converged solutions}: R \to 0 \end{aligned} \tag{2.16}$$

Where k indicates the local iteration counter with an initial approximation solution $x^{(0)}$ and R is the measured error. The current stresses, which follows the form of Eq. (2.16), can be obtained either using Eqs. (2.12)-(2.13) or (2.14)-(2.15). Thus, current stress tensor at the iteration k from a given total strain tensor are written as:

$$\begin{aligned} \sigma_{ij}^{t} &= S_{ij}^{t} + \frac{1}{3}\sigma_{kk}^{t}\delta_{ij} \\ &= \frac{1}{\bar{J}^{t}}\left[e_{ij}^{t} + \frac{1}{2} g_1^{t} \sum_{n=1}^{N} J_n \left[\exp[-\lambda_n \Delta\psi^{t}] q_{ij,n}^{t-\Delta t} - g_2^{t-\Delta t} \frac{1-\exp[-\lambda_n \Delta\psi^{t}]}{\lambda_n \Delta\psi^{t}} S_{ij}^{t-\Delta t} \right] \right] \\ &+ \frac{1}{3\bar{B}^{t}}\left[\varepsilon_{kk}^{t} + \frac{1}{3} g_1^{t} \sum_{n=1}^{N} B_n \left[\exp[-\lambda_n \Delta\psi^{t}] q_{kk,n}^{t-\Delta t} - g_2^{t-\Delta t} \frac{1-\exp[-\lambda_n \Delta\psi^{t}]}{\lambda_n \Delta\psi^{t}} \sigma_{kk}^{t-\Delta t} \right] \right] \delta_{ij} \end{aligned} \tag{2.17}$$

The effective shear $\bar{J}^{t}$ and bulk $\bar{B}^{t}$ compliances and the nonlinear parameters in the Eq. (2.17) are functions of the current effective stresses $\bar{\sigma}^{t}$ and temperatures T^{t}. The current temperature is defined by $T^{t} = T^{t-\Delta t} + \Delta T^{t}$. The current deviatoric and

volumetric strains $e_{ij}^{t} \equiv e_{ij}^{t,m}$ and $\varepsilon_{kk}^{t} \equiv \varepsilon_{kk}^{t,m}$ are obtained from the structural level at Mth global iteration. The initial approximation (trial) stress tensor is determined using the following approximation of nonlinear parameters:

$$\begin{aligned} g_{\beta}^{t,tr} &= g_{\beta}^{t,(0)} = g_{\beta}(\bar{\sigma}^{t-\Delta t}, T^{t-\Delta t}), \qquad \beta = 0,1,2 \\ a^{t,tr} &= a^{t,(0)} = a\ (\bar{\sigma}^{t-\Delta t}, T^{t-\Delta t}) \end{aligned} \tag{2.18}$$

The trial current stress tensor is formed based on the given variables and history variables from the previous converged step:

$$\begin{aligned} \sigma_{ij}^{t,tr} &= \sigma_{ij}^{t-\Delta t} + \Delta\sigma_{ij}^{t,tr} \\ \Delta\sigma_{ij}^{t,tr} &= \Delta S_{ij}^{t,tr} + \frac{1}{3}\Delta\sigma_{kk}^{t,tr}\delta_{ij} \end{aligned} \tag{2.19}$$

Where the trial incremental deviatoric and volumetric stresses are given by:

$$\begin{aligned} \Delta S_{ij}^{t,tr} &= \frac{1}{\bar{J}^{t,tr}}\left[\Delta e_{ij}^{t} + \frac{1}{2} g_1^{t,tr}\sum_{n=1}^{N} J_n(\exp[-\lambda_n \Delta\psi^{t}]-1) q_{ij,n}^{t-\Delta t}\right] \\ \Delta\sigma_{kk}^{t,tr} &= \frac{1}{\bar{B}^{t,tr}}\left[\Delta\varepsilon_{kk}^{t} + \frac{1}{3} g_1^{t,tr}\sum_{n=1}^{N} B_n(\exp[-\lambda_n \Delta\psi^{t}]-1) q_{kk,n}^{t-\Delta t}\right] \end{aligned} \tag{2.20}$$

During the local iteration, the residual tensor is expressed in terms of the total stress tensor:

$$R_{ij}^{t,(k+1)} = \sigma_{ij}^{t,(k+1)} - \sigma_{ij}^{t,k} \tag{2.21}$$

and the nonlinear parameters in Eq. (2.17) is defined by $g_\beta^{t,k} = g_\beta(\bar{\sigma}^{t,(k)}, T^t)$ and $a^{t,(k)} = a(\bar{\sigma}^{t,(k)}, T^t)$. Once convergence is achieved, the consistent tangent stiffness matrix in Eq. (2.22), the current stress tensor, and history variables in Eqs. (2.10) and (2.11) are updated and sent to the structural level. If coupled thermo-mechanical problems are considered, it is also necessary to determine $\frac{\partial \sigma_{ij}^t}{\partial T^t}$ tensor. The consistent tangent stiffness is expressed by:

$$C_{ijkl}{}^{t} = \frac{\partial \sigma_{ij}{}^{t}}{\partial \varepsilon_{kl}{}^{t}} = \frac{1}{\bar{J}^t}\delta_{ik}\delta_{jl} + \frac{1}{3}\left[\frac{1}{\bar{B}^t} - \frac{1}{\bar{J}^t}\right]\delta_{ij} \tag{2.22}$$

2.1.2 NEWTON-RAPHSON'S (NR) METHOD

The iterative procedure using the NR's method to find a solution of x that satisfies F(x) =0 is summarized as:

$$x^{k+1} = x^k - \frac{F(x^k)}{F'(x^k)}$$

$$F'(x) = \frac{dF(x)}{dx}$$

$$converged\ \ solutions: \ R \to F \to 0 \tag{2.23}$$

This procedure requires that F(x) and F'(x) are continuous near the solution x and the magnitude of F'(x) should not be very small. In this study, an iterative scheme is

developed in order to achieve the correct stress state for a given strain tensor. The residual tensor can be defined by using either the incremental strains or total strains. The component of residual mechanical strain tensor is expressed by:

$$R_{ij}^{t,(k)} = \Delta e_{ij}^{t,(k)} + \frac{1}{3}\Delta \varepsilon_{kk}^{t,(k)}\delta_{ij} - \Delta \varepsilon_{ij}^{t} \tag{2.24}$$

The incremental deviatoric and volumetric strain tensors at iteration k are defined using Eqs. (2.14)-(2.15). The current incremental strains $\Delta \varepsilon_{ij}^{t} \equiv \Delta \varepsilon_{ij}^{t,m}$ are obtained from the structural level at the m^{th} global iteration. The initial approximation (trial) stress tensor is determined using Eqs. (2.18)-(2.20). A Jacobian tensor, which in the uniaxial case is F'(x), is formed by taking the derivative of the residual tensor in Eq. (2.24) with respect to the incremental stress tensor as:

$$\frac{\partial R_{ij}{}^{t}}{\partial \Delta\sigma_{kl}{}^{t}} = \bar{J}^{t}\delta_{ik}\delta_{jl} + \frac{1}{3}\left(\bar{B}^{t} - \bar{J}^{t}\right)\delta_{ij}\delta_{kl}$$

$$+\frac{\partial \Delta\bar{\sigma}^{t}}{\partial \Delta\sigma_{kl}{}^{t}}\left\{\begin{array}{l} \dfrac{\partial \bar{J}^{t}}{\partial \Delta\bar{\sigma}^{t}}\sigma_{ij}{}^{t} + \dfrac{1}{3}\left(\dfrac{\partial \bar{B}^{t}}{\partial \Delta\bar{\sigma}^{t}} - \dfrac{\partial \bar{J}^{t}}{\partial \Delta\bar{\sigma}^{t}}\right)\sigma_{kk}{}^{t}\delta_{ij} - \\ \dfrac{1}{2}\dfrac{\partial g_1{}^{t}}{\partial \Delta\bar{\sigma}^{t}}\displaystyle\sum_{n=1}^{N} J_n\left[exp[-\lambda_n\Delta\psi^{t}]q_{ij,n}^{t-\Delta t} - g_2^{t-\Delta t}\left(\dfrac{1-exp[-\lambda_n\Delta\psi^{t}]}{\lambda_n\Delta\psi^{t}}\right)S_{ij}{}^{t-\Delta t}\right] - \\ \dfrac{1}{2}\dfrac{\partial a_{\sigma}{}^{t}}{\partial \Delta\bar{\sigma}^{t}}g_1{}^{t}\displaystyle\sum_{n=1}^{N} J_n\left[\begin{array}{l} exp[-\lambda_n\Delta\psi^{t}]\left(\dfrac{\lambda_n\Delta t q_{ij,n}{}^{t-\Delta t}}{a_{\sigma}{}^{t2}} + \dfrac{S_{ij}{}^{t-\Delta t}}{a_{\sigma}{}^{t}}\right) - \\ g_2{}^{t-\Delta t}\left(\dfrac{1-exp[-\lambda_n\Delta\psi^{t}]}{\lambda_n\Delta\psi^{t}}\right)S_{ij}{}^{t-\Delta t} \end{array}\right] \end{array}\right\}$$

$$-\frac{\partial \Delta\bar{\sigma}^{t}}{\partial \Delta\sigma_{kl}{}^{t}}\left\{\begin{array}{l} \dfrac{1}{9}\dfrac{\partial g_1{}^{t}}{\partial \Delta\bar{\sigma}^{t}}\displaystyle\sum_{n=1}^{N} B_n\left[exp[-\lambda_n\Delta\psi^{t}]q_{kk,n}^{t-\Delta t} - g_2^{t-\Delta t}\left(\dfrac{1-exp[-\lambda_n\Delta\psi^{t}]}{\lambda_n\Delta\psi^{t}}\right)\sigma_{kk}{}^{t-\Delta t}\right]\delta_{ij} - \\ \dfrac{1}{9}\dfrac{\partial a_{\sigma}{}^{t}}{\partial \Delta\bar{\sigma}^{t}}g_1{}^{t}\displaystyle\sum_{n=1}^{N} B_n\left[\begin{array}{l} exp[-\lambda_n\Delta\psi^{t}]\left(\dfrac{\lambda_n\Delta t q_{kk,n}{}^{t-\Delta t}}{a_{\sigma}{}^{t2}} + \dfrac{\sigma_{kk}{}^{t-\Delta t}}{a_{\sigma}{}^{t}}\right) - \\ g_2{}^{t-\Delta t}\left(\dfrac{1-exp[-\lambda_n\Delta\psi^{t}]}{\lambda_n\Delta\psi^{t}}\right)\sigma_{kk}{}^{t-\Delta t} \end{array}\right]\delta_{ij} \end{array}\right\} \quad (2.25)$$

Where $$\frac{\partial \Delta\bar{\sigma}^{t}}{\partial \Delta\sigma_{kl}{}^{t}} = \frac{3}{2}\frac{S_{ij}{}^{t}}{\Delta\sigma^{t}}\left(\delta_{ik}\delta_{jl} - \frac{1}{3}\delta_{ij}\delta_{kl}\right)$$

Next, the consistent tangent stiffness matrix is defined by taking the inverse of the partial derivative of the incremental strain with respect to the incremental stress at the end of the current time step. Using Eq. (2.25), the consistent tangent stiffness, $C_{ijkl}{}^{t}$, at the converged state is:

$$C_{ijkl}{}^{t} \equiv \frac{\partial \Delta\sigma_{ij}{}^{t}}{\partial \Delta\varepsilon_{kl}{}^{t}} = \left[\frac{\partial R_{ij}{}^{t}}{\partial \Delta\sigma_{kl}{}^{t}} \right]^{-1} ; R_{ij}{}^{t} \to 0 \tag{2.26}$$

Once convergence has been achieved, the stress and the hereditary integrals for each Prony series are calculated and stored for next time step integration. The complete numerical algorithm, which is used to provide the correct stress and its corresponding nonlinear parameters for a given strain increment, is presented in the following steps.

1 Input variables: (At the mth global iteration)

$\varepsilon_{ij}^{t-\Delta t}$, $\Delta\varepsilon_{ij}^{t,(m)}$, $\Delta t^{(m)}, \Delta T^{t,(m)}$

History : $\sigma_{ij}^{t-\Delta t}, T^{t-\Delta t}$, $q_{ij,n}^{t-\Delta t}$, $q_{kk,n}^{t-\Delta t}$

2 Initial approximation variables:

$g_{\beta}^{t,tr} = g_{\beta}(\bar{\sigma}^{t-\Delta t}, T^{t-\Delta t}); \beta = 0,1,2 \qquad a^{t,tr} = a\ (\bar{\sigma}^{t-\Delta t}, T^{t-\Delta t})$

$\overline{J}^{t,tr} = \overline{J}^{t}\ (g_{\beta}^{t,tr}, a^{t,tr}) \qquad \overline{B}^{t,tr} = \overline{B}^{t}\ (g_{\beta}^{t,tr}, a^{t,tr})$

$\Delta\sigma_{ij}^{t,tr} = \Delta\sigma_{ij}^{t,tr}(\Delta S_{ij}^{t,tr}, \Delta\sigma_{kk}^{t,tr}) \qquad \sigma_{ij}^{t,(0)} = \sigma_{ij}^{t-\Delta t} + \Delta\sigma_{ij}^{t,tr}$

3 Iterate for k=0,1,2,3... (k=local iteration counter)

3.1 Compute nonlinear parameters:

$g_{\beta}^{t,(k)} = g_{\beta}(\bar{\sigma}^{t,(k)}, T^{t,(m)}); \ \beta = 0,1,2 \qquad a^{t,(k)} = a\ (\bar{\sigma}^{t,(k)}, T^{t,(m)})$

where $T^{t,(m)} = T^{t-\Delta t} + \Delta T^{t,(m)}$

3.2 Compute current stress:

(i) FP method:

$\sigma_{ij}^{t,(k+1)} = f(\sigma_{ij}^{t,(k)}, \varepsilon_{ij}^{t,(m)}, T^{t,(m)}),$ *where* $\varepsilon_{ij}^{t,(m)} = \varepsilon_{ij}^{t-\Delta t} + \Delta\varepsilon_{ij}^{t,(m)}$

(ii) NR method:

$$\Delta\sigma_{ij}^{t,(k+1)} = \Delta\sigma_{ij}^{t,(k)} + \left[\frac{\partial R_{ij}^{t,(k)}}{\partial \Delta\sigma_{kl}}\right]^{-1} R_{kl}^{t,(k)} \qquad \sigma_{ij}^{t,(k+1)} = \sigma_{ij}^{t-\Delta t} + \Delta\sigma_{ij}^{t,(k+1)}$$

3.3 Evaluate residual tensor:

(i) FP method: $R_{ij}^{t,(k+1)} = \sigma_{ij}^{t,(k+1)} - \sigma_{ij}^{t,(k)}$

(ii) NR method: $R_{ij}^{t,(k+1)} = \Delta e_{ij}^{t,(k+1)} + \frac{1}{3}\delta_{ij}\Delta\varepsilon_{kk}^{t,(k+1)} - \Delta\varepsilon_{ij}^{t,(m)}$

IF $\| R_{ij}^{t,(k+1)} \| \leq$ Tol THEN GOTO 4 and EXIT

ENDIF GOTO 3

4. Update stress, consistent tangent stiffness, and history variables:

$\sigma_{ij}^{t,(k+1)} \rightarrow \sigma_{ij}^{t}$, C_{ijkl}^{t} , $q_{ij,n}^{t,(k+1)} \rightarrow q_{ij,n}^{t}$, $q_{kk,n}^{t,(k+1)} \rightarrow q_{kk,n}^{t}$

2.2 NUMERICAL IMPLEMENTATION AND VERIFICATION

The above numerical algorithm of thermo-mechanical viscoelastic constitutive model is implemented at each material point (Gaussian integration point) within the 3D continuum elements. The material subroutine (UMAT) of the ABAQUS [41] FE code is used. The 3D nonlinear viscoelastic material response can also be integrated with other typed of elements e.g: 1D (truss, beam) or 2D (plane stress, plane strain) by imposing uniaxial or in-plane stress-strain relations to the 3D constitutive model. Verification is performed with the thermo-mechanical viscoelastic experimental data available in the literature. Test data on FM73 adhesive polymers reported by Peretz and Weitsman [11]-[12] and epoxy Hercules 3502 of Harper and Weitsman [13] are used. The proposed

integration algorithm is also examined in terms of computational efficiency and accuracy.

2.2.1 VISCOELASTIC RESPONSES OF FM73 ADHESIVE POLYMERS

The efficiency and accuracy of the recursive-iterative algorithm with the fixed point (FP) and Newton Raphson (NR) iterative schemes are first examined using the thermo-mechanical viscoelastic tests on FM73 adhesive. Peretz and Weitsman [11]-[12] performed 15 minutes creep followed by 15 minutes recovery tests on FM73 adhesive under various uniaxial stresses: 10-30 MPa and temperatures: 30-60^{o}C. The Schapery [6] single integral model was used to represent the thermo-mechanical viscoelastic behaviors. The calibrated time-dependent parameters (Prony series) and elastic properties for FM73 adhesive are given in Table 2.1. From the experimental results, Peretz and Weitsman [11]-[12] have established that the nonlinear stress and temperature dependent material parameters for the FM73 adhesive, which were calibrated from the creep-recovery tests, can be fitted using the following functions:

$$g_0 = \left(1 + 0.15\frac{\sigma}{50}\right)\left(1 + 0.91\frac{T - T_0}{T_0}\right)$$

$$g_1 = \left(1 + 1.435\left(\frac{\sigma}{50}\right)^{2.4}\right)\left(exp\left[-8.5\frac{T - T_0}{T_0}\right]\right)$$

$$g_2 = \left(1 + 0.75\left(\frac{\sigma}{50}\right)^{2}\right)\left(exp\left[12.12\frac{T - T_0}{T_0}\right]\right)$$

$$a = exp\left[-1.75\frac{\sigma}{50} - 40\frac{T - T_0}{T_0}\right] \tag{2.27}$$

Where T_0 is the reference temperature, which is 303 K; the stress σ and temperature T are in MPa and Kelvin, respectively.

Table 2.1. Elastic properties and Prony series coefficients for the FM73 adhesive polymer.

n	$\lambda_n(\sec^{-1})$	$D_n \times 10^{-6}(MPa^{-1})$
1	1	21.00
2	10^{-1}	21.60
3	10^{-2}	11.84
4	10^{-3}	15.88
5	10^{-4}	21.58
6	10^{-5}	20.05
$E = 2710\,MPa$		$\nu = 0.35$

Convergence behaviors using the FP and NR methods are presented with linear ramp and creep loadings. Figure 2.1 illustrates nonlinear elastic responses under a linear stress and temperature ramp loading. The nonlinear responses are generated from the recursive algorithm with the FP and NR iterative methods. Iteration processes are performed both

at the material and structural levels. Iteration procedures at the material level from the FP and NR methods are monitored at two stress levels: 30 and 40 MPa, as shown in Fig. 2.2. It is seen that the NR method gives faster convergent solutions at the material level in terms of iteration numbers than the ones using FP method, while at the structural level both methods require two iterations. The total CPU time required to complete the above job using the NR and FP methods are 3.68 and 3.75 seconds, respectively. Even with less number of iteration, the NR method reduces only 2% CPU time. This is due to more computational efforts, which require calculating the residual strain tensor, the derivative of the residual tensor and its inverse, are needed in using the NR method.

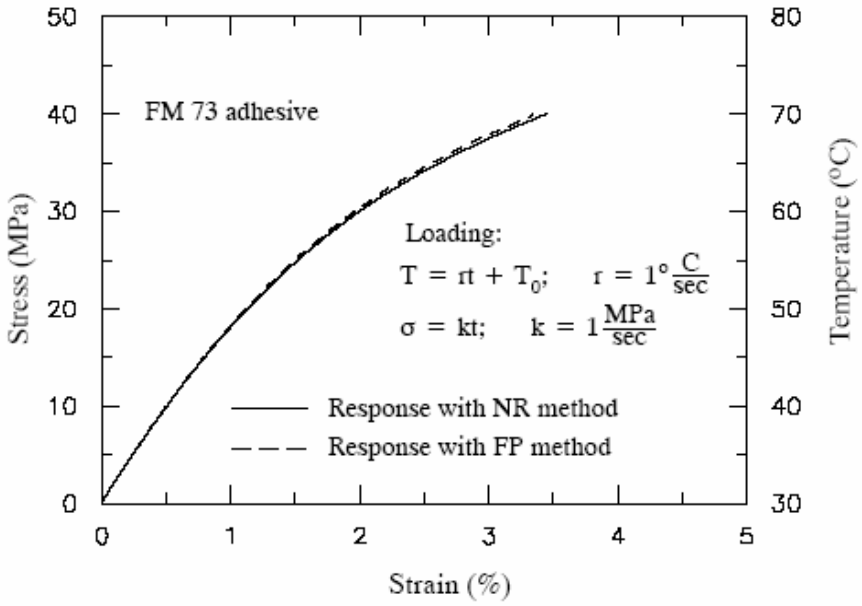

Figure 2.1. Stress--strain responses on FM73 adhesive under stress and temperature ramp loading using the recursive algorithm with the Newton Raphson (NR) and Fixed Point (FP) iterative methods.

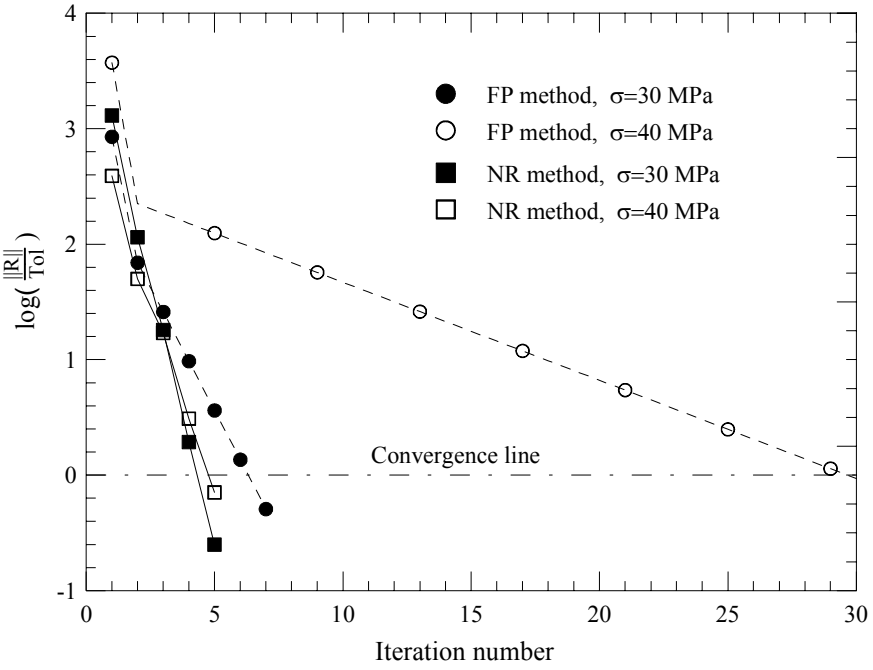

Figure 2.2. Residual at the material level from ramp loading using the NR and FP methods.

Convergence behaviors of the NR and FP methods are also presented for creep loading under constant stress (30 MPa) and temperature (60^{o}C), shown in Fig. 2.3. The responses under these load and temperature show high nonlinear behaviors. Figure 2.4 illustrates iteration processes at the material levels during the initial and final creep tests. Total CPU time using the NR and FP methods are 4.64 and 5.3 seconds, respectively. The NR method gives more efficient solutions provided that the residual function is continuous; its derivative exists; and is nonsingular within the loading range.

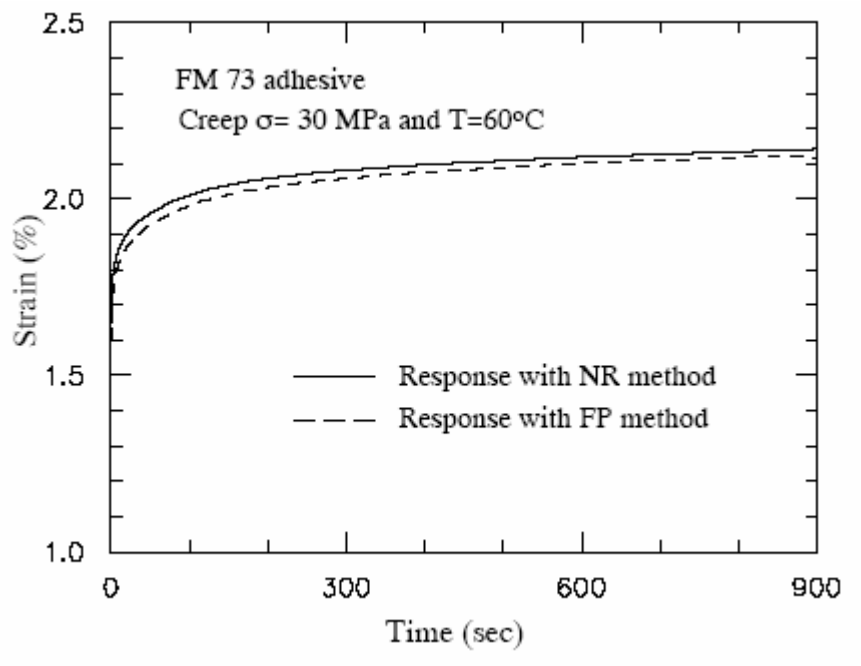

Figure 2.3 Creep strain responses on FM73 adhesive using the recursive algorithm with the NR and FP iteration methods.

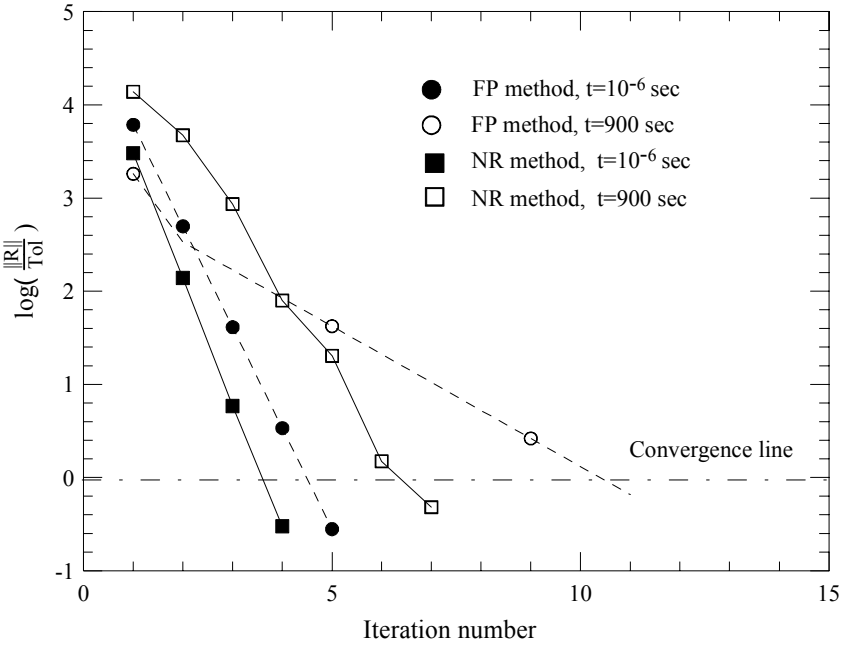

Figure 2.4 Residual at the material level from creep loading using the NR and FP methods.

The time-dependent responses from the recursive-iterative algorithm are verified using available experimental data for several thermo-mechanical loading histories. Figures 2.5 and 2.6 show creep and stress-strain responses for the FM73 adhesive under stress and temperature loading history illustrated in the figures. Both NR and FP iterative methods are used and compared with the experimental data. Good predictions are shown. The rest of this study will use recursive algorithm with the NR iterative method.

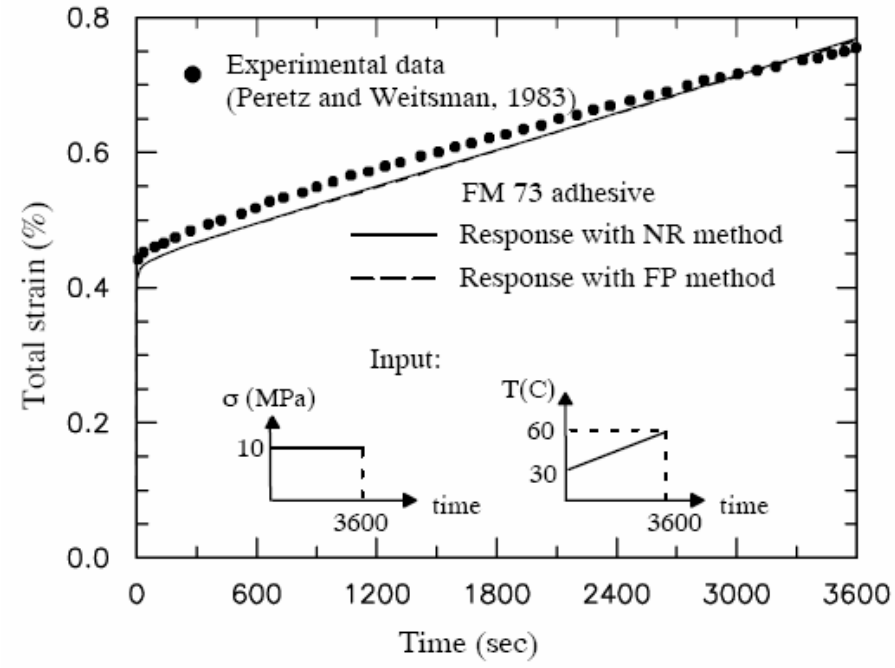

Figure 2.5 Creep strain responses under linear temperature ramp and fixed stress.

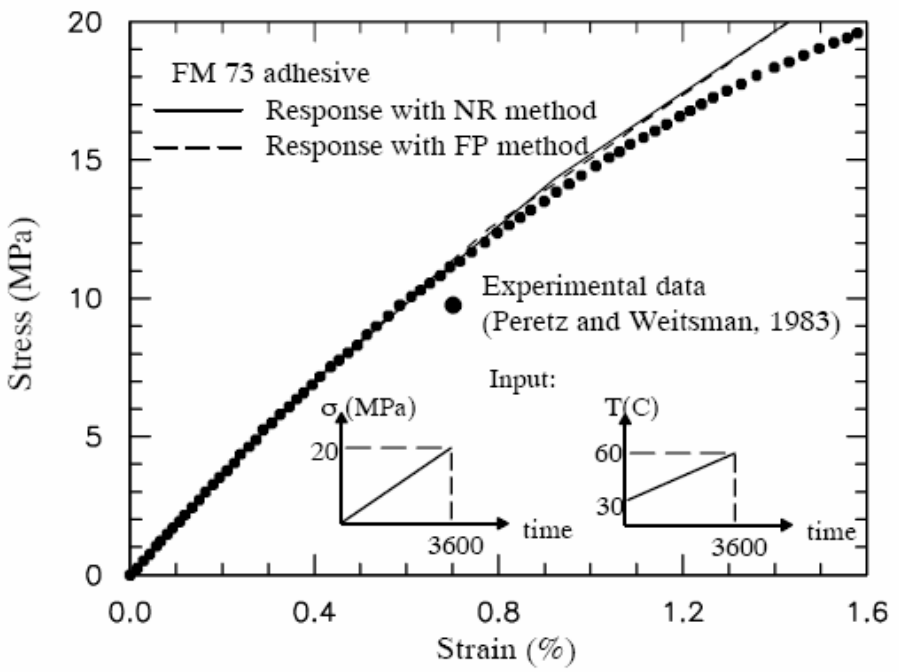

Figure 2.6 Stress-strain responses under linear stress and temperature ramp.

Prediction of Creep strains responses for the FM 73 adhesive under several load levels and temperatures are illustrated in Fig. 2.7. Good predictions are shown for all cases. Figures 2.8 and 2.9 present strain predictions of temperature and stress recovery, respectively. The temperature recovery tests were performed by reducing the testing temperature to the reference temperature at the constant load. The stress recovery tests were performed by removing the applied stresses at the fix temperature.

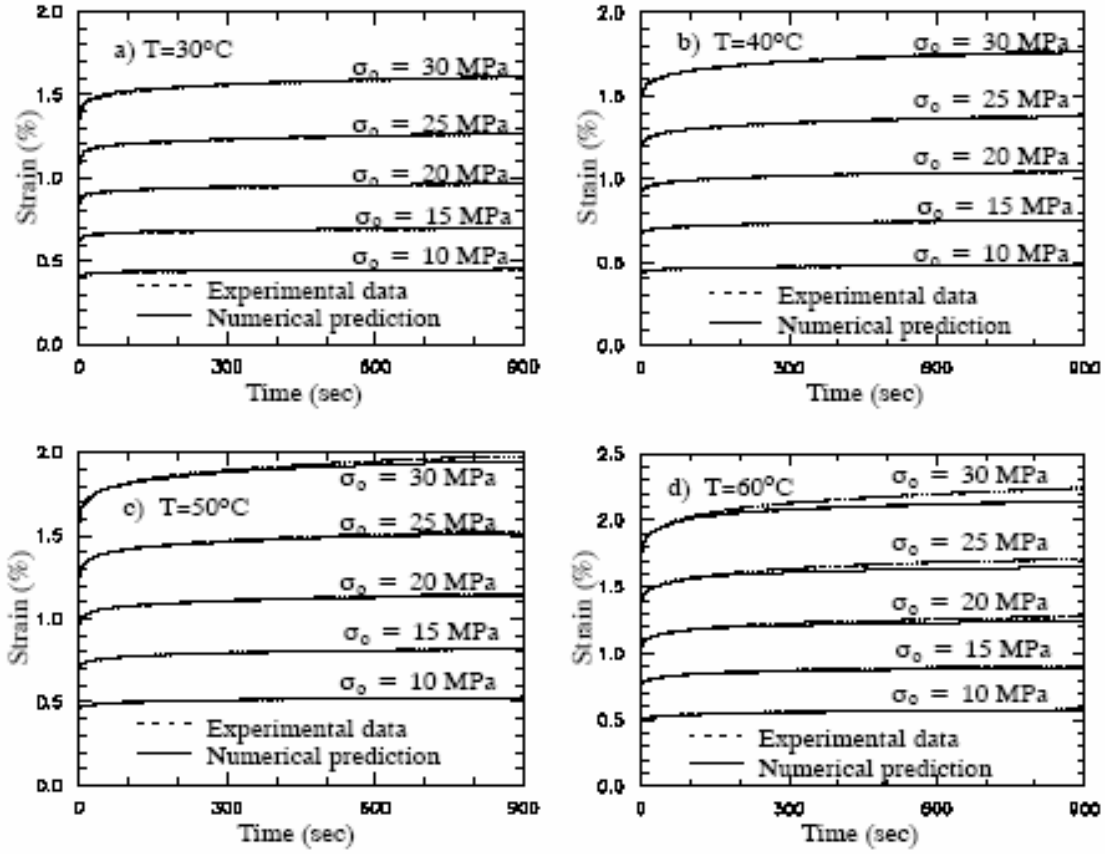

Figure 2.7 Creep strain responses of FM 73 adhesive under several stresses and temperatures (numerical prediction using the NR method; experimental data of Peretz and Weitsman, 1983).

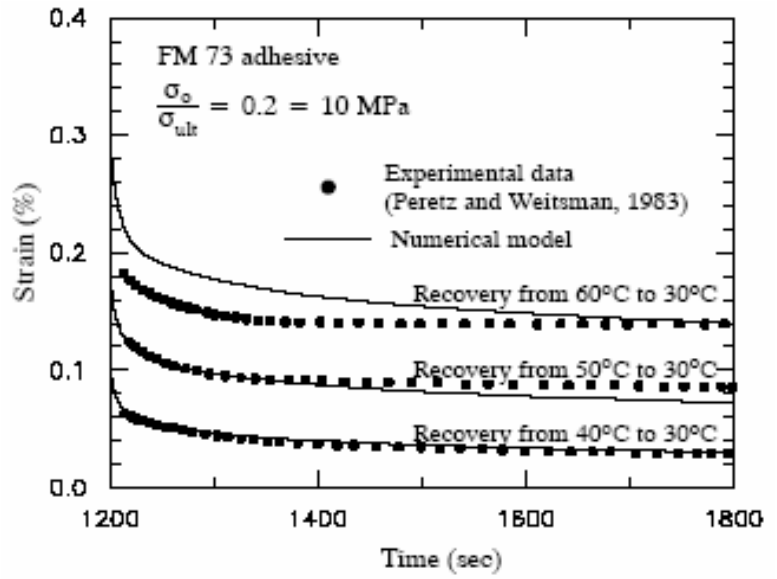

Figure 2.8 Temperature recovery responses of FM 73 adhesive at constant stress (numerical prediction using the NR method; experimental data of Peretz and Weitsman, 1983).

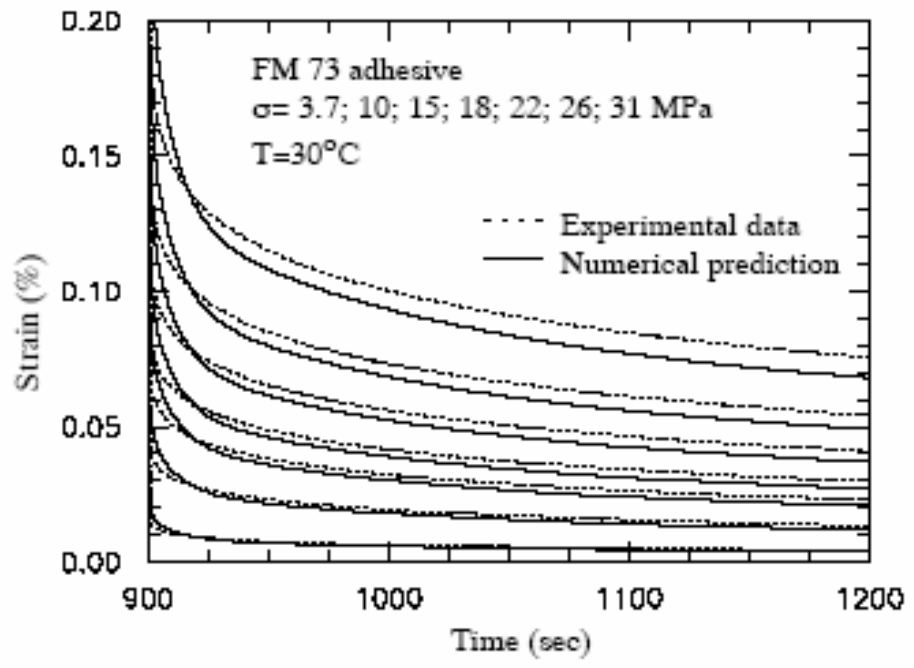

Figure 2.9 Stress recovery responses of FM 73 adhesive at constant temperature (numerical prediction using the NR method; experimental data of Peretz and Weitsman, 1982).

2.2.2 VISCOELASTIC RESPONSES OF EPOXY HERCULES 3502 POLYMERS

The capability of the recursive-iterative algorithm in predicting thermo-mechanical viscoelastic behaviors is also verified for responses under nonlinear ramp loadings. For this purpose, thermo-mechanical experimental tests on epoxy Hercules 3502 of Harper and Weitsman [13] are used. The time and temperature dependent material properties were characterized using creep recovery tests under constant stress 10 MPa and several temperatures ranging from 50-130^{o}C. Table 2.2 gives the elastic and time-dependent material properties of the Hercules 3502. The temperature dependent parameters were fitted with exponential functions:

$$g_0 = exp\left[0.675\left(\frac{T-T_0}{T_0}\right)^{0.787}\right]$$

$$g_1 = exp\left[-5.79\left(\frac{T-T_0}{T_0}\right)^{1.11}\right]$$

$$g_2 = exp\left[4.5\left(\frac{T-T_0}{T_0}\right)^{2.48}\right]$$

$$a_T = exp\left[-13.7\left(\frac{T-T_0}{T_0}\right)^{0.985}\right], \text{ (Harper and Weitsman [13])} \qquad (2.28)$$

Where T_0 is the reference temperature, which is 303 K; the temperature T is in Kelvin.

Table 2.2. Elastic properties and Prony series coefficients for the Hercules 3502 polymer.

N	$\lambda_n(\sec^{-1})$	$D_n \times 10^{-6}(MPa^{-1})$
1	1	2.10
2	10^{-1}	4.70
3	10^{-2}	2.50
4	10^{-3}	9.90
5	10^{-4}	26.60
6	10^{-5}	20.10
7	10^{-6}	104.2
8	10^{-7}	496.5
9	10^{-8}	562.2
$E = 4292\,MPa$		$\nu = 0.35$

Figures 2.10-2.12 illustrate creep strain responses for epoxy Hercules 3502 under three different combinations of stress and temperature histories. The recursive numerical algorithm with the NR iterative method is used. Good predictions are shown for all loading histories.

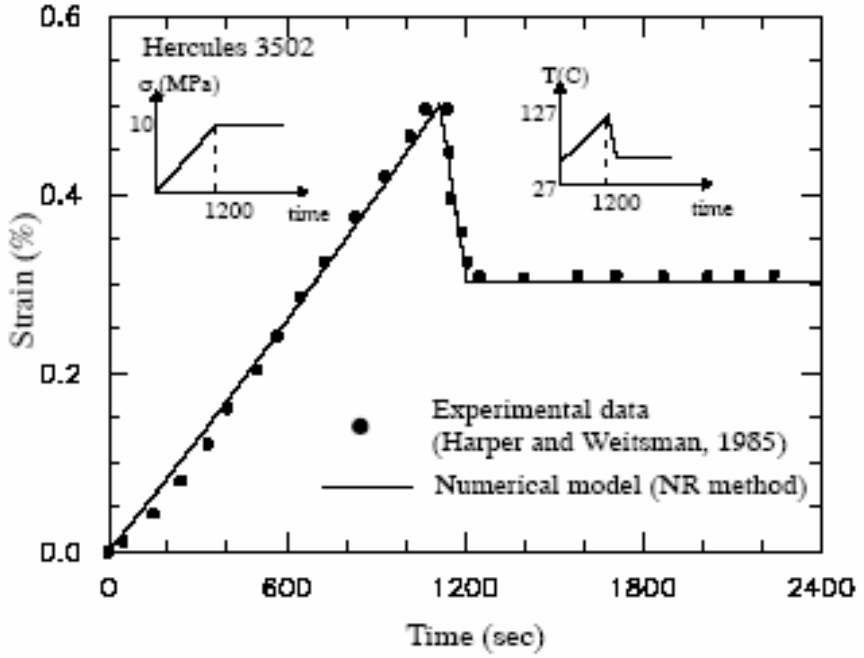

Figure 2.10 Strain responses for the Hercules epoxy 3502 under ramp stress and temperatures.

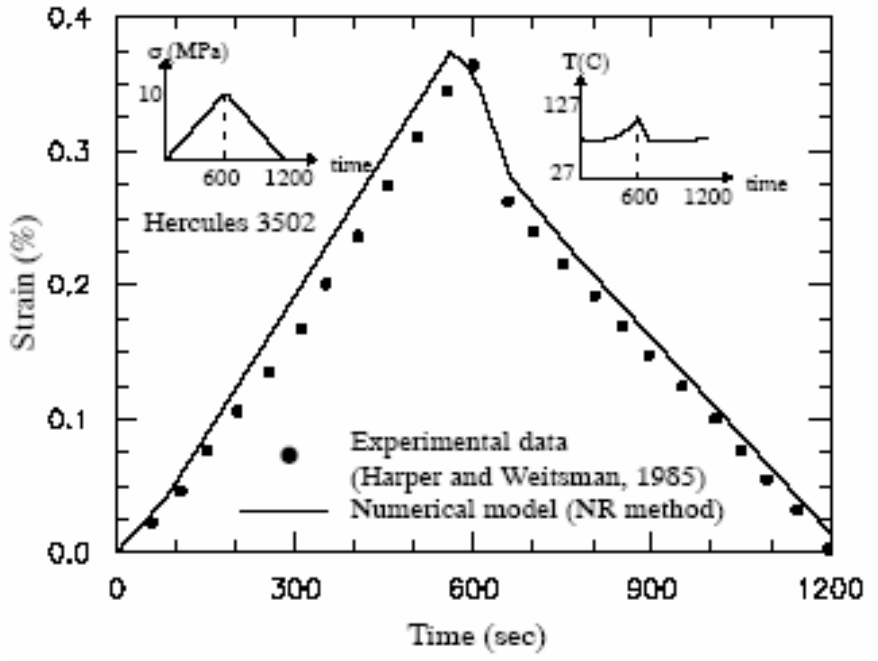

Figure 2.11 Strain responses for the Hercules epoxy 3502 under cyclic stress and ramp temperature.

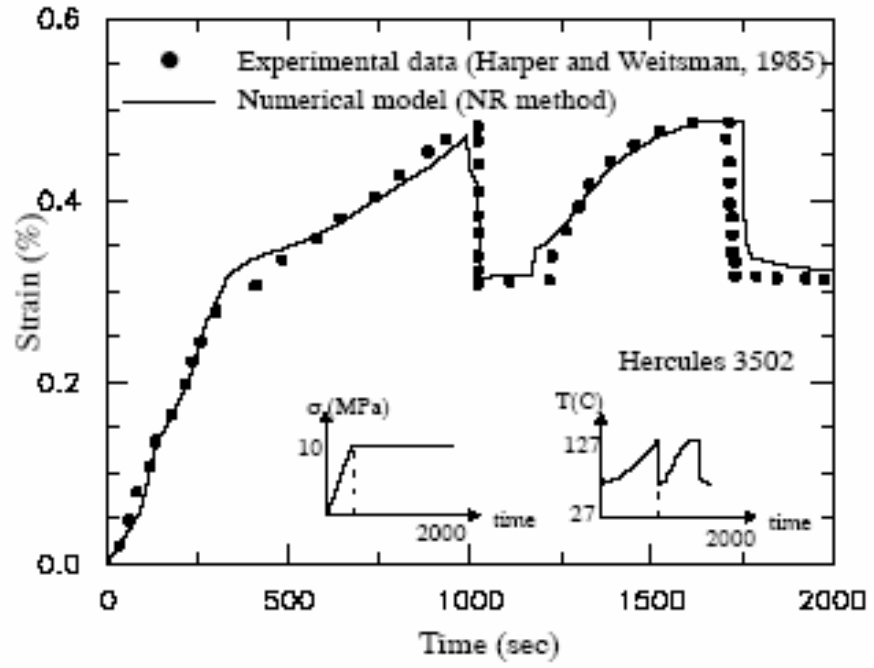

Figure 2.12 Strain responses for the Hercules epoxy 3502 under ramp stress and cyclic temperature.

2.3 THERMO-VISCOELASTIC RESPONSES UNDER MULTIAXIAL DEFORMATIONS

The capability of the recursive-iterative algorithm in predicting nonlinear multiaxial responses is presented for creep analysis of a plate with a hole. The rectangular plate has dimensions of 60x20x5 mm and hole diameter of 5 mm, which gives stress concentration factor K=2.44. FE model with 8-node brick element (C3D8) is generated. The FM73 adhesive material tested by Peretz and Weitsman [12]) is used. Axial and transverse strain responses under a uniform axial stress of 10 MPa and two different temperatures 303K and 323K are monitored near the stress concentration location and

compared with the analytical solutions, as illustrates in Figs. 2.13 (a) and (b). Good agreement between the analytical and numerical results is observed.

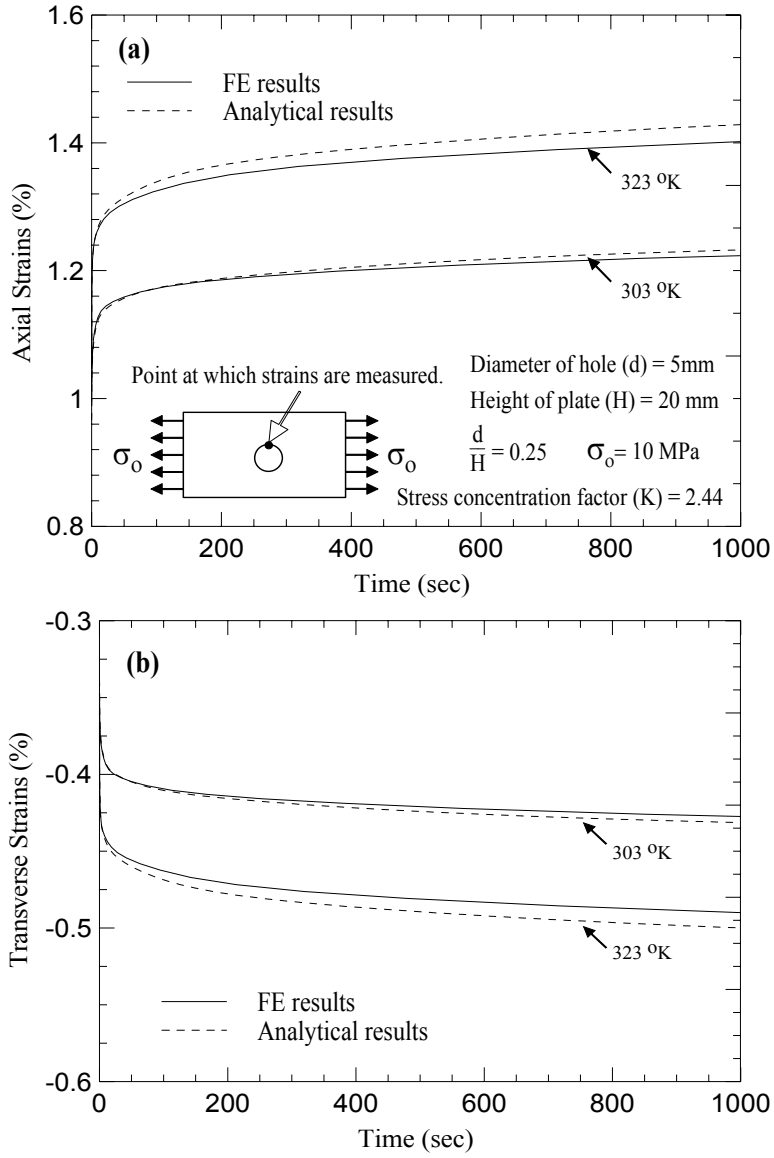

Figure 2.13 Creep strains measured at the notched edge under uniform applied stress 10 MPa: a) axial strain and b) transverse strain.

2.4 NUMERICAL ASSESSMENTS OF THE THERMORHEOLOGICALLY COMPLEX MATERIALS UNDER THERMOMECHANICAL LOADING HISTORIES

The concept of the TSM has been discussed extensively by Schwarzl and Staverman [22], Tobolsky et al. [44] in terms of the micro and macro structural configurations of polymers at various temperatures. The behaviors of the TSM are mainly demonstrated for creep and relaxation cases at constant temperatures. Morland and Lee [45] and Wineman and Rajagopal [46] presented extension of the time temperature superposition of the TSM to time temperature varying histories. In summary, materials are characterized as TSM when the following criteria are met:

1) The time dependent compliance/modulus on a logarithmic scale has the same shape for all temperatures.
2) During creep/relaxation at various temperatures, the material microstructures change to the same configuration and at different speeds (rate of change). Higher temperatures increase the speed and lower temperatures slow down the process.
3) The initial and long time compliance/modulus is independent of temperature.

The more general thermo-viscoelastic behaviors are attributed to the TCM, in which the effects of temperatures on material's initial and long term properties and loading rates are incorporated. This section presents the numerical exercises of the recursive-iterative algorithm in modeling material responses under various thermo-mechanical loading histories. Both TSM and TCM materials are considered and the responses from

the TSM and TCM are compared. The goal of this numerical study is to observe the capability of TSM and TCM in predicting thermo-viscoelastic responses. The FM73 material reported by Peretz and Weistman [12] is used and the material properties are given in Table 2.1 and Eq. 2.27.

The first case deals with the creep behaviors of the TSM and TCM under a constant stress of 25 MPa and isothermal temperatures of 40°C and 50°C. The purpose of this study is to observe the effect of temperature dependent parameters on the initial elastic response and creep behavior of the polymer. Figure 2.14 shows the creep behaviors of the FM-73 adhesive from the TSM and TCM analyses. It is found that there is an initial increase in the elastic compliance for TCM due to the presence of the non linear temperature dependent parameter (g_0), which accounts for the increase or decrease in the compliance/stiffness with temperature. The nonlinear parameters g_2 has shown significant effects at the early time-dependent stage and its effect is slowly decreasing with the increase of time. The parameter g_1 has insignificant effect due to the relatively short term creep behaviors. In general, the parameters $g_1 g_2$ leads to significant increase in the long-term strain responses. Unlike the TCM, the creep responses under TSM showed constant jump since the temperature effects are incorporated only through the parameter a_T

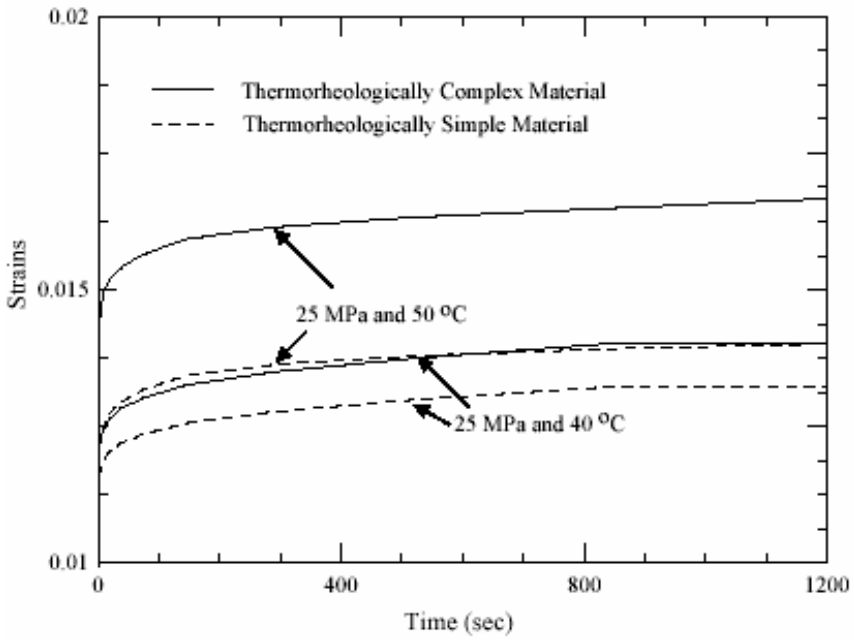

Figure 2.14. Strain responses under different constant temperature and fixed stress.

The second study examines the behaviors of the TSM and TCM under linear ramping of temperatures at different rates. The responses are also compared with the one of the temperature independent materials. It is shown that the slower rate of loading leads to more accumulation of the strains, shown in Fig. 2.15, while higher rate shows less strain buildup with the rise of the temperature. For the TCM with the increase of temperatures the slope of the temperature-strain curve decreasing and the difference in the strains from the two temperature rates increases. It is also observed that at different rates the viscoelastic behavior shifts equally in case of TSM while the TCM exhibits different amount of shifting due to the existence of g_0, g_1 and g_2 parameters. The temperature independent materials show different strains for the two temperature rates due to the time dependent material properties. The same amount of strain shifting as the

one of temperature independent material responses is exhibited by the TSM. The deviation of the TSM responses from the time-independent material is attributed to the shift factor a_T.

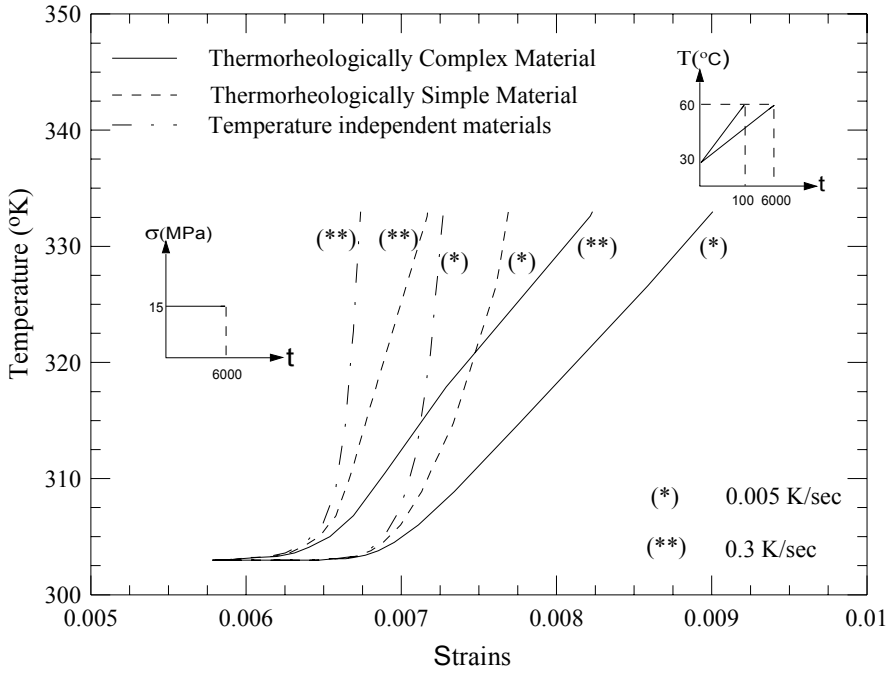

Figure 2.15 Strain responses under different temperature rates and fixed stress.

The third study presents the responses under multiple temperature loading histories and constant stress. Figures 2.16 (a)-(c) show the comparison of the responses from the TSM and TCM. In all cases, higher strain responses have been observed for TCM due to the presence all non linear temperature dependent parameters. For the TSM, since the time-temperature dependent properties are only carried through the horizontal shift factor, therefore the delayed recovery behavior is not prominent. It is noted that the initial strains for the TSM and temperature independent material are having the same values, but due to the presence of the horizontal shift factor in TSM there is a constant

difference in the strains value at the end of recovery which is same as the difference just before the unloading.

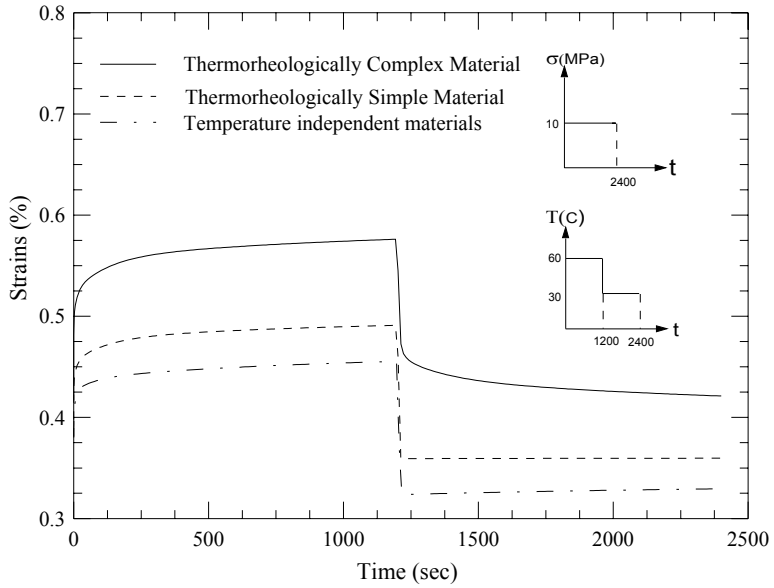

Figure 2.16 (a) Strain responses under constant temperature loading followed by recovery and fixed stress.

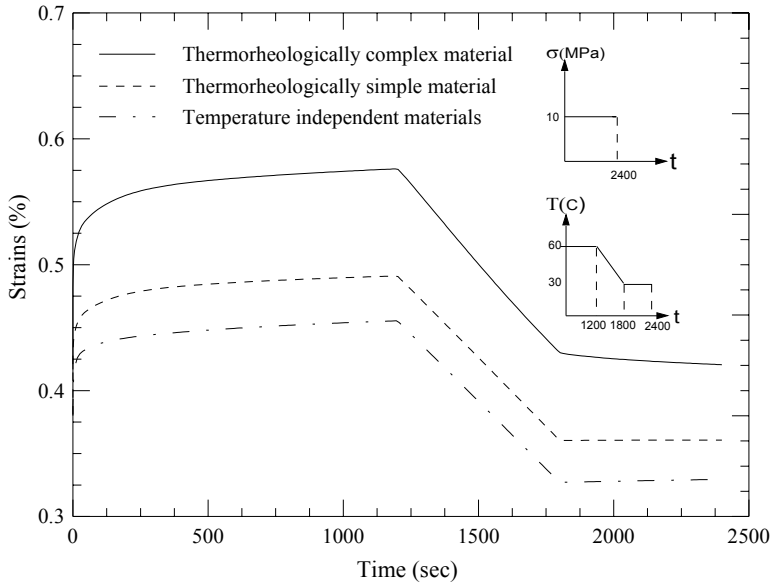

Figure 2.16 (b) Strain responses under constant temperature-linear temperature drop-recovery and fixed stress.

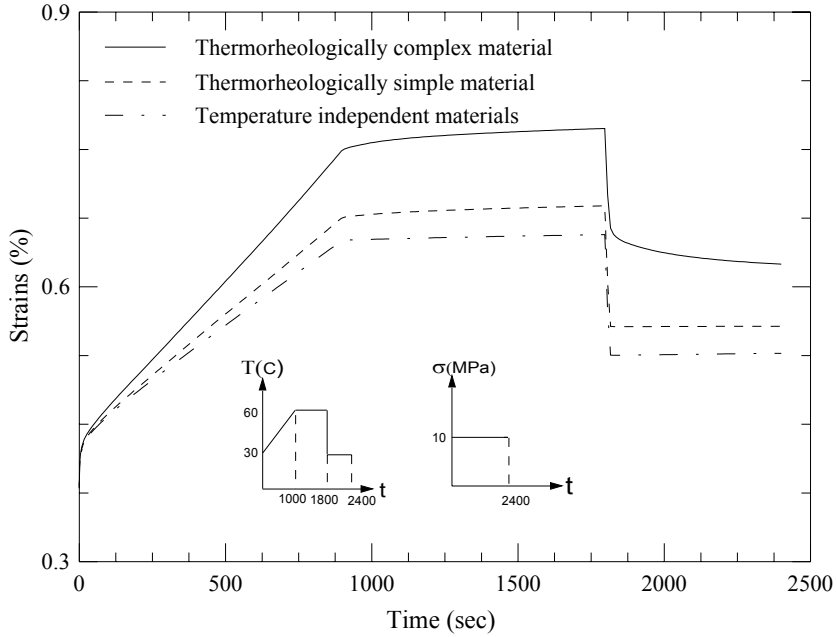

Figure 2.16 (c) Strain responses under linear ramping- constant temperature-recovery and fixed stress.

Finally, material responses under a constant stress and cyclic temperatures are presented. Two different cyclic frequencies are conducted, which are 1/200 cycle/sec and 1/2000 cycle/sec. The triangular temperature cycle with low cyclic rate is performed since the temperature loadings are often occur at low frequencies as compare to the mechanical loadings. In addition, most polymers are a good insulator having low thermal conductivity properties. This characteristic results in slow temperature changes. Figures 2.17 (a) and (b) shows the temperature-strains responses from the TSM, TCM and the temperature independent materials. The TSM and temperature independent material time-dependent responses follow the same trend and the responses at lower frequency have been shifted from the higher frequency by same amount except at the

beginning of the cycle. The shifting between the TSM and time-independent responses are carried by the parameter a_T, which indicate constant shifting. The nonlinear temperature dependent parameters in the TCM results in higher strains. It is also shown that upon unloading, there are accumulated unrecoverable strains in the TCM. It is also observed that low frequency delays the strains.

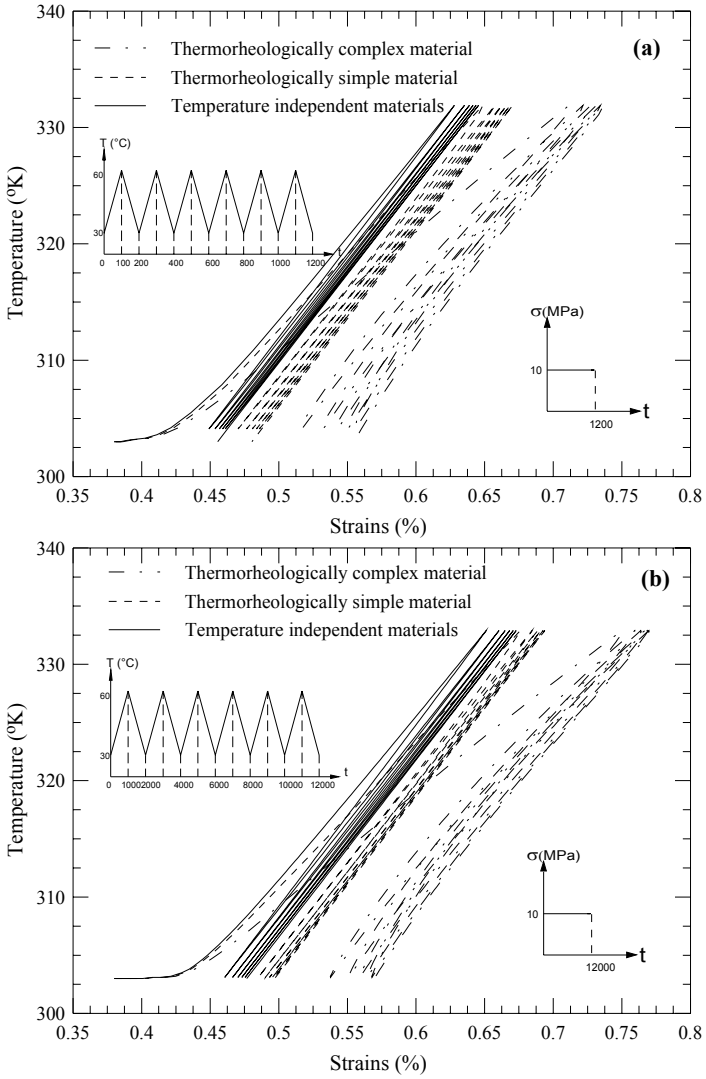

Figure 2.17 (a) and (b) Strain responses under cyclic loadings with different frequencies and fixed stress.

The analyses for the cyclic stresses and temperature are also performed. The same cyclic pattern is used for both stress and temperature. It is found that the strain accumulations that were prominent in the Fig. 2.17 (a) and (b) due to creep are reduced to very low value in case of the cyclic stress, shown in figure Fig. 2.18 (a) and (b).

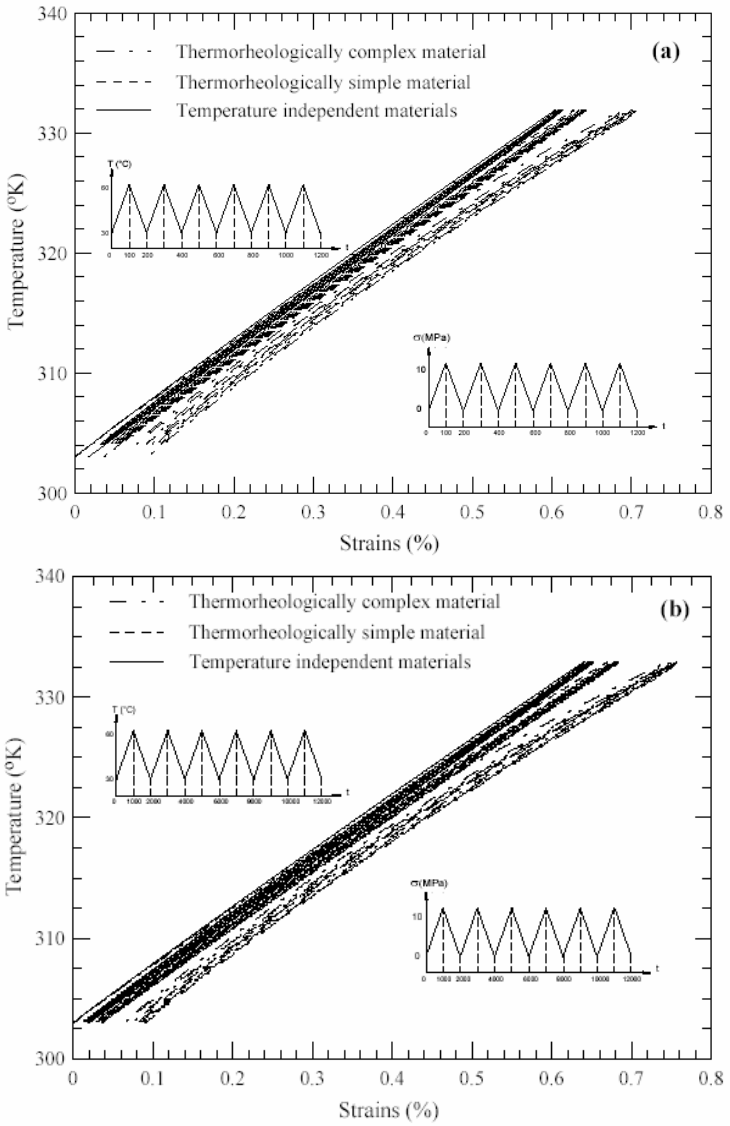

Figure 2.18 (a) and (b) Strain responses under cyclic temperature loadings with different frequencies and cyclic stress.

CHAPTER III

FINITE ELEMENT METHOD FOR THERMO-MECHANICAL VISCOELASTIC ANALYSES OF BONDED JOINTS

Adhesive polymers are widely used for joining structural components made of similar and dissimilar materials. The advantages of using adhesive bonding includes flexibility in design, light weight, cost competitive, and more uniform stress distribution over an entire bonded surface. Typical applications of the adhesives are in the aircraft structural components, automotive components, naval transportations and railway carriages for joining composite to steel. One of the important requirements of these polymeric adhesives is its durability and capability to sustain mechanical loads under various environmental conditions. Therefore, it is necessary to predict the short-term and long-term performances of adhesive bonded joints under complex loading conditions. This chapter presents the integration of the proposed numerical algorithm of TCM with the displacement based FE framework for analyzing thermo-mechanical viscoelastic behaviors of single lap-joints. Time dependent crack propagation analyses for opening and shearing failure modes are also performed.

Finite element (FE) structural analyses have been employed to study time-dependent behaviors of adhesive bonded lap joint structures. Most of the studies are done for the TSM adhesives. This requires generating numerical algorithms of time-dependent constitutive material models that can be integrated with the FE framework. Several numerical algorithms of nonlinear viscoelastic behaviors for isotropic and TSM models have been proposed (Henriksen [30]; Roy and Reddy, [47]; Lai and Bakker, [31]; Haj-Ali and Muliana, [32]). These algorithms are compatible with general displacement-based FE code. Yadagirz et al. [48] presented direct formulation for the viscoelastic analysis of adhesively bonded joints using FE method. Hereditary integrals using Prony series for the relaxation modulus were used in the stress-strain relations. An eight-node quadratic isoparametric plane strain element was used to model the adherends. The developed FE procedure was applied to model a single lap joint having two identical adherends and a linear viscoelastic adhesive layer. The adhesive layer was modeled with three parameter viscoelastic solid model. Roy and Reddy [47] developed two-dimensional (2D) FE computational procedure for the analysis of the strains and stresses in adhesively bonded joints. The adhesive layer was modeled using the Schapery's nonlinear single integral model. A similar integration approach to Henriksen's was formulated with additional material parameter to account for moisture sorption. The effects of temperatures, stresses and moisture were carried through the time shift factors, which refer to TSM. The numerical procedure was validated by comparing the obtained results with analytical and experimental results available in the literature. Carpenter [49] presented a numerical algorithm for viscoelastic adhesive with direct time integration.

The direct integration procedure showed computationally effective and required minimal storages. The direct integration process presented permitted the use of higher order integration formulae which allows for large time increments. The proposed algorithm was validated using the analytical model of Delale and Erdogan [50].

Lap joint model has also been used by many researchers to experimentally characterize the elastic and viscoelastic properties of the adhesives. Sancaktar [51] characterized stress-strain in adhesive bonded lap joints. Two approaches, i.e. semi-empirical and theoretical, were assessed. The semi-empirical approach includes Ludwik and Zhurkov's equations to describe failure stresses under constant strain-rates and constant stresses that included temperature effects. The theoretical approach was used to describe adhesive shear stress/strain behavior by utilizing viscoelastic or nonlinear elastic constitutive equations. Ahn et al. [52] characterized thermo-mechanical properties of adhesive bonded joints. It was shown that shear strengths increased with decreasing temperatures and/or increasing testing speeds due to the viscoelastic behavior, especially at high temperatures.

3.1 FINITE ELEMENT ANALYSES OF ADHESIVE LAP JOINT

Time dependent FE analyses of a symmetric lap joint specimen, having aluminum adherends and adhesive layers, at different temperatures are presented. The numerical algorithm of nonlinear viscoelastic constitutive model of TCM presented in chapter II is integrated as material points (Gaussian points) within each element in the FE model. Three dimensional viscoelastic analysis of the lap joint is performed using ABAQUS FE

code. The adherend is modeled as linear elastic. A user material subroutine (UMAT) is used for the thermo-mechanical viscoelastic behaviors of the adhesive layers.

Static and creep test data of Jurf and Vinson [40] on the FM73M adhesive single lap joint is used to validate the FE model. The geometry of the single lap joint is given in figure 3.1. The dimensions of adherend thickness H and the joint overlap length L have significant effects on the stress distribution within the adhesives layers, while the adhesive thickness is predetermined by the manufacturer. Renton [40] conducted parametric study on the effects of L and H. It was found that the dimensions of the lap joint specimen with L = h=9.5 mm (0.375 in) resulted in the most uniform shear stress and smallest normal stress distribution across the adhesive layer of the single lap joint. The FE model for the lap joint is generated using 3D continuum elements (C3D8). Five layers of the elements are generated across the bond thickness. The boundary conditions for the FE analysis are shown in figure 3.2(a). The uniform load is applied at the end such that the stresses in the adhesive layers remain in the linear. The same load (P) is applied at all temperatures. Figure 3.2 (b) shows the uniformly distributed shear stress around the adhesive joint after the application of the load.

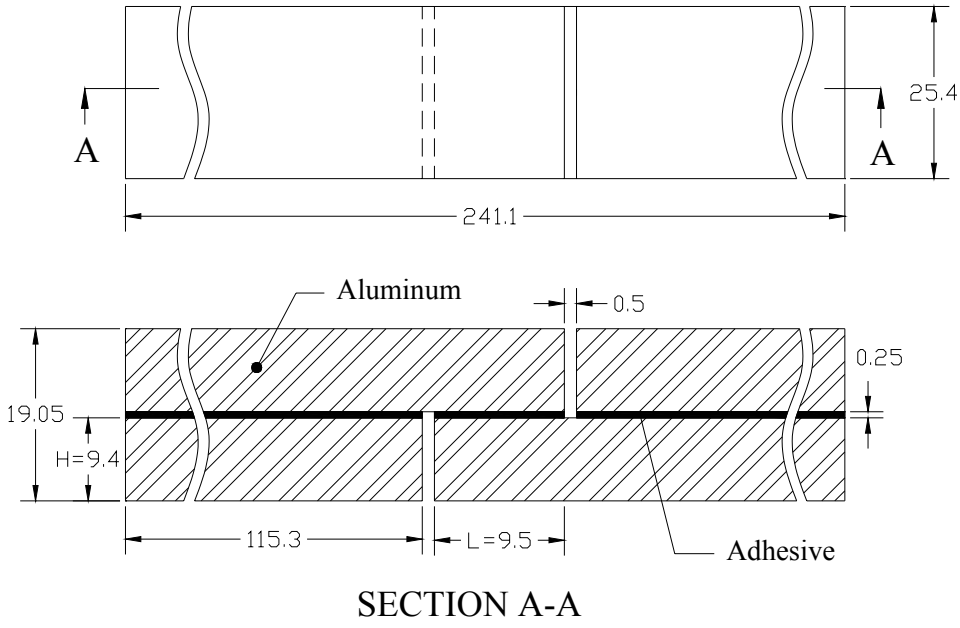

Figure 3.1. A geometry of the symmetric single-lap joint (all dimensions in mm, not to scale).

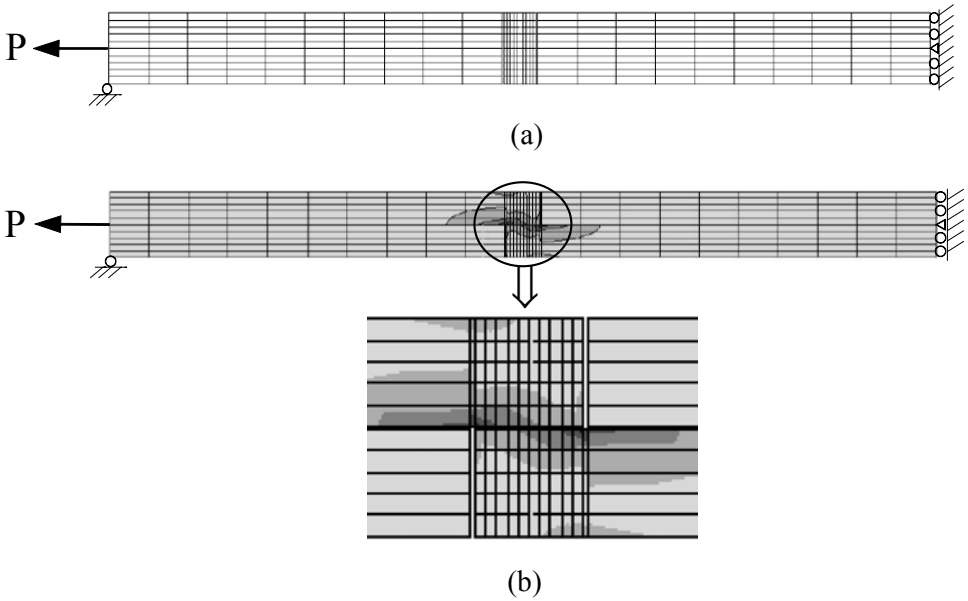

Figure 3.2. (a) FEA model of the symmetric lap joint; (b) Uniformly distributed shear stress around the adhesive bondline.

The tests were performed at several temperatures: 22-106^{o}C. The effect of moisture is also investigated by exposing the specimen at three different moisture contents dry (i.e. no humidity), 63% and 95 %. It was also concluded that the effect of the moisture as an external plasticizer on the shear properties of these adhesives is equivalent to raising the environmental temperature. In this study the behavior of the adhesives with the increase of temperatures at three different humidity levels are investigated. Elastic properties of the studied materials are shown in table 3.1.

Table 3.1. Elastic properties of aluminum and FM73M.

Material	E (MPa)	υ
FM73M	2700	0.35
Aluminum	69000	0.33

Static test was first performed at a constant rate of 0.2mm/min to determine the ultimate shear strength. The load-deflection curves from the FE model and experimental test at 22°C are shown in figure 3.3. The purpose of this analysis is to validate the FE geometry model. Both the adherend and adhesive is assumed to be linear elastic. Good agreement is found between the experimental and FE results. Next, the FE geometry model is further verified with another static test data of a lap joint, reported by Chalkley and Chiu [53]. They used a similar geometry as in figure 3.2 to perform a FE analysis of the lap joint with steel adherends. The shear stresses along the interface area are normalized by the average shear stress along the bondline and the distance along the

bondline is normalized with respect to the length of the bondline. Figure 3.4 shows comparisons of normalized shear stresses along the bonded area determined from the FE analysis and experimental data.

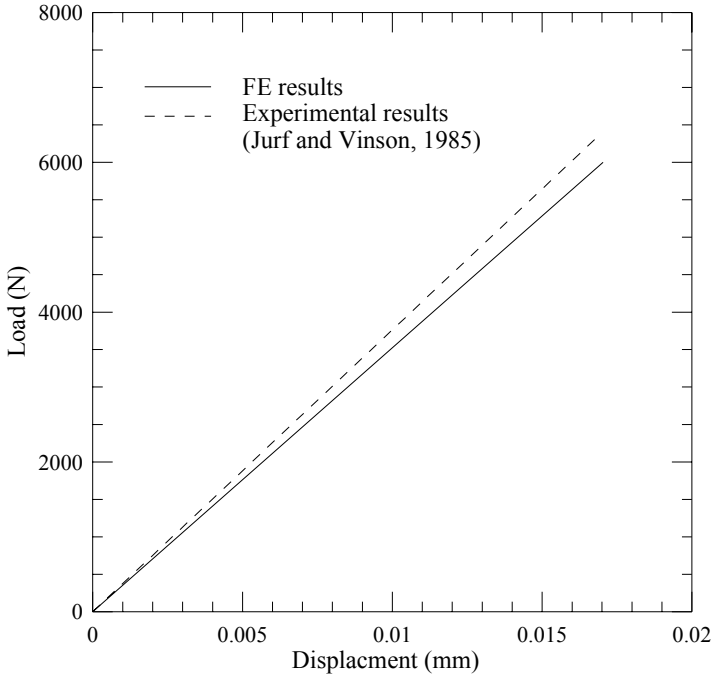

Figure 3.3. Load displacement curve for lap-joint at 22 °C.

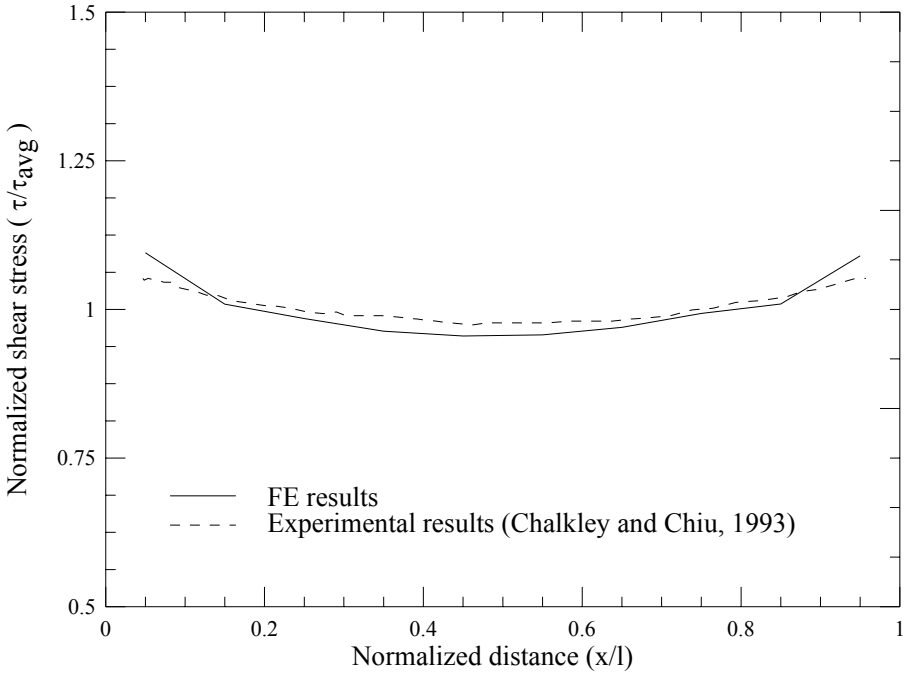

Figure 3.4. Normalized shear stress vs. normalized distances along a bondline in the test specimen.

3.1.1 CHARACTERIZATION OF THE TIME-TEMPERATURE DEPENDENT MATERIAL PARAMETERS

To determine the time-temperature dependent parameters, the experimental data of Jurf and Vinson [40] are used. Short-term creep tests at different temperature ranging: 22^{o}C-106^{o}C and at different load levels from 85 to 105 kg were performed. Shear creep compliance at dry (i-e no humidity), 63% and 95% moisture contents are also measured for the FM73M adhesive at different temperatures. With no humidity, only the comparison of dry FM73M up to 80°C is presented in this study since above this temperature the adhesive exhibits a rubbery state and tertiary creep. Peretz and Weitsman [12] have also reported that the FM-73 exhibited tertiary creep at 70°C. The

FM73M material used in Jurf and Vinson [40] has the glass transition temperature (Tg) of 99°C. Jurf and Vinson [40] also investigated the moisture effect on the structural properties and it was concluded that increasing the moisture has the same effect on the creep compliance behavior as increasing the temperature.

The material parameters in Eq. (2.2) can be obtained from series of creep data at different temperatures. The test data performed at the lowest level are used to calibrate temperature dependent properties. Since at this load level the all stress dependent parameters are equal to one. The nonlinear instantaneous elastic parameters (g_0^T) are calculated using the following expression $g_0^T = \frac{D_0^T}{D_0^{T_0}}$. Where D_0 is the instantaneous value of the compliance at different temperatures and $D_0^{T_0}$ is the instantaneous compliance at reference temperatures. The values of the g_0^T at dry condition are presented in table 3.2.

Table 3.2. Values of g_0^T for FM73M at dry condition.

Temperature (°C)	g_0^T
22	1.00
38	1.25
50	1.52
59	1.94
69	2.48
80	3.92

The time-temperature superposition principle (TTSP), proposed by Leaderman [2], is used to characterize long-term behaviors of various viscoelastic materials. For a class of thermorheologically complex material (TCM), vertical shifting of the short-term data prior to the horizontal shifting is required (Griffith et al., [19]; Yen and Williamson, [21]). Since the adhesive is modeled as TCM, both vertical and horizontal shifting is performed in the TTSP to create master curves for predicting long-term material behaviors from a series of short-term creep tests at elevated temperatures. The horizontal distance required to shift the short-term creep/relaxation responses to the master curve is equal to the log of the inverse of the time-temperature shift factor a^{T^t} in Eq. 2.3. Vertical shifting is associated with instantaneous elastic temperature dependent behaviors. The amount of vertical shifting is defined by:

$$a_v = \left(g_0^T - 1\right) D_0 \tag{3.1}$$

Figure 3.5 illustrates shear creep compliances of the specimens under constant load (P=1kN) and at several temperatures. A master curve at the reference temperature of 22 ^{o}C is created. The master curve represents creep behaviors up to 862 hours (3000 times longer than the conducted creep tests). The vertical shift factors are computed using Eq. 3.1 with the previously calibrated g_0, reported in table 3.2. The horizontal time shift factors, measured graphically for the studied specimens, are also given in table 3.3.

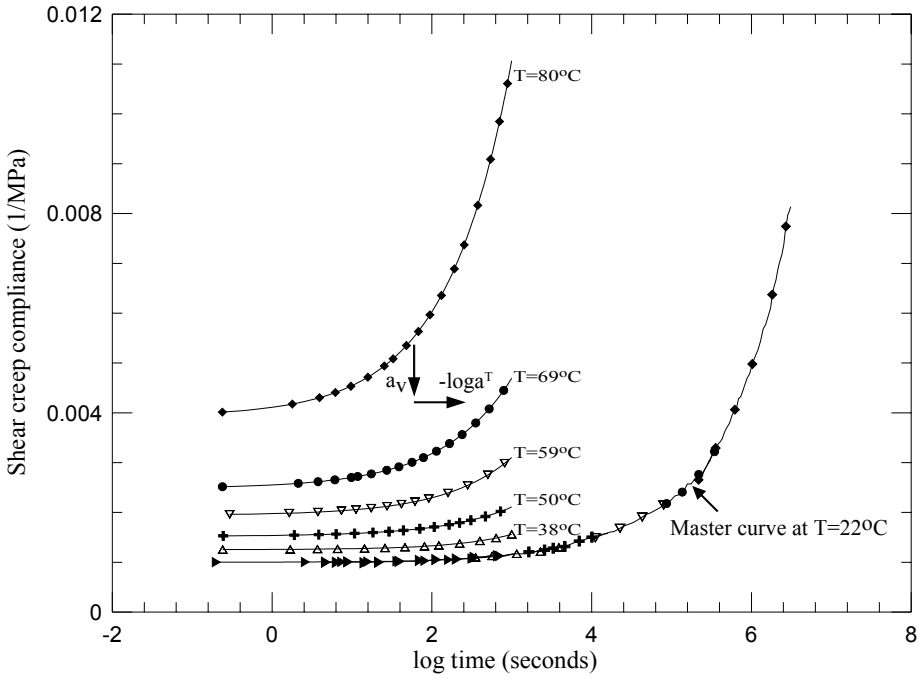

Figure 3.5. Shear creep compliance at different temperatures and master curve at the reference temperature.

Table 3.3. Horizontal shift factors (a^T) and vertical shift factor (a_v) for the FM73M at dry condition.

Temperature (°C)	a^T	a_v
22	1	0
38	0.223872	0.000252
50	0.063095	0.000519
59	0.012589	0.000943
69	0.002818	0.001480
80	0.000316	00029272

In order to create longer time responses in the TTSP, short-term creep tests with longer time periods at several elevated temperature are required. Another way to extend long-term material behaviors is using extrapolation of the available creep data. Next, the master curve from the TTSP is plotted in double logarithmic scales, and expressed in terms of linear equation as shown in figure 3.6. This allows extending the material long-term prediction using a linear extrapolation function.

Figure 3.6 presents a long-term response created from the TTSP and the linearly extended TTSP response, which can predict up to 14000 hours (19 months) of the shear creep compliances. It should be noted that the linear extrapolation creep strains will only be valid for limited times, at which the tertiary creep stage has not been occurred yet or the materials have not exhibited microstructural changes. The long-term Prony coefficients with second unit time are calibrated by matching the extended long-term responses, shown in figure 3.7. The long-term Prony parameters are presented in table 3.4. Using the calibrated long-term Prony series and temperature-dependent parameters, the long-term shear creep strains for the simple shear lap joint specimens under different temperature can be predicted.

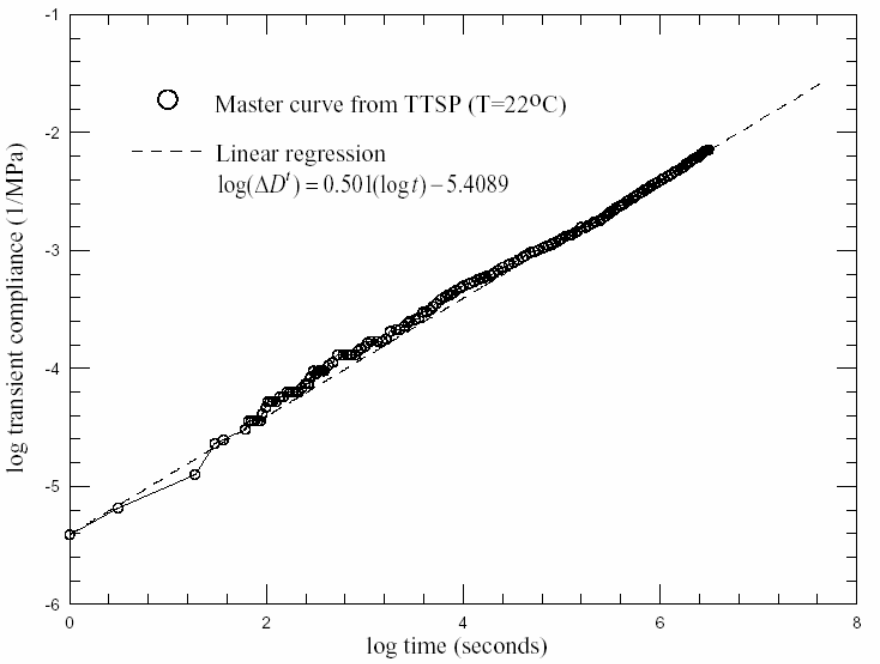

Figure 3.6. Extended shear creep compliance master curve at the reference temperature.

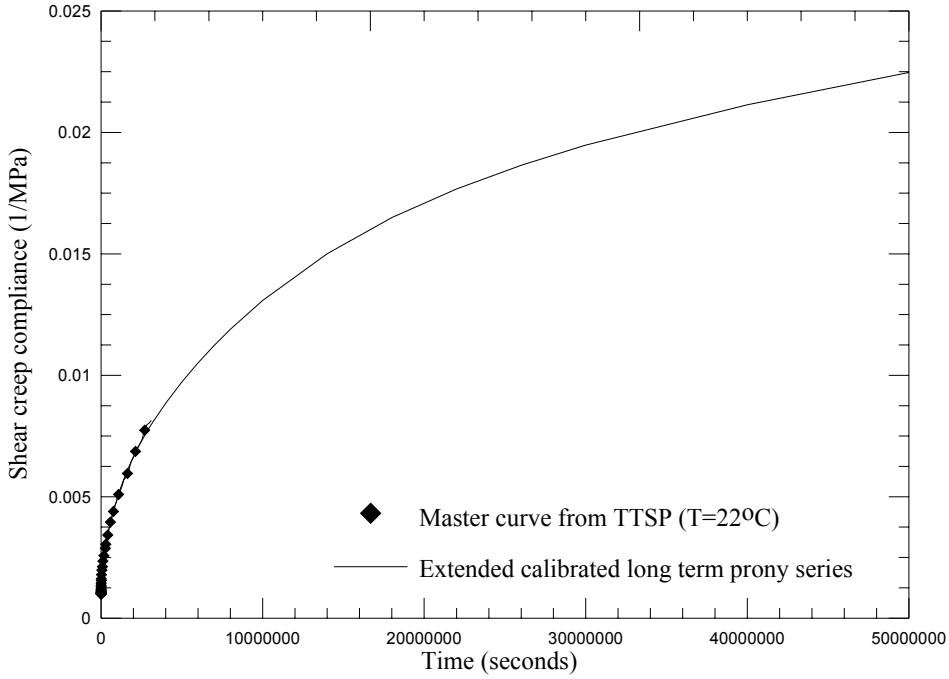

Figure 3.7. Long term Prony parameters at the reference temperature.

Table 3.4. Long term Prony parameters for the FM73M at dry condition.

N	$\lambda_n(\sec^{-1})$	$D_n \times 10^{-6}(1/MPa)$
1	1	3.70
2	10^{-1}	0.296
3	10^{-2}	40.7
4	10^{-3}	33.3
5	10^{-4}	55.6
6	10^{-5}	259
7	10^{-6}	1000
8	10^{-7}	3810
9	10^{-8}	7040

Next, viscoelastic analysis of the lap joint is performed using the calibrated long term Prony coefficients and temperature dependent material parameters. Figures 3.8 and 3.9 shows fitted functions of the horizontal shift factors (a^{T^t}) and g_0^T values, which are used in the UMAT subroutine to predict the response of the adhesive at different temperature. All other stress dependent parameters ($g_i^\sigma (i = 0,1,2)$ and a^σ) and nonlinear temperature parameters ($g_i^T (i = 1,2)$) are set equal to one.

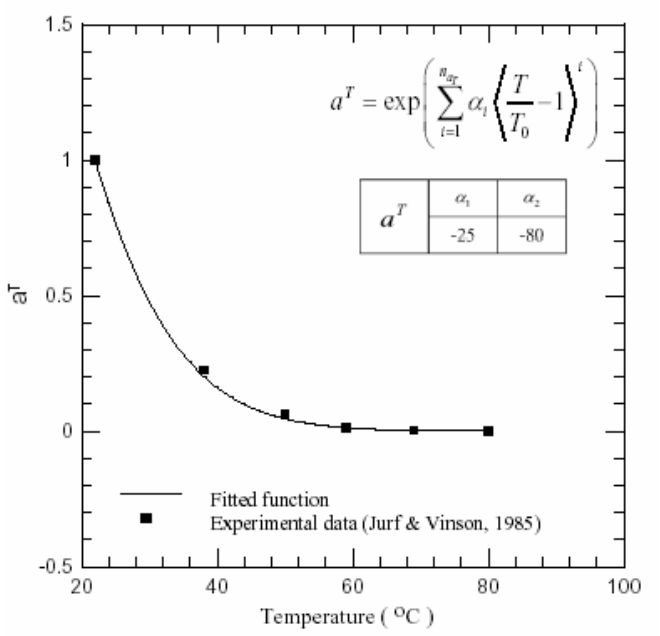

Figure 3.8. Horizontal shift factor values against temperature for FM73M at dry condition.

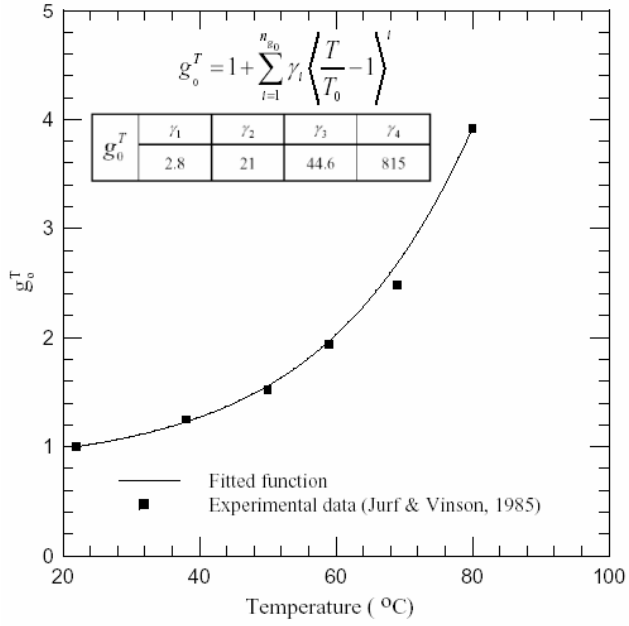

Figure 3.9. Values of g_0 against temperature for FM73M at dry condition.

.

Figure 3.10 shows the shear creep compliance from the experimental data and FE analyses of the lap joint at several temperatures. The strains are measured at the nodes of the middle element of the adhesive layer at the interface. The stresses are calculated at the centroidal points of the element at different temperatures. The time dependent shear compliance is calculated by dividing the shear strains and shear stress in the middle element. Good agreement is observed at all temperatures.

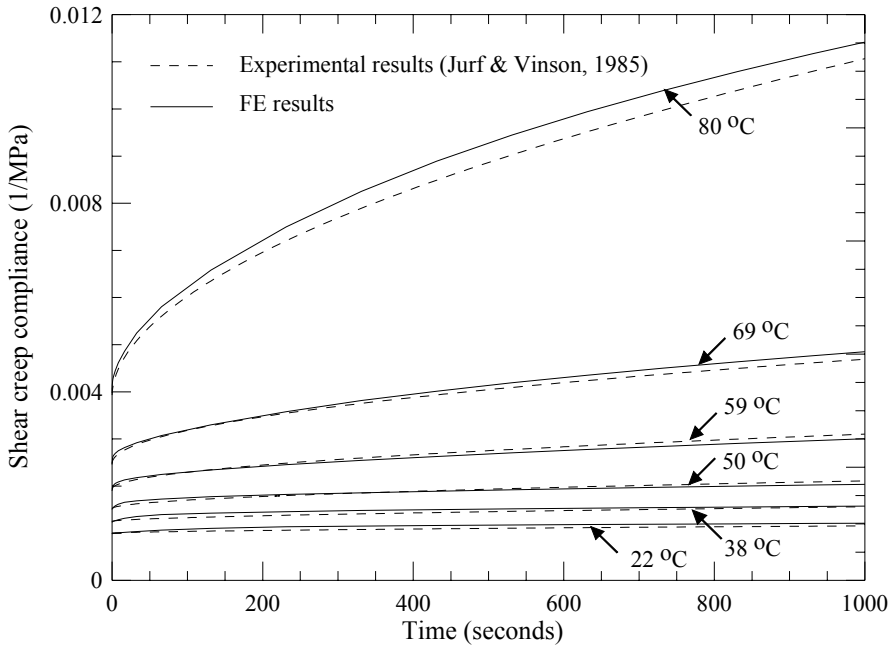

Figure 3.10. Shear creep compliances calculated from the FE analysis and the experimental data of the lap-joint at different temperatures.

The FE analyses of the adhesively bonded joints at two humidity levels i-e 63% and 95% are also performed. The long term properties and nonlinear temperature dependent parameters are calibrated in a similar method as for dry (i-e no humidity) FM-73M using

the experimental data reported by Jurf and Vinson [40]. The long term prony parameters for 63 % and 95% humidity levels are shown in the table 3.5 and the nonlinear temperature dependent parameters i-e fitted functions of the horizontal shift factors (a^{T^t}) and g_0^T values are shown in the figure 3.11 (a) – (d). All other stress dependent parameters ($g_i^\sigma (i = 0,1,2)$ and a^σ) and nonlinear temperature parameters ($g_i^T (i = 1,2)$) are set equal to one.

Table 3.5. Long term Prony parameters at 53% and 95% humidity level.

N	$\lambda_n(\sec^{-1})$	$D_n \times 10^{-6}(1/MPa)$ Humidity = 63%	$D_n \times 10^{-6}(1/MPa)$ Humidity = 95%
1	1	0.1	0.1
2	10^{-1}	0.8	0.8
3	10^{-2}	110	100
4	10^{-3}	90	800
5	10^{-4}	150	1000
6	10^{-5}	1100	11200
7	10^{-6}	2700	88500
8	10^{-7}	28000	24000
9	10^{-8}	18000	90000

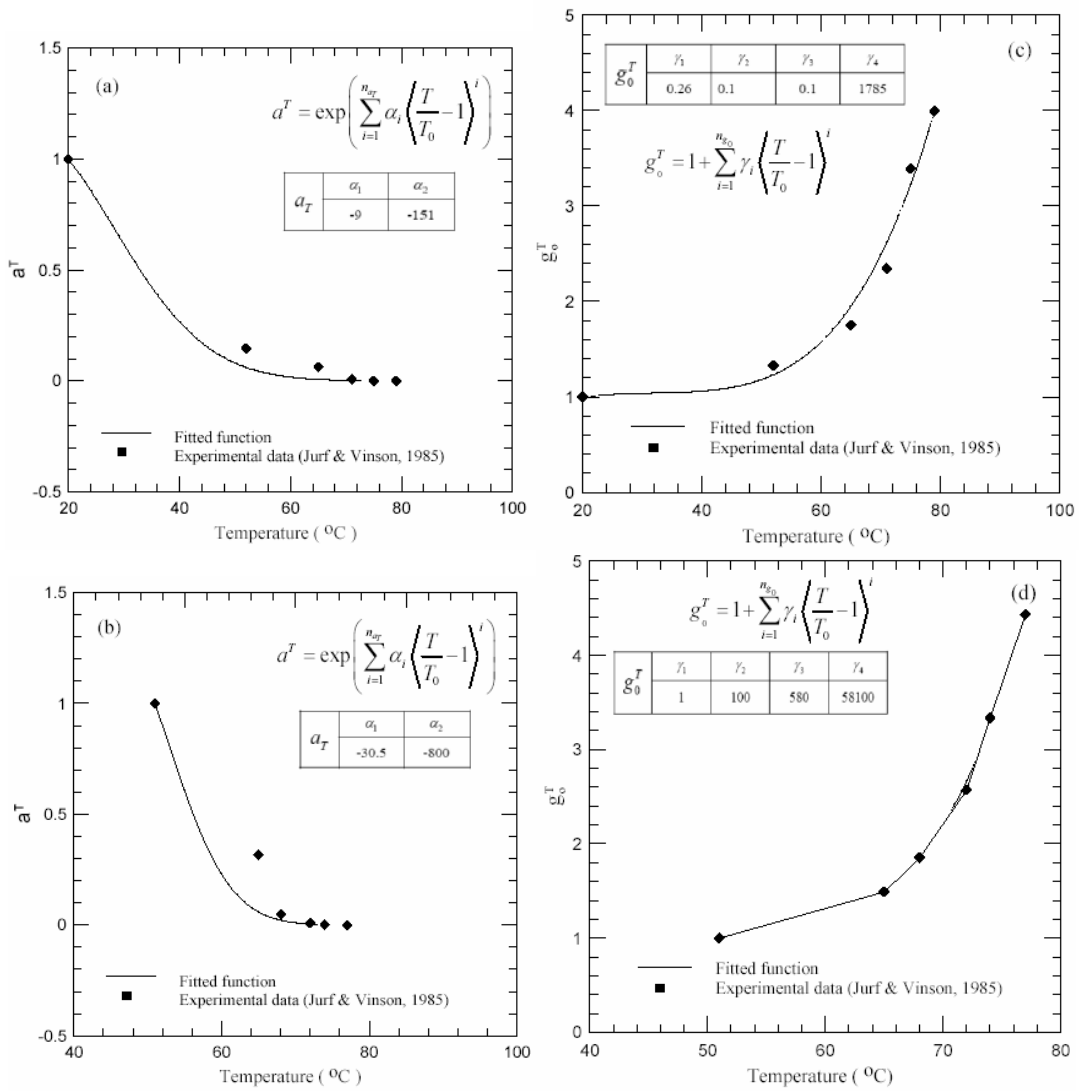

Figure 3.11. Horizontal shift factor (a) 63% (b) 95% humidity. g_0^T at (c) 63% (d) 95% humidity.

Figure 3.12 (a) and (b) present the shear creep compliances obtained from the FE analyses and the experimental results reported by the Jurf and Vinson [40]. The responses are shown for 63% and 95% moisture contents at different temperatures. Some deviations in the predictions of the viscoelastic responses have been observed. The

primary reason found is due to the mismatch in the fitted curves and experimental date points. Overall results are in good agreements with the experimental data.

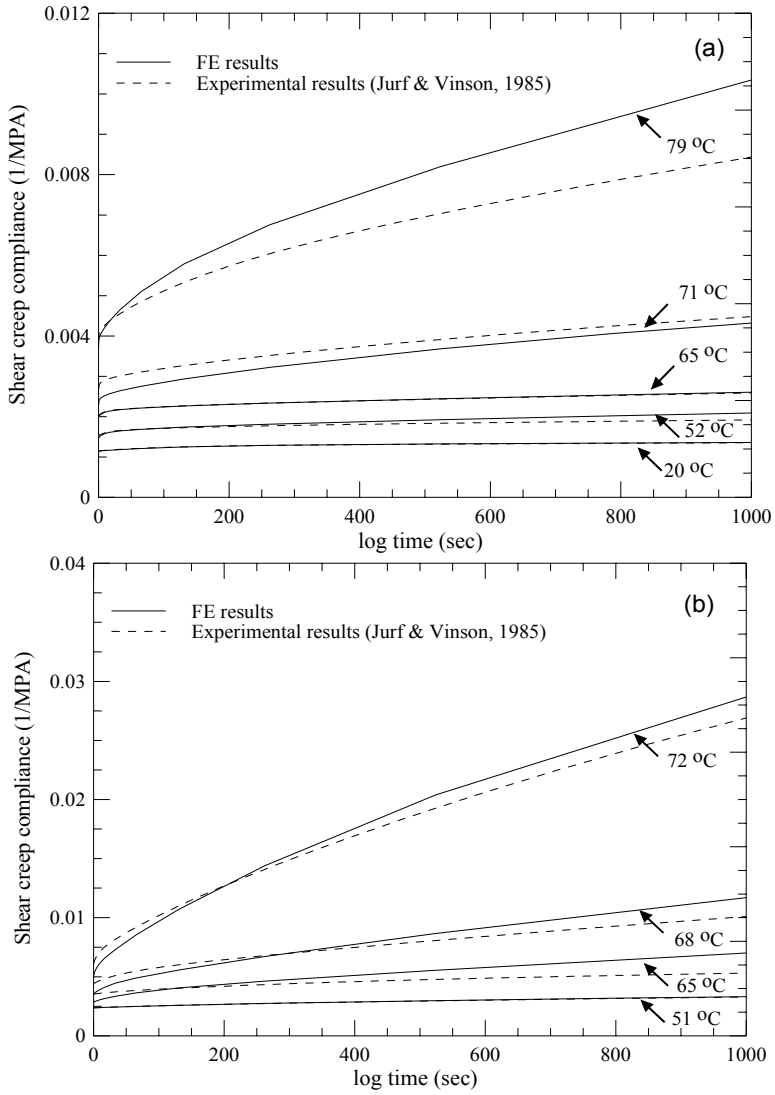

Figure 3.12. Shear creep compliances calculated from the FE analysis and the experimental data of the lap-joint at different temperatures and at humidity (a) 63% (b) 95%.

3.2 NONLINEAR TIME-DEPENDENT FAILURE ANALYSES OF ADHESIVE BONDED JOINTS

One of the important characteristics of adhesive bonded joints is their durability under service loads. FE crack propagation analyses on linear viscoelastic media have also been performed by several researchers (Krishnaswamy et al.,[54] ; Warby et al., [55]; Chen and Dillard, [56]; Dubious et al., [57]; and Rahulkumar et al. [58]). Most studies were performed on the TSM.

In this section, the capability of the recursive-iterative algorithm integrated within the FE framework for simulating time-dependent crack propagations of adhesive bonded joints under thermo-mechanical loadings are presented. The purposes of these numerical studies are to predict crack initiation and complete failure time. FE models for mode I (opening) and mode II (shearing) bonded joint failures are generated using plane strain elements (CPE4). For this purpose, a 2D plane strain condition is imposed to the 3D recursive-iterative algorithm. The mode I failure analysis is performed on a double cantilever beam (DCB) specimen, which is taken from a study by Allen and Searcy [59] While, for mode II analysis, the lap-joint specimen tested by Jurf and Vinson [40] is modeled. Figures 3.13 (a) and (b) illustrates the lap joint geometries for simulating mode I and mode II failures, respectively.

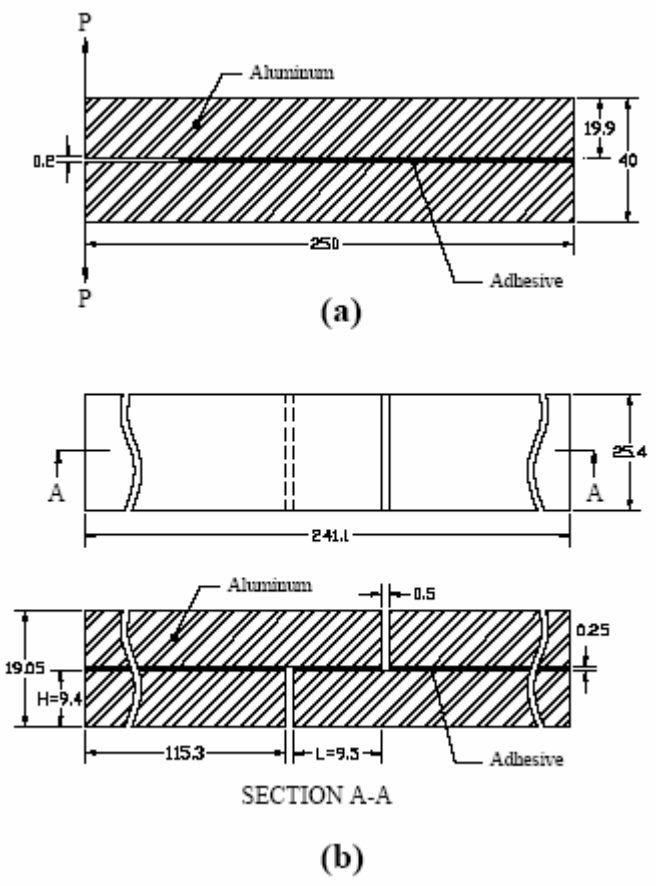

Figure 3.13. Geometry models for Mode I and Mode II time-dependent crack propagation analyses on adhesive bonded joints (a) Double cantilever beam (b) Lap joint (not to scale).

The nonlinear viscoelastic constitutive model is incorporated for the adhesive layers made of FM73M polymer. The aluminum adherends in both lap joints are modeled as linear elastic materials and the temperature effects in the adherends' elastic properties are neglected. It is noted that in order to simulate more accurate time-dependent crack propagation analyses under thermo-mechanical loadings, detail constitutive model of the adherends under elevated temperature should be incorporated. In addition, detail crack

initiation prediction should also incorporate plastic deformation and prestresses due to the different coefficient of thermal expansions in the adherend and adhesive materials.

3.2.1 MODE I (OPENING) TIME-DEPENDENT CRACK PROPAGATION

Convergence studies are first performed to determine suitable number of elements used in the crack propagation analyses. Finer meshes are required for the adhesive layers. Total 4 and 64 numbers of meshes are generated along the adhesive's thickness and bonded length, respectively. Cohesive elements are applied along the predetermined failure path, which is located at the mid-height of the adhesive layers. The last four nodes near the fix end are tied, in which crack will no longer allow propagating. Thus, complete debonding is determined once the current crack tip reaches the tied node. The crack opening displacement (COD) failure criterion, available in the ABAQUS FE code [41], is used to evaluate crack initiation and propagation:

$$f = \frac{\delta_n^{\,t}}{\delta_{ncr}} \tag{3.2}$$

Where $\delta_n^{\,t}$ is the current normal opening displacement across the cohesive surface δ_{ncr} is the critical opening displacement. The critical displacement δ_{ncr} is first determined using failure analyses of a quasi static problem based on the critical stress failure criterion:

$$f = \sqrt{\left(\frac{\sigma}{\sigma_{cr}}\right)^2 + \left(\frac{\tau}{\tau_{cr}}\right)^2} \tag{3.3}$$

Where σ_{cr} and τ_{cr} are the axial and shear critical stress, respectively. Thus, the critical displacement δ_{ncr} is the opening displacement when the failure criterion in Eq. (3.3) reaches one. Load-displacement response of the quasi-static DCB specimen under displacement control with rate of 0.2 mm/min at 295K is shown in Fig. 3.14. The failure criterion in Eq. (3.2) is monitored at the distance 3 mm ahead the current crack tip. When the failure criterion reaches one, crack is initiated and the fracture energy is released to create two traction free surfaces. The energy released rate can be determined from the experimental crack propagation. The load at which crack initiate is around 200 N, which corresponds to 5 MPa critical stresses. The critical opening displacement δ_{ncr} is found to be equal to 0.002 mm. These parameters correspond to the opening failure within the adhesive materials.

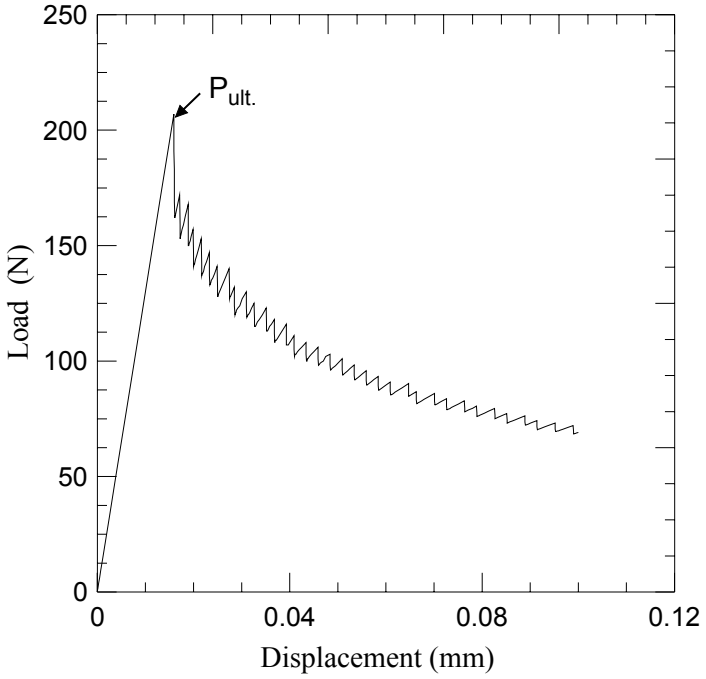

Figure 3.14. Load vs. displacement plot for double cantilever beam (Mode I) at a displacement rate of 0.2 mm/min.

Next, time-dependent crack propagation analysis of the double cantilever is performed with the COD failure criterion. Two constant loads: 140 N and 160 N, which correspond to 70 and 80% failure load, are applied under several isothermal temperatures for one hour. Figures 3.15 (a) and (b) present the cumulative crack length for two loads at several temperatures. As expected, higher load and temperatures accelerate crack initiation and complete debonding time. Table 3.6 presents crack initiation time and debonding time under 70% and 80% failure load.

Table 3.6. Crack propagation for Mode I for different displacement rates and temperatures.

Temperature (K)	Crack Initiation Time (seconds)		De-bonding time (seconds)	
	140 N	160 N	140 N	160 N
295	---	2097	---	---
305	---	52.4	---	---
310	---	1.64	---	323
315	3500	4e-4	---	10.9
320	1050	3e-4	---	11.2
323	262	2e-4	---	0.5

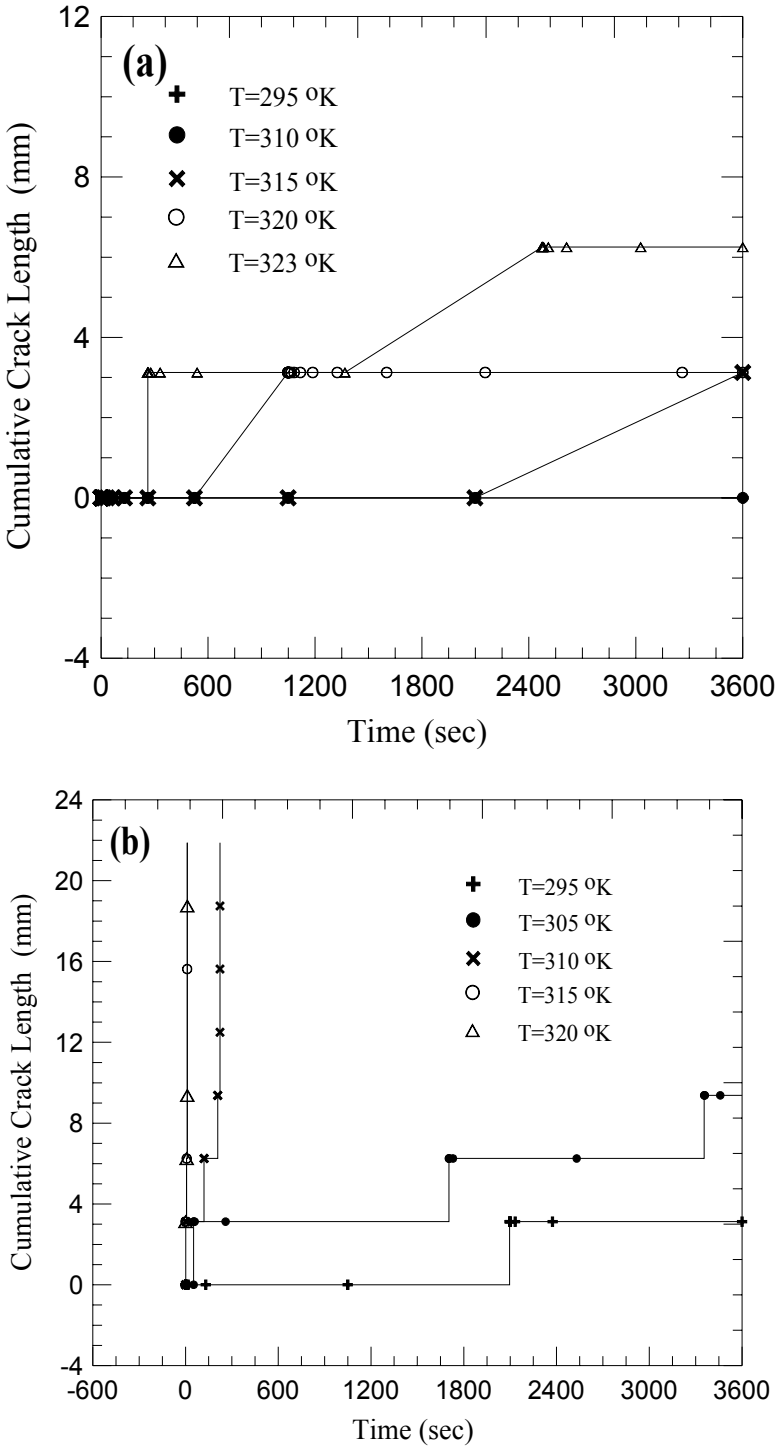

Figure 3.15. Cumulative crack length vs. time for a double cantilever beams in mode I under creep load of (a) 140 N (b) 160N.

3.2.2 MODE II (SHEARING) TIME-DEPENDENT CRACK PROPAGATION

Similar procedure is adopted for the mode II failure analyses. In this case, 40 meshes are generated along the bonded length for the adhesive layers and total 5 elements are used along the adhesive's thickness. Cohesive elements are applied along the predetermined failure paths, which are located at top and bottom interface between the adhesive layers and the aluminum adherend. Stress based failure criterion, Eq. (3.3), is used. This failure criterion corresponds to the separation between adhesive and aluminum. Figures 3.16 (a) and (b) show the crack propagation analysis for mode II based on the critical stress. Analyses are run at displacement rates of 0.1 mm/min and 0.2 mm/min and at different temperatures. Softer material reaches the critical stress level slower than the stiffer material does, which cause slow crack propagation. The crack propagates equally in the anti-symmetric failure paths at the top and bottom interface. Table 3.7 shows the crack initiation and debonding time for different displacement rates and at different temperatures.

Table 3.7. Crack propagation for Mode II for different displacement rates and temperatures.

Temperature (K)	Crack Initiation Time (seconds)		De-bonding time (seconds)	
	0.1 mm/min	0.2 mm/min	0.1 mm/min	0.2 mm/min
295	6.16	3.07	15.2	7.37
311	6.70	3.34	19.1	9.31
323	7.41	3.68	23.0	12.1

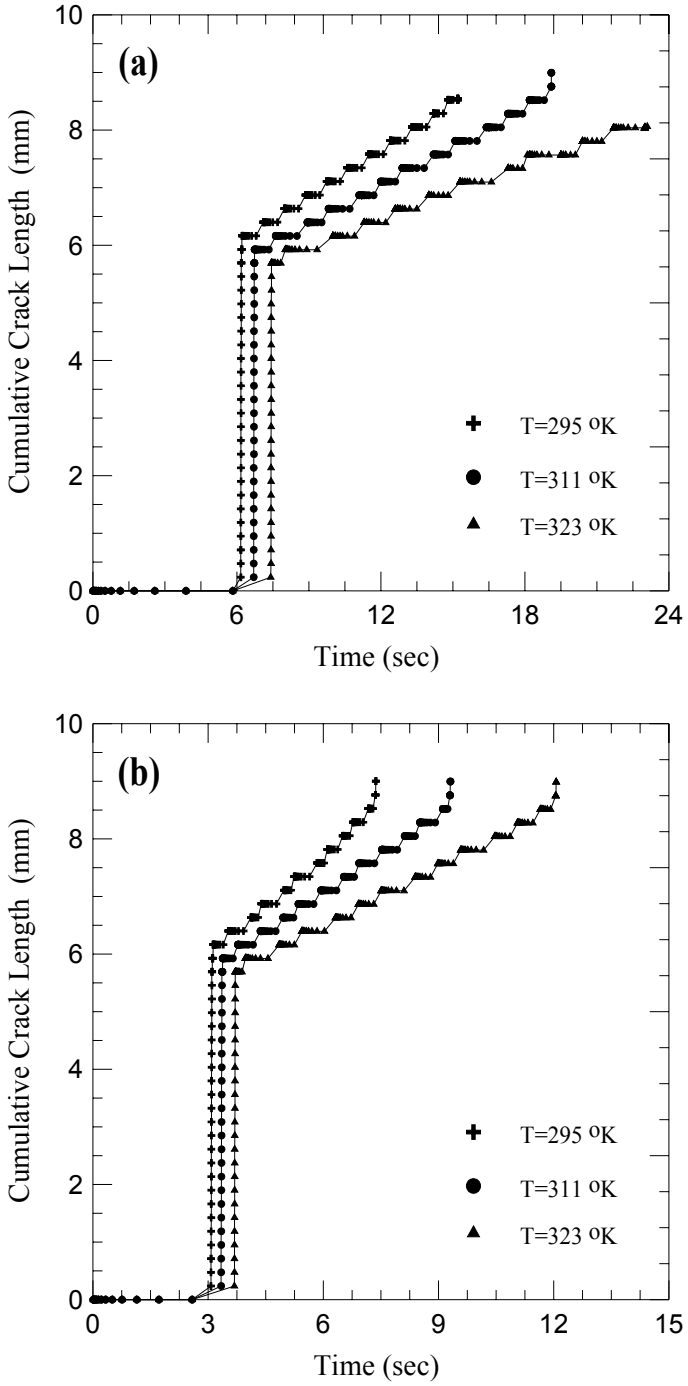

Figure 3.16. Cumulative crack length vs. time at displacement rate of (a) 0.1 mm/min (b) 0.2 mm/min.

CHAPTER IV

INTEGRATION OF THE THERMO-VISCOELASTIC ALGORITHM WITH THE MICROMECHANICAL MODEL OF PARTICULATE REINFORCED COMPOSITES

This chapter describes integration of the proposed thermo-viscoelastic algorithm with a micromechanical model for predicting effective viscoelastic responses of composite systems reinforced with solid spherical micro particles. The solid spherical particle is taken as linear elastic, while the polymer follows thermo viscoelastic material responses. The micromechanical formulation is generalized to include an explicit time-scale for modeling time-dependent behavior and is designed to be compatible with general displacement based finite element (FE) analyses. Comparisons with detailed unit-cell FE models are presented to verify the capability of the above micromechanical model for predicting the overall nonlinear viscoelastic behaviors.

Polymer composite materials can be precisely tailored to meet a desired performance by varying reinforcement types and in-situ material properties. However, polymers that are commonly used in composite materials are often brittle with poor resistance to fracture. Thus, nano or micro size particles are added to increase the toughness of the composite systems. Experimental studies have been performed to evaluate constituent and microstructural parameters that govern the effective mechanical properties of the composites. For polymers reinforced with microscale spherical beads, it was found that decreasing particle sizes at constant particle volume fractions increases

the composite strength; while increasing volume fractions decrease the strength [Cho et. al. [60], Leiden et. al. [61] and Wong et. al [62]. The effective moduli of the composites depend strongly on the particle contents and are less influenced by the particle sizes (Biwa et. al. [63], Leiden et. al. [61], Wong et. al [62] and Yang et. al. [64]). On the other hand, for composites reinforced with nano scale particles, the particle size significantly influences both the modulus and strength of the composites (Leiden et. al. [61]. In addition, surface treatment on particles increases the composite strength due to improvement in interface adhesion (Wong et. al [62]). Furthermore, polymeric based composites often exhibit nonlinear viscoelastic behaviors. Limited experimental studies have been done on the viscoelastic behaviors of particulate reinforced polymer composites (Alberola et. al. [65], Aniskevich et. al. [66] and Tsou et. al. [67]).

From the experimental observations, analytical and numerical modeling approaches have been proposed to evaluate the effective mechanical responses of composite systems having several microstructural geometries and in-situ material properties. Micromechanical modeling approaches have been widely used for predicting overall mechanical behaviors of composite systems due to their ability in incorporating different constituent microstructures and properties. Each constituent is represented by a homogeneous and continuous medium. Several analytical methods based on volume average have been proposed to evaluate effective elastic and inelastic responses of particulate reinforced composites (Eroshkin et. al [68], Levesque et. al. [69], Mura [70], Nemat-Nasser et. al. [71]). These micromechanical models formulate detail microstructural geometries, which allows for predicting exact composite responses.

However, it is often difficult to evaluate the exact solutions especially when material nonlinearity or inelastic behaviors are also considered. Finite element (FE) methods are often used for modeling microstructures of particulate reinforced composites. The FE method allows generating composite systems having certain particle numbers with detail particle size and shape, easily incorporating different constitutive material models for all the constituents, and modeling various mechanism between the constituents (Chen et. al. [72], Dommelen et. al. [73], Kari et. al. [74] and Levesque et. al. [69]). Simulating overall composite behaviors by incorporating detail microstructural mechanism is often computationally expensive. Moreover, it is not always necessary or possible to generate detail microstructural geometries for evaluating overall composite behaviors.

This study formulates a simplified micromechanical model for predicting nonlinear viscoelastic responses of polymeric based composite systems reinforced with solid spherical micro particles. The proposed numerical algorithm for thermo-viscoelastic behaviors of polymers is integrated into the micromechanical model. The micromechanical model is suitable for implementation in general displacement based FE structural analyses. The composite microstructures are simplified with uniformly distributed cubic particles over an infinite medium. A unit-cell model with four particle and polymer subcells is generated. It is assumed that all particles are surrounded by polymeric matrix. In addition, the particle contacts are not considered in the micromechanical formulations, which is best for estimating composite performance having low to medium volume fractions. The nonlinear stress-temperature dependent viscoelastic material responses are attributed to the polymer subcells, while the particle

subcell remains linear elastic. The micromechanical homogenization is developed in terms of the average strains and stresses in the subcells. The traction continuity and displacement compatibility at the subcells' interfaces are imposed. Due to the nonlinear and time-dependent response in the polymeric matrix, the linearized micromechanical relations will often deviate from the nonlinear constitutive equations. Thus, a stress-strain correction algorithm is formulated to satisfy the micromechanical constraints and nonlinear constitutive equations. Detail FE unit-cell models of solid spherical particle embedded in the viscoelastic medium are generated using 3D continuum elements. The responses form the detail FE models are compared with the ones generated from the proposed micromechanical model.

4.1 THE MICROMECHANICAL MODEL

The micromechanical homogenization schemes are derived in terms of the average stress-strain relations in the subcells, which was proposed by Haj-Ali and Pecknold [75] to generate effective responses of unidirectional fiber reinforced composite systems. For composite systems with nonlinear constitutive models in the individual constituents, the linearized micromechanical relations often violate the constitutive equations. Thus, iterative correction schemes are formulated to satisfy both the micromechanical constraints and the nonlinear constitutive equations. This linearized homogenization and corrector schemes have been successfully applied to model nonlinear and time-dependent behaviors of composite materials having unidirectional and randomly oriented fiber reinforcement (Haj-Ali et. al. [76]- [77]).

This study will adopt the micromechanical homogenization and corrector schemes of (Haj-Ali et. al. [75]-[77]) for modeling nonlinear time-dependent responses of particulate reinforced polymer composites. The particles are in the form of solid spheres made of linear elastic materials. The nonlinear time-dependent constitutive model is attributed to the polymeric matrix. Figure 4.1 illustrates the simplified micromechanical model for the polymer composite with randomly distributed solid spherical particles. The solid spherical particulate composites are idealized with uniformly distributed arrays of cubic particles in x_1, x_2, and x_3 axes of the Cartesian coordinate. This geometry representation is similar to the one proposed by Aboudi et. al. [78] to study functionally graded materials with non-uniform fiber spacing. A representative volume element (RVE) consists of a cubic particle embedded in the center of the matrix with cubic domain. A one eight unit-cell consisting of four subcells is modeled due to symmetry. The first subcell is a particle constituent, while subcells 2, 3, and 4 represent the matrix constituents. The micromechanical relations provide equivalent homogeneous material responses from the heterogeneous microstructures and simultaneously recognize behaviors of the individual constituents from the overall composite responses. The two-ways micro-macro mechanical relations refer to a concurrent micromechanical model.

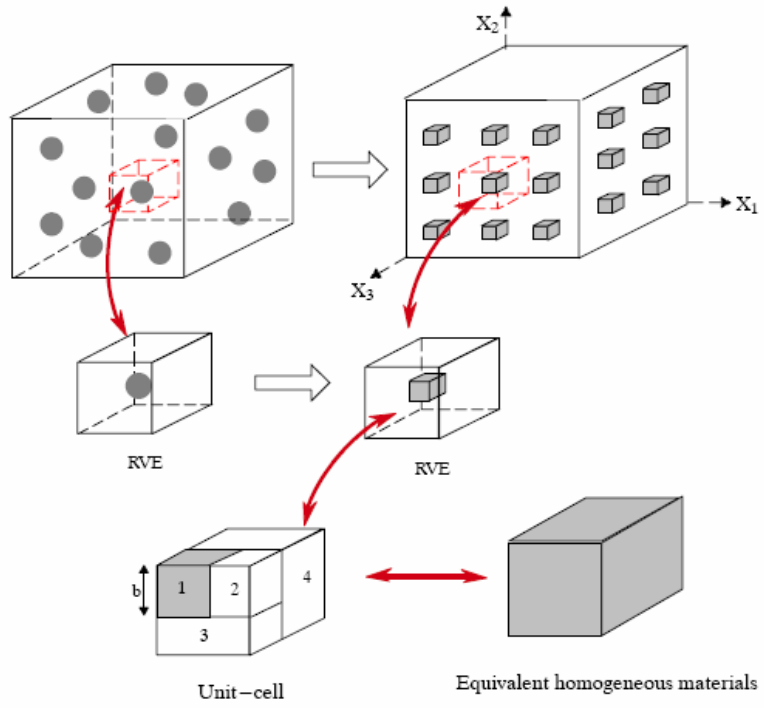

Figure 4.1. Representative unit-cell model for the particulate reinforced polymers.

4.1.1 LINEARIZED MICROMECHANICAL RELATIONS

The effective properties of a heterogeneous medium can be approximated using volume averaged of individual constituents. The average stresses and strains are defined by:

$$\bar{\sigma}_{ij} = \frac{1}{V}\int_V \sigma_{ij}(x_k)dV \qquad i, j = 1,2,3 \tag{4.1}$$

$$\bar{\varepsilon}_{ij} = \frac{1}{V}\int_V \varepsilon_{ij}(x_k)dV \tag{4.2}$$

An overbar indicates effective material quantities. For small deformation, the strain is expressed by $\varepsilon_{ij}=\frac{1}{2}[u_{i,j}+u_{j,i}]$, where u_i is the component of the displacement tensor. The average stresses and strains represent the stresses and strains of the fictitious homogeneous media that are related by composite effective stiffness or compliance:

$$\overline{\sigma}_{ij} = \overline{C}_{ijkl}\overline{\varepsilon}_{kl} \tag{4.3}$$

$$\overline{\varepsilon}_{ij} = \overline{S}_{ijkl}\overline{\sigma}_{kl} \tag{4.4}$$

The goal of the micromehanical formulation is to provide composite effective stiffness and compliances. Following Haj-Ali and Pecknold [75], in a heterogeneous periodic medium, a basic unit-cell that represents geometrical and material characteristics can be defined. Each unit-cell is divided into a number of subcells and the spatial variation of the displacement field in each subcell is assumed such that the stresses and deformations are spatially uniform. Traction continuity at an interface between subcells is satisfied in an average sense. Thus, the average stresses and strains in the unit-cell model are defined by:

$$\overline{\sigma}_{ij} = \frac{1}{V}\sum_{\alpha=1}^{N}\int_{V^{(\alpha)}}\sigma_{ij}^{(\alpha)}(x_k^{(\alpha)})dV^{(\alpha)} = \frac{1}{V}\sum_{\alpha=1}^{N}V^{(\alpha)}\sigma_{ij}^{(\alpha)} \tag{4.5}$$

$$\overline{\varepsilon}_{ij} = \frac{1}{V}\sum_{\alpha=1}^{N}\int_{V^{(\alpha)}}\varepsilon_{ij}^{(\alpha)}(x_k^{(\alpha)})dV^{(\alpha)} = \frac{1}{V}\sum_{\alpha=1}^{N}V^{(\alpha)}\varepsilon_{ij}^{(\alpha)} \tag{4.6}$$

The superscript a denotes the subcell number and N is the number of subcells. The stress $\sigma_{ij}^{(\alpha)}$ and strain $\varepsilon_{ij}^{(\alpha)}$ are the average stress and strain within each subcell. The unit-cell volume V is:

$$V = \sum_{\alpha=1}^{N} V^{(\alpha)} \tag{4.7}$$

The micromechanical model of solid spherical particle reinforced composites is represented by a unit-cell model with four subcells, as illustrated in Fig. 4.1. The volume of the unit-cell is taken as one. The volume of the subcell 1, which is model as a cube of edge length b, represents the particle volume fraction of the composite systems. Thus, the magnitude of b is always less than one. The volumes of the four subcells are then expressed as:

$$V^{(1)} = b^3,\ V^{(2)} = b^2(1-b),\ V^{(3)} = b(1-b),\ V^{(4)} = (1-b) \tag{4.8}$$

The micromechanical relations within the four subcells in Fig. 4.1 are derived by assuming perfect bond along the interfaces of the subcells. Thus, displacement compatibility and traction continuity at the subcells' interface should be satisfied. In the case of both particle and matrix are isotropic, the outcome of the homogenized micromechanical model is also isotropic. The homogenized strain relations are summarized in the following:

$$\bar{\varepsilon}_{11} = \frac{1}{V^{(1)}+V^{(2)}}\left[V^{(1)}\varepsilon_{11}^{(1)} + V^{(2)}\varepsilon_{11}^{(2)}\right] = \varepsilon_{11}^{(3)} = \varepsilon_{11}^{(4)} \tag{4.9}$$

$$\bar{\varepsilon}_{22} = \frac{1}{V^{(1)}+V^{(2)}}\left[V^{(1)}\varepsilon_{22}^{(1)} + V^{(2)}\varepsilon_{22}^{(2)}\right] = \varepsilon_{22}^{(3)} = \varepsilon_{22}^{(4)} \tag{4.10}$$

$$\bar{\varepsilon}_{33} = \frac{1}{V^{(1)}+V^{(2)}}\left[V^{(1)}\varepsilon_{33}^{(1)} + V^{(2)}\varepsilon_{33}^{(2)}\right] = \varepsilon_{33}^{(3)} = \varepsilon_{33}^{(4)} \tag{4.11}$$

$$\bar{\gamma}_{12} = V^{(1)}\gamma_{12}^{(1)} + V^{(2)}\gamma_{12}^{(2)} + V^{(3}\gamma_{12}^{(3)} + V^{(4)}\gamma_{12}^{(4)} \tag{4.12}$$

$$\bar{\gamma}_{13} = V^{(1)}\gamma_{13}^{(1)} + V^{(2)}\gamma_{13}^{(2)} + V^{(3}\gamma_{13}^{(3)} + V^{(4)}\gamma_{13}^{(4)} \tag{4.13}$$

$$\bar{\gamma}_{23} = V^{(1)}\gamma_{23}^{(1)} + V^{(2)}\gamma_{23}^{(2)} + V^{(3}\gamma_{23}^{(3)} + V^{(4)}\gamma_{23}^{(4)} \tag{4.14}$$

The homogenized stresses are written in the following:

$$\begin{aligned} \bar{\sigma}_{11} &= V^{(A)}\sigma_{11}^{(A)} + V^{(3)}\sigma_{11}^{(3)} + V^{(4)}\sigma_{11}^{(4)} \\ \sigma_{11}^{(A)} &= \sigma_{11}^{(1)} = \sigma_{11}^{(2)} \end{aligned} \tag{4.15}$$

$$\begin{aligned} \bar{\sigma}_{22} &= V^{(A)}\sigma_{22}^{(A)} + V^{(3)}\sigma_{22}^{(3)} + V^{(4)}\sigma_{22}^{(4)} \\ \sigma_{22}^{(A)} &= \sigma_{22}^{(1)} = \sigma_{22}^{(2)} \end{aligned} \tag{4.16}$$

$$\begin{aligned} \bar{\sigma}_{33} &= V^{(A)}\sigma_{33}^{(A)} + V^{(3)}\sigma_{33}^{(3)} + V^{(4)}\sigma_{33}^{(4)} \\ \sigma_{33}^{(A)} &= \sigma_{33}^{(1)} = \sigma_{33}^{(2)} \end{aligned} \tag{4.17}$$

$$\bar{\tau}_{12} = \tau_{12}^{(1)} = \tau_{12}^{(2)} = \tau_{12}^{(3)} = \tau_{12}^{(4)} \tag{4.18}$$

$$\bar{\tau}_{13} = \tau_{13}^{(1)} = \tau_{13}^{(2)} = \tau_{13}^{(3)} = \tau_{13}^{(4)} \tag{4.19}$$

$$\bar{\tau}_{23} = \tau_{23}^{(1)} = \tau_{23}^{(2)} = \tau_{23}^{(3)} = \tau_{23}^{(4)} \tag{4.20}$$

Where the total volume of subcells 1 and 2 in Eqs. (4.15)-(4.17) is $V^{(A)} = V^{(1)} + V^{(2)}$

The proposed micromechanical models consists of four subcells with six components of strains need to be determined for every subcell. This requires forming 24 equations. The first sets of equations are determined from the strain compatibility equations, which can be rearranged as:

$$\underset{(12x1)}{\left\{ \mathbf{R}_{\varepsilon} \right\}} = \underset{(12x24)}{\left[\mathbf{A}_1 \right]} \underset{(24x1)}{\left\{ \begin{matrix} \boldsymbol{\varepsilon}^{(1)} \\ \boldsymbol{\varepsilon}^{(2)} \\ \boldsymbol{\varepsilon}^{(3)} \\ \boldsymbol{\varepsilon}^{(4)} \end{matrix} \right\}} - \underset{(12x6)}{\left[\mathbf{D}_1 \right]} \underset{(6x1)}{\left\{ \bar{\boldsymbol{\varepsilon}} \right\}} \tag{4.21}$$

where $\mathbf{R}_{\varepsilon}$ is the residual vector arising from imposing strain compatibility relations. In the case of linear elastic responses are exhibited for all subcells, the vector $\mathbf{R}_{\varepsilon}$ is zero. The second sets of equations are formed based on traction continuity relations. Up to this stage, the components of effective stress tensor $\bar{\sigma}_{ij}$ remain unknown, thus, rearranging Eqs. (4.15)-(4.20) should avoid the presence of $\bar{\sigma}_{ij}$. The equations based on the traction continuity relations within subcells:

$$\underset{(12x1)}{\{\mathbf{R}_\sigma\}} = \underset{(12x24)}{[\mathbf{A}_2]} \underset{(24x1)}{\begin{Bmatrix} \boldsymbol{\varepsilon}^{(1)} \\ \boldsymbol{\varepsilon}^{(2)} \\ \boldsymbol{\varepsilon}^{(3)} \\ \boldsymbol{\varepsilon}^{(4)} \end{Bmatrix}} - \underset{(12x6)}{[\mathbf{O}]} \underset{(6x1)}{\{\bar{\boldsymbol{\varepsilon}}\}} \tag{4.22}$$

The residual vector $\mathbf{R}_\sigma$ results from satisfying traction continuity relations. For linear elastic constituents, the components of $\mathbf{R}_\sigma$ are zero. The matrix $\mathbf{O}$ is the zero matrix and the components of matrix $\mathbf{A}_1$, $\mathbf{A}_2$ and $\mathbf{D}_1$ are given as follows:

$$\mathbf{A}_1 = \begin{bmatrix} \underset{(3x3)}{\frac{V^{(1)}}{V^{(A)}}\mathbf{I}} & \underset{(3x3)}{0} & \underset{(3x3)}{\frac{V^{(2)}}{V^{(A)}}\mathbf{I}} & \underset{(3x3)}{0} & \underset{(3x3)}{0} & \underset{(3x3)}{0} & \underset{(3x3)}{0} & \underset{(3x3)}{0} \\ \underset{(3x3)}{0} & \underset{(3x3)}{0} & \underset{(3x3)}{0} & \underset{(3x3)}{0} & \underset{(3x3)}{\mathbf{I}} & \underset{(3x3)}{0} & \underset{(3x3)}{0} & \underset{(3x3)}{0} \\ \underset{(3x3)}{0} & \underset{(3x3)}{0} & \underset{(3x3)}{0} & \underset{(3x3)}{0} & \underset{(3x3)}{0} & \underset{(3x3)}{0} & \underset{(3x3)}{\mathbf{I}} & \underset{(3x3)}{0} \\ \underset{(3x3)}{0} & \underset{(3x3)}{V^{(1)}\mathbf{I}} & \underset{(3x3)}{0} & \underset{(3x3)}{V^{(2)}\mathbf{I}} & \underset{(3x3)}{0} & \underset{(3x3)}{V^{(3)}\mathbf{I}} & \underset{(3x3)}{0} & \underset{(3x3)}{V^{(4)}\mathbf{I}} \end{bmatrix}$$

$$\mathbf{A}_2 = \begin{bmatrix} \underset{(3x3)}{-\mathbf{C}_{ax}^{(1)}} & \underset{(3x3)}{0} & \underset{(3x3)}{\mathbf{C}_{ax}^{(2)}} & \underset{(3x3)}{0} & \underset{(3x3)}{0} & \underset{(3x3)}{0} & \underset{(3x3)}{0} & \underset{(3x3)}{0} \\ \underset{(3x3)}{0} & \underset{(3x3)}{-\mathbf{C}_{sh}^{(1)}} & \underset{(3x3)}{0} & \underset{(3x3)}{-\mathbf{C}_{sh}^{(1)}} & \underset{(3x3)}{0} & \underset{(3x3)}{0} & \underset{(3x3)}{0} & \underset{(3x3)}{0} \\ \underset{(3x3)}{0} & \underset{(3x3)}{-\mathbf{C}_{sh}^{(1)}} & \underset{(3x3)}{0} & \underset{(3x3)}{0} & \underset{(3x3)}{0} & \underset{(3x3)}{\mathbf{C}_{sh}^{(3)}} & \underset{(3x3)}{0} & \underset{(3x3)}{0} \\ \underset{(3x3)}{0} & \underset{(3x3)}{-\mathbf{C}_{sh}^{(1)}} & \underset{(3x3)}{0} & \underset{(3x3)}{0} & \underset{(3x3)}{0} & \underset{(3x3)}{0} & \underset{(3x3)}{0} & \underset{(3x3)}{\mathbf{C}_{sh}^{(4)}} \end{bmatrix} \tag{4.23}$$

Where:

$$\mathbf{C}_{ax} = \begin{bmatrix} C_{1111} & C_{1122} & C_{1133} \\ C_{2211} & C_{2222} & C_{2233} \\ C_{3311} & C_{3322} & C_{3333} \end{bmatrix} \quad \mathbf{C}_{sh} = \begin{bmatrix} C_{1212} & 0 & 0 \\ 0 & C_{1212} & 0 \\ 0 & 0 & C_{1212} \end{bmatrix}$$

$$\mathbf{D}_1 = \begin{bmatrix} \underset{(3x3)}{\mathbf{I}} & \underset{(3x3)}{0} \\ \underset{(3x3)}{\mathbf{I}} & \underset{(3x3)}{0} \\ \underset{(3x3)}{\mathbf{I}} & \underset{(3x3)}{0} \\ \underset{(3x3)}{0} & \underset{(3x3)}{\mathbf{I}} \end{bmatrix}$$

4.1.2 STRESS CORRECTION ALGORITHM

The linearized micromechanical relations are exactly satisfied only when all subcells exhibit linear elastic responses. Due to the nonlinear and time-dependent response in the matrix subcells, the linearized micromechanical relations will usually violate the constitutive equations. This study uses the linearized micromechanical relations in incremental forms and performs an iterative correction scheme. The corrector scheme is needed to satisfy both the micromechanical constraints and the nonlinear viscoelastic constitutive equations, otherwise very small time step is required to better approximate the nonlinear responses. The above micromechanical relations are used to define trial stresses and strains for each subcell at the beginning of time increment (backward Euler method). The nonlinear stress-strain relations in one or more of the subcells result in nonzero residual vectors $\mathbf{R}_{\varepsilon}$ and $\mathbf{R}_{\sigma}$. These residuals are then used to correct the trial solution. This process is repeated until a converged solution that satisfies both micromechanical and nonlinear equations is achieved. The stress correction algorithm is shown in figure 4.2.

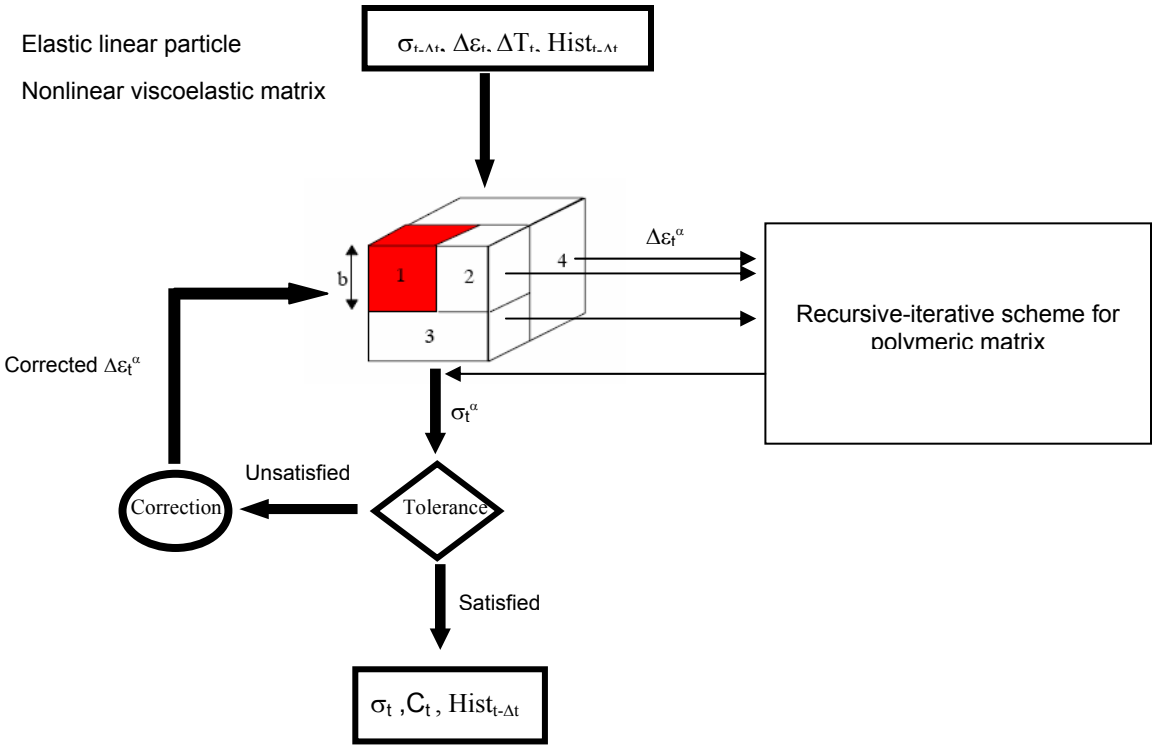

Figure 4.2 Stress-Strain correction algorithm.

4.2 NUMERICAL IMPLEMENTATION AND VERIFICATION

The capability of the proposed micromechanical model in predicting nonlinear viscoelastic properties of the particle reinforced composite is presented. For this purpose, the micromechanical model is implemented in a 3D continuum element using a material subroutine of ABAQUS [41] FE code. Nonlinear viscoelastic responses evaluated using the micromechanical model is compared with the detailed FE model of the composite representative volume element (RVE) are also generated.

Two detailed FE unit-cell models of different composite's representative volume element (RVE) are generated, illustrated in Fig. 4.3. The first unit-cell model consists of single particle embedded in a cubic polymeric matrix. Due to the three-plane symmetric condition, one-eight unit-cell can be used. The second unit-cell model consists of 9 particles placed at each corner and center of the cubic polymeric matrix. All particles are surrounded by matrix medium. Thus contact between particles is avoided but particles interaction is recognized. The simplified one-eight unit-cell consists of two particles at the farthest distance. Both unit cell models assume the particle to be linear elastic and the matrix to be modeled as pure polymer. The FM-73 polymer is used for this study. The time-temperature and stress dependent properties are taken from the experimental data reported by Peretz and Weitsman (1982), which are previously given in Table 2.1 and Eq. 2.27.

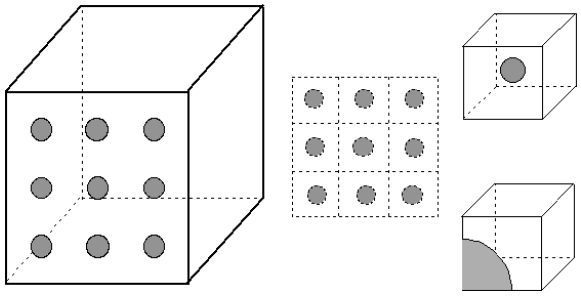

(a)

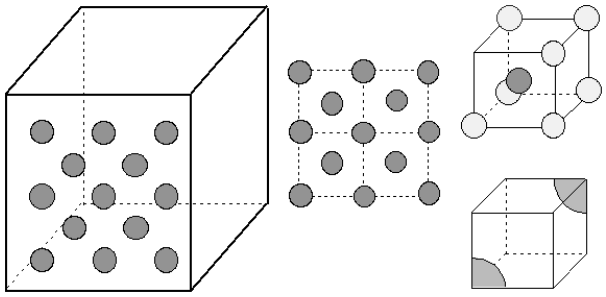

(b)

Figure 4.3. Finite element unit-cell model. (a) one particle (b) two particle.

The first verification is done on creep responses under different temperatures and stresses. Detailed unit-cell model that consists of two particle are used for comparisons. Figure 4.4 (a)–(b) shows the creep responses for composites having 5% volume fraction. The solid lines indicate the results from the micromechanical model and the dotted line shows the results from the FE unit-cell model. Good agreements are shown for all cases.

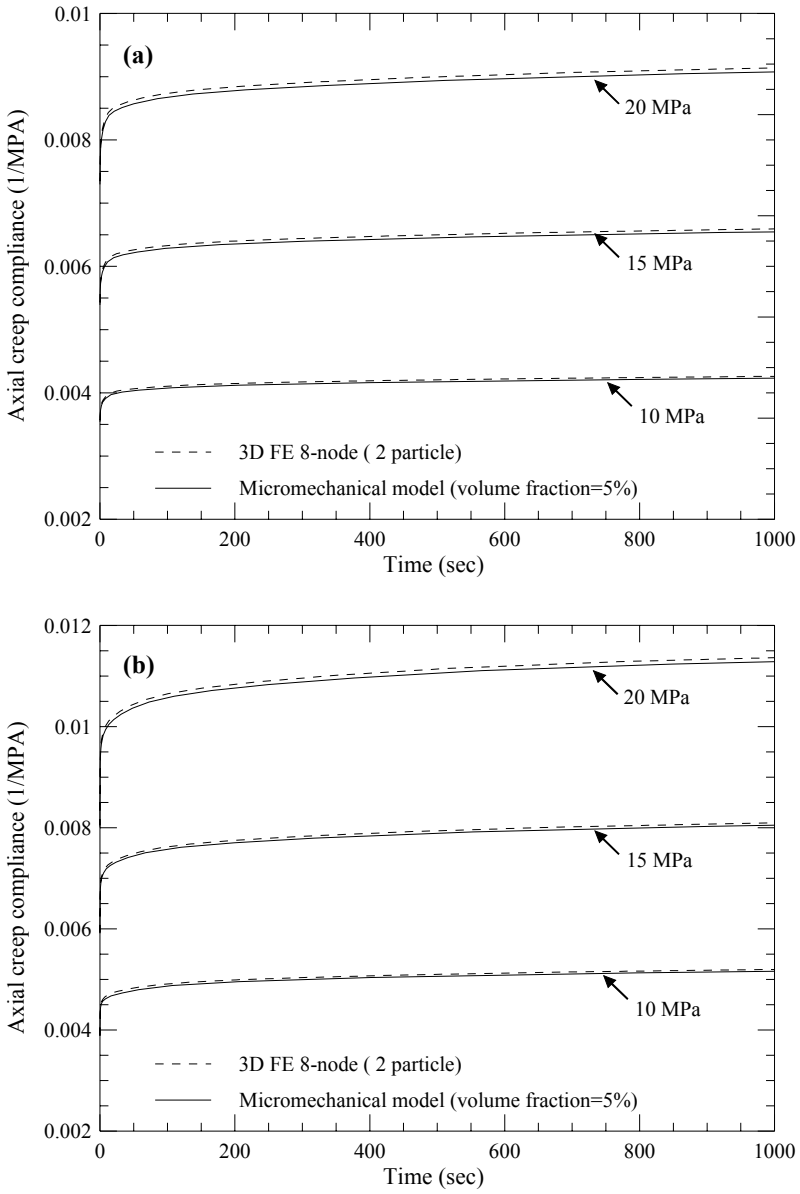

Figure 4.4. Creep strain responses under different stress levels and at temperatures. (a) 303 ˚K (b) 333 ˚K.

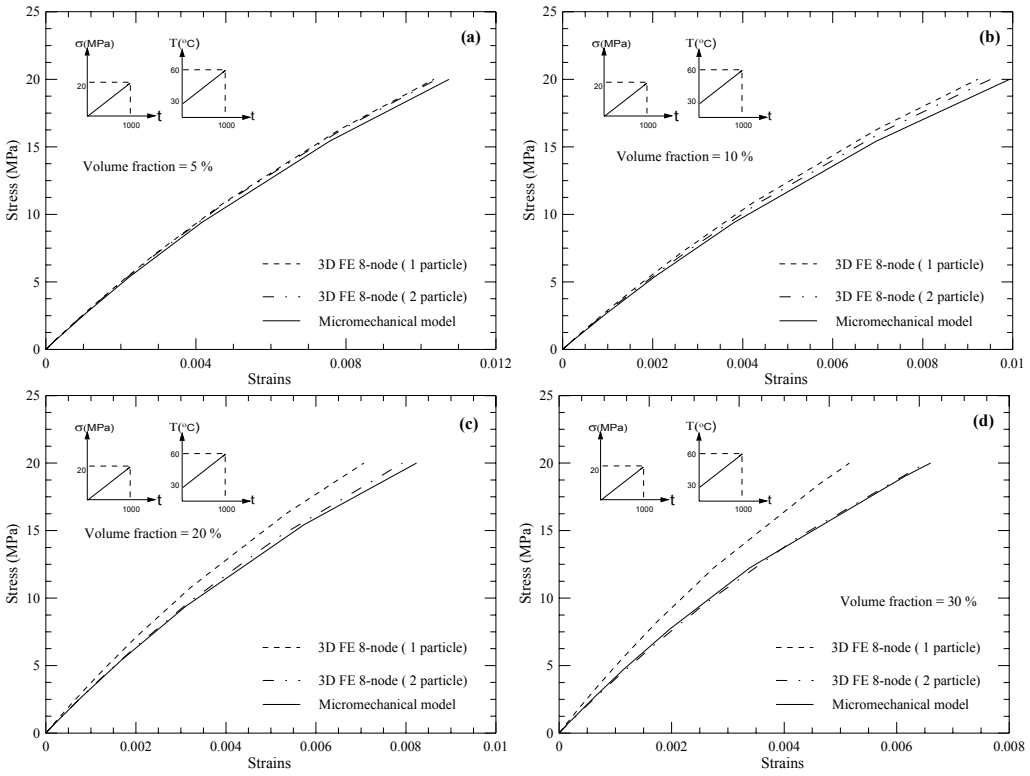

Figure 4.5. Creep strain responses under linear stress and temperature ramping at different volume fractions. (a) 5% (b) 10 % (c) 20% (d) 30%.

Next, the composites behaviors under ramp temperature and stress loading have been analyzed for composites having 5-30% volume fractions. Fig. 4.5 (a)–(d) show the time dependent nonlinear responses from the one particle, two particles and the micromechanical models at 5%, 10%, 20% and 30% volume fractions respectively. It is seen that with the increase of volume fraction the results from the one particle FE unit-cell model deviate from the ones of micromechanical and two particle models. For the same volume fraction, the unit-cell model with single particle has larger particle size as compared to the one of the two particle model. Thus, as the particle's radius approaching the edge length of the cubic matrix, particles contact will occur. This explains the deviations shown from the single particle unit cell model. In the case of two particle

model, for the studied volume fraction, the shortest distance between two particles are relatively large. This indicates no particles are in contact.

CHAPTER V

CONCLUSIONS AND FURTHER RESEARCH

5.1 CONCLUSIONS

A recursive-iterative algorithm is developed for predicting nonlinear viscoelastic behaviors of isotropic materials that belong to the TCM. The algorithm is derived based on implicit stress integration solutions within a general displacement based FE structural analyses for small deformations and uncoupled thermo-mechanical problems. Linearized predictor and corrector schemes are performed simultaneously at the structural and material levels. The corrector scheme is used to minimize error arising from linearization. Previously developed recursive-iterative algorithm for a stress-dependent hereditary integral model (Haj-Ali and Muliana, 2004) is modified to include time-temperature effects. The recurrence formula allows bypassing the need to store entire strain histories at each Gaussian integration point. Two types of iterative procedures, which are fixed point (FP) and Newton-Raphson (NR) methods, are examined within the recursive algorithm. Furthermore, a consistent tangent stiffness matrix is formulated to accelerate convergence and avoid divergence. The efficiency and accuracy of the proposed algorithm are evaluated using available experimental data and several structural analyses. The performance of the proposed algorithm under multi-axial conditions is verified with analytical solutions of creep responses of a plate with a hole. Next, the recursive-iterative algorithm is used to predict the overall response of single lap-joint. Numerical simulations of time-dependent crack propagations of adhesive bonded joints are also presented. For this purpose, the recursive algorithm is

implemented in cohesive elements. The numerical assessment of the TCM and TSM behaviors has also been performed. The result showed that the TCM are able to describe thermo-viscoelastic behavior under general loading histories, while the TSM behaviors are limited to isothermal conditions. The proposed numerical algorithm can be easily used in a micromechanical model for predicting the overall composite responses. Examples are shown for the solid spherical particle reinforced composites. Detailed unit-cell FE models of the composite systems are generated to verify the capability of the above micromechanical model for predicting the overall nonlinear viscoelastic behaviors.

5.2 FURTHER RESEARCH

The current study for thermo-mechanical time dependent behavior of the polymer and polymeric based systems are limited to conditions without damage and failure. The time-shifting methods are applicable only within limited times at which tertiary creep and/or micro-structural changes have not yet occurred. In order to better understand the complete responses, failure criterion should also be incorporated to study the effect of micro-structural changes or damage accumulation in the polymer. Other environmental factors such as moisture can also significantly affect the creep deformation of the material. In addition, polymers at high temperatures experience thermal oxidation that degrades their material properties. Therefore moisture dependence and material degradation on the long-term polymers behavior need to be studied. It is also necessary to develop time-dependent material model undergoing simultaneous thermo-hygro-mechanical and oxidation mechanisms.

REFERENCES

[1] Staverman, A. J and Schwarzl, F., Thermodynamics of Viscoelastic Behaviour (Model Theroy), Proceedings of the Physical Sciences (Series B), 1952; 5(55): 474-485.

[2] Leaderman, H, Elastic and Creep Properties of Filamenteous Materials and Other High Polymers, Textile Foundation, Washington: McGraw Hill; 1943.

[3] Green A. E and Rivlin, R. S., The Mechanics of Nonlinear Materials with Memory Part I, Archive for Rational Mechancis and Analysis, 1957; 1: 1.

[4] Green A. E, Rivlin, R. S. and Spencer, A. J., The Mechanics of Nonlinear Materials with Memory Part II, Archive for Rational Mechancis and Analysis, 1959; 3: 82.

[5] Green A. E and Rivlin, R. S., The Mechanics of Nonlinear Materials with Memory Part III, Archive for Rational Mechancis and Analysis, 1960; 4: 387.

[6] Schapery, R. A., Stress Analysis of Viscoelastic Composite Materials, J. Composite Materials, 1967; 1(3): 228-241

[7] Caruthers, J. M, Adolf, D. B., Chambers, R. S. and Shrikand, P, A, Thermodynamically Consistent Nonlinear Viscoelastic Approach for Modeling Glassy Polymers, Polymer, 2004; 45:4577-4597

[8] Adolf, D. B, Chambers, R. S, and Caruthers, J. M, Extensive Validation of a Thermodynamically Consistent, Nonlinear Viscoelastic Model for Glassy Polymers, Polymer, 2004; 45:4599-4621

[9]Coleman, B. D. and Noll, W, Foundation of Linear Viscoelasticity, Reviews of Modern Physics, 1961; 33:239-255

[10] Ward, I. M and Onat, E. T., Nonlinear Mechanical Behavior of Oriented Polypropylene, J. of Mechanics and Physics of Solids, 1963; 11:217-228

[11] Peretz, D. and Weitsman, Y., Non Linear Viscoelastic Characterization of FM-73 Adhesives, Journal of Rheology, 1982; 26(3):245-261

[12] Peretz, D. and Weitsman, Y., The Non Linear Thermo Viscoelastic Characterization of FM-73 Adhesives, Journal of Rheology, 1983; 27(2):97-114

[13] Harper, B. D. and Weitsman, Y., Characterization Method for a Class of Thermorhelogically Complex Materials, Journal of Rheology, 1985, 29(1):49-66

[14] Knauss, W. G. and Emri, I, Volume Change and the Nonlinearly Thermo-Viscoelastic Constitution of Polymers, Polymer Engineering and Science, 1985; 27(1):49-66

[15] Zhang, L., Ernst, L. J., and Brouwer. H. R, A Study of Nonlinear Viscoelasticity of an Unsaturated Polyester Resin. Part I. Uniaxial Model, Mechanics of Materials, 1997; 26:141-166

[16] Knauss, W.G. and Zhu, W, Nonlinear Viscoelastic Behavior of Polycarbonate I. Response under Pure Shear, Mechanics of Time Dependent Materials, 2002; 6:231-269.

[17] Park, S. J., Liechti, K. M., and Roy, S., Simplified Bulk Experiments and Hygrothermal Non Linear Viscoelasticity, Mechanics of Time Dependent Materials, 2004; 8:303-344

[18] Popelar's K., Multiaxial Nonlinear Viscoelastic Characterization and Modeling of a Structural Adhesive, J. Eng. Mater. Technol. Trans. ASME, 1997;119:205–210

[19] Griffith, W. I., Morris, D. H., and Brinson, H. F, The Accelerated Characterization of Viscoelastic Composite Materials, 1980, VPI&VSU Report, VPI-E-80-5

[20] Tuttle, M. E., Accelerated Viscoelastic Characterization of T300/5208 Graphite-Epoxy Laminates, Ph.D. Dissertation, Blackburg, VA: Virginia Polytechnic Institute and State University, 1984

[21] Yen, S. C., and Williamson, F. L, Accelerated Characterization of Creep Response of an Off Axis Composite Material, Composite Science and Technology, 1980; 38:103-118.

[22] Schwarzl, F and Staverman, A. J., Time-Temperature Dependence of Linear Viscoelastic Behavior, Journal of Applied Physics, 1952; 23(8):838-843.

[23] Feng, C. W, Keong, C. W, Hsueh, Y. P, Wang, Y. Y. and Sue, H. J, Modeling of Long-Term Creep Behavior of Structural Epoxy Adhesives, International Journal of Adhesion & Adhesives, 2005; 25:427–436

[24] Qvale, D and Chandar, K. R., Viscoelastic Characterization of Polymers Under Multiaxial Compression, Mechanics of Time-Dependent Materials, 2004;8:193–214

[25] Zienkiewicz, O. C., Watson, M., and King, I. P., A Numerical Method of Viscoelastic Stress Analyses, Int. J. Mechanical Science, 1968; 10:807-827.

[26] Zienkiewicz, O. C. and Cheung, Y. K., The Finite Element Method in Structural and Continuum Mechanics, London: McGraw Hill;1967

[27] Bazant, Z. P., Matrix Differential Equation and Higher-order Numerical Methods for Problems of Nonlinear Creep, Viscoelasticity and Elasto-plasticity, Int. J. Numerical Method in Engineering, 1972; 4 (1):11-15.

[28] Taylor, R.L., Pister, K.S., and Goudreau, G.L., Thermomechanical Analysis of Viscoelastic Solids, International Journal for Numerical Methods in Engineering, 1970; 2:45-59.

[29] Feng, W. W., A Recurrence Formula for Viscoelastic Constitutive Equations, Int. J. Nonlinear Mechanics, 1992; 27 (4):675-678.

[30] Henriksen, M., Nonlinear Viscoelastic Stress Analysis - A Finite Element Approach, Computer and Structures, 1984; 18(1):133-139.

[31] Lai, J. and Bakker, A., 3-D Schapery Representation for Nonlinear Viscoelasticity and Finite Element Implementation, Computational Mechanics, 1996; 18:182-191.

[32] Haj-Ali, R. M. and Muliana, A, Numerical Finite Element Formulation of the Schapery Nonlinear Viscoelastic Material Model, Int. J. Numerical Meth. in Eng., 2004; 59 (1):25-45.

[33] Simo, J.C., and Hughes, T.J.R., Computational Inelasticity, New York: Springer Verlag, 1998.

[34] Kennedy, T.C. and Wang, Three-Dimensional Nonlinear Viscoelastic Analysis of Laminated Composites, Journal of Composite Materials, 1994; 28(10):902-25

[35] Yi, S., Hilton, H. H., and Ahmad, M. F., Nonlinear Thermo-Viscoelastic Analysis of Interlaminar Stresses in Laminated Composites, Journal Applied Mechanics, 1996; 63: 218-224.

[36] Hilton, H. and Yi. S, Anisotropic Viscoelastic FE Analysis of Mechanically and Hygrothermally Loaded Composites, Composite Engineering, 1993; 3:123-135.

[37] Zocher, M. A., Groves, S. E., and Allen, D. H, A Three-dimensional Finite Element Formulation for Thermoviscoelastic Orthotropic Media, Int. J. Numerical Method in Eng., 1997; 40:2267-2280.

[38] Poon, H. and Ahmad, F., A Material Point Time Integration Procedure for Anisotropic, Thermo-rheologically Simple, Viscoelastic Solids, Computational Mechanics, 1998; 21:236-242.

[39] Poon, H. and Ahmad, F., A Finite Element Constitutive Update Scheme for Anisotropic, Viscoelastic Solids Exhibiting Non-linearity of the Schapery Type, International Journal of Numerical Method in Engineering, 1999; 46:2027-2041.

[40] Jurf, R. A. and Vinson, J. R., Effect of Moisture on the Static and Viscoelastic Shear Properties of Epoxy Adhesives, Journal of Material Science, 1985; 20:2979-2989

[41] ABAQUS, User's Manual, Version, 6.5, Baltimore, Maryland, Hibbitt, Karlsson and Sorensen Inc., 2005.

[42] Schapery, R. A., Viscoelastic Behavior and Analyses of Composite Materials, Composite Material, 1974; 5:85-168.

[43] Sadkin, Y. and Aboudi, J., Viscoelastic Behavior of Thermo-rheologically Complex Resin Matrix Composites, Composites Science and Technology, 1989; 36:351-365

[44] Tobolsky, A. V., Structure and Properties of Polymers, New York: John Wiley; 1960

[45] Morland, L. W. and Lee, E. H, Stress Analysis for Linear Viscoelastic Materials with Temperature Variation, Trans. Soc. Rheology, 1960; 4:233-246

[46] Wineman, A. S and K. R. Rajagopal, Mechanical Response of Polymers: An Introduction, London: Cambridge University Press, 2000

[47] Roy, S. and Reddy, J. N., A Finite Element Analysis of Adhesively Bonded Composite Joints with Moisture Diffusion and Delayed Failure, Computers and Structures, 1988; 29(6):1011-1031.

[48] Yadagirz, S., Reddy, C., and Reddy, T., Viscoelastic Analysis of Adhesively Bonded Joints, Computers and Structures, 1987; 27(4):445-458.

[49] Carpenter, W. C., Viscoelastic Analysis of Bonded Connections, Computers & Structures, 1990; 36(6):1141-l 152.

[50] Delale, F and Erdogan, F., Viscoelastic Analysis of Adhesivelv Bonded Joints. J. Appl. Mech., 1980; 48:331-338.

[51] Sancaktar, E., Material Characterization of Structural Adhesives in the Lap Shear Mode, International Journal of Adhesion and Adhesives, 1985; 5(2):66-68.

[52] Ahn, K. J, Eom, Y. S and Shim, Y. T, Characterization of Structural Adhesives for Load Bearing Composite Structural Applications, Composite Structures, 1994; 27:57-64.

[53] Chalkley, P. D. and Chiu. W. K., An Improved Method for Testing the Shear Stress/Strain Behavior of Adhesives, International Journal of Adhesion and Adhesives, 1993; 13(4):237-242.

[54] Krishnaswamy, P, Tuttle, M.E, Emery, A.F and Ahmad, J., Finite Element Modeling of Crack Tip Behavior in Viscoelastic Materials, Part I: Linear Behavior, International Journal for Numerical Methods in Engineering, 1990; 30:371-387.

[55] Warby, M. K., Waltonb, J. R. and Whiteman, J. R., A Finite Element Model of Crack Growth in a Finite Body in the Context of Mode I Linear Viscoelastic Fracture, Computer Methods in Applied Mechanics and Engineering , 1992; 97:375-397.

[56] Chen, B. and Dillard, D.A., Numerical Analysis of Directionally Unstable Crack Propagation in Adhesively Bonded Joints, International Journal of Solids and Structures, 1998; 38:6907 -6924.

[57] Dubois, F., Chazal, C., and Petit, C., A Finite Element Analysis of Creep-Crack Growth in Viscoelastic Media, Mechanics of Time-Dependent Materials, 1999; 2:269-286.

[58] Rahulkumar, P., Jagota, A., Bennison, S.J., and Saigal, S., Cohesive Element Modeling of Viscoelastic Fracture:Application to Peel Testing of Polymers, International Journal of Solids and Structures, 2000; 37:1873 -1897.

[59] Allen, D. H. and Searcy, C. R., A Micromechanical Model for a Viscoelastic Cohesive Zone", International Journal of Fracture, 2001; 107:159-176.

[60] Cho, J., Joshi, M. S., and Sun, C. T., Effects of Inclusion Size of Mechanical Properties of Polymeric Composites with Micro and Nano Particles, Composite Sci. Technol., 2006; in press.

[61] Leiden, J. and Woodhams, R. J., The Strength of Polymeric Composites Containing Spherical Fillers, J. Applied Polymer Sci., 1974; 18:1639-1651.

[62] Wong, F. C. and Ait-Kadi, A., Mechanical Behavior of Particulate Composites: Experiments and Micromechanical Predictions, J. Applied Polymer Sci., 1995; 55:263-278.

[63] Biwa, S., Ito, N., and Ohno, N., Elastic Properties of Rubber Particles in Toughened PMMA: Ultrasonic and Micromechanical Evaluation, Mechanics of Materials, 2001; 33: 717-728.

[64] Yang, W., Shi, Li, Z. M, Xie, B. H, Feng, J. M, and Yang, M. B, Mechanical Properties of Glass Bead-filled Linear Low-density Polyethylene, J. Elastomers and Plastics, 2004; 36:251-262

[65] Alberola, N. D. and Mele. P., Viscoelasticity of Polymers Filled by Rigid or Soft Particles: Theory and Experiment, Polymers Composites, 1996; 17:751-759.

[66] Aniskevich, K. and Hristova, J., Creep of Polyester Resin Filled with Mineral, J. Applied Polymers Sci., 2000; 77:45-52.

[67] Tsou, A. H. and DelleFave, D. L., Creep of a Glass-flake-reinforced Epoxy Adhesive for Space Applications, Polymer, 1996; 37(24):5381-5386.

[68] Eroshkin, O. and Tsukrov, I., On Micromechanical Modeling of Particulate Composites with Inclusions of Various Shapes, Int. J. Solids and Structures, 1995; 42:409-427.

[69] Levesque, M., Derrien, K., Mishnaevski, L., Baptiste, D. and Gilchrist, M. D., A Micromechanical Model for Nonlinear Viscoelastic Particle Reinforced Polymeric Composite Materials: Undamaged State, Composites A, 2004; 35:905-913.

[70] Mura, T., Micromechanics of Defects in Solids, Dordrecht: Martinous Nijhoff Publishers, 1987.

[71] Nemat-Nasser, S. and Hori, M., Micromechanics: Overall Properties of Heterogeneous Materials, 2nd Ed., New York: Elsevier, 1999

[72] Chen, X. H. and Mai, Y. W., Micromechanics of Rubber-toughened Polymers, J. Materials Science, 1998; 33:3529-3539.

[73] Dommelen, J. A. W., Brekelmans, W. A. M, and Baaijens, F. P. T, Micromechanics of Particle-Modified Semi-crystalline Materials, Fifth World Congress on Computational Mechanics, Vienna, Austria, 2002

[74] Kari, S., Berger, H., Rodriguez-Ramos, R., and Gabbert, U., Computational Evaluation of Effective Material, New York: Elsevier; 2005

[75] Haj-Ali, R. M., and Pecknold, D. A., Hierarchical Material Models with Microstructure for Nonlinear Analysis of Progressive Damage in Laminated Composite Structures, Structural Research Series No. 611, UILU-ENG-96-2007, Department of Civil Engineering, University of Illinois at Urbana-Champaign, 1996

[76] Haj-Ali, R. M., Kilic, H., and Zureick, A. H., Three-Dimensional Micromechanics-Based Constitutive Framework for Analysis of Pultruded Structures, Journal of Engineering Mechanics, 2001; 127(7):653-660.

[77] Haj-Ali, R. M. and Muliana, A. H., Micromechanical Models for the Nonlinear Viscoelastic Behavior of Pultruded Composite Materials, Int. J. Solids and Structures, 2003;40:1037-1057.

[78] Aboudi, J., Pindera, M. J., and Arnold, S. M., Thermoelastic Theory for the Response of Materials Graded in Two Directions, Int. J. Solids and Structures, 1996; 33: 931-966.

VITA

Name:	Kamran-Ahmed Khan
Address:	A-944 Sector 11-B North Karachi, Karachi -75850, Pakistan
Email Address:	kamrankhan@tamu.edu
Education:	B.Eng., NED University of Engineering and Technology, Karachi, Pakistan, 2002
	M.S, Dept. of Mechanical Engineering, Texas A&M University, College Station, Texas, 2006